ISSN 1000-9620

Marine Science Bulletin

Volume 6 • Number 1 2004

ISSN 1000-9620
01>
9 771000 962001

NATIONAL MARINE DATA AND
INFORMATION SERVICE OF CHINA

MARINE SCIENCE BULLETIN

Vol.6 No.1 May, 2004

CONTENTS

Profile Method for Measuring Apparent Optical Parameters (AOP) in Class-II Waters ····· *Li Tongji* (李铜基) *et al.* (1)

Characteristics of K_d(490) around Nansha Islands in the South China Sea ····· *Zhang Qingling* (张清凌) *et al.* (9)

Research on the Evaluation of Marine Environmental Quality by Using the GIS Technology ····· *Wang Lihua* (王立华) *et al.* (18)

Laboratory Simulation on Phosphorus Releasing near the Water/Sediment Interface in the East China Sea off the Changjiang Estuary ····· *Zheng Libo* (郑丽波) *et al.* (26)

Distribution of Dissolved Inorganic Phosphate in Nansha Islands Sea Area, Southern South China Sea ····· *Cheng* Saiwei (程塞伟) *et al.* (32)

Application of SAR Imagery in Submarine Topography Surveys ····· *Zhang Ningchuan* (张宁川) *et al.* (38)

Thermodynamic Analysis of Heavy Metals Biosorption by Two Macroalgae ····· *Chen Lidan* (陈丽丹) *et al.* (47)

Calculation of Environmental Capacity of Petroleum Hydrocarbon in Jiaozhou Bay ····· *Li Keqiang* (李克强) *et al.* (53)

Studies on Biquaternary Ammonium Salt Algaecide for Removing Red Tide Algae ····· *Liu Jiesheng* (刘洁生) *et al.* (60)

Statistical Study of Trace Elemental Concentrations in Major Types of Organisms from Typical Chinese Coastal Waters ····· *Guo Weidong* (郭卫东) *et al.* (66)

Harmful Ciliates and Dominant Genus in Culture Ponds of Young Abalone ····· *Huang Jianrong* (黄建荣) *et al.* (73)

The Relation of Standard Metabolic Rate to Water Temperature and Body Weight of Schlegels Black Rockfish (*Sebastodes Fuscescens*) ····· *Ma Zhimin* (马志敏) *et al.* (80)

Bottom Sediment Transport in the Flood and Ebb Channels of the Changjiang Estuary ····· *Liu Gaofeng* (刘高峰) *et al.* (88)

LIBRARY
MAR 0 1 2005
National Oceanic &
Atmospheric Administration
U.S. Dept. of Commerce

Profile Method for Measuring Apparent Optical Parameters (AOP) in Class-Ⅱ Waters

Li Tongji (李铜基), Chen qinglian (陈清莲)
National Ocean Technology Centre, Tianjin 300111, *China*

Abstract The profile method is the principal method first to be chosen to measure the apparent optical parameters of waters. This paper first introduces the profile method briefly, then modifies the applied algorithm in the light of the properties of the class-Ⅱ waters and lastly, analyses the effect of application.

LIBRARY
Pacific Islands Fisheries Science Ce
NOAA Fisheries
Honolulu, Hawai'i

Keywords Profile method; apparent optical parameters; class-Ⅱ waters

Introduction

To acquire marine information by applying the satellite has become a subject of concern to the international remote-sensing community and marine community. Ocean water colour remote-sensing is to detect the content of matter in the water by using the satellite-borne optical sensors, and, among others, the water-leaving radiance is the basic physical quantity in ocean water colour remote sensing and the optical manifestation of the water pigment components. *In-situ* accurate acquisition of the water-leaving radiance will be beneficial to the development of the biological optical algorithm and the atmospheric correction algorithm as well as the radiance correction of satellite-based remote sensors and the plausibility check of its data.

In the ocean water colour remote sensing, the seawater is usually divided into two classes —— class-Ⅰ seawater and class-Ⅱ seawater[1]. The class-Ⅰ water means that its optical properties are mainly determined by phytoplankton and its degraded matter pigment while the optical properties of the class-Ⅱ seawater are determined by the non-chlorophyll degraded matters, which include mainly the coloured dissolved organic matter (CDOM), suspended matter, deloris and bacteria, *etc.*. It can thus be seen that there are many factors affecting the optical properties of the Class-Ⅱ seawater. It is the complexity of the light field in the class-Ⅱ seawater that increases the difficulty in measuring its optical properties.

There are mainly three methods available for the *in-situ* measurement of the water-leaving radiance[2]: profile method, above-water measurement method and semi-empirical method with inherent optical parameters, among which the profile method is the first to be chosen internationally because it is less subjected to the effect of environmental factors (such as the direct solar light reflection, the sky diffuse reflection, *etc.*) and what it obtains is the internal information of the waters, which may be used in the detailed analysis and treatment of such problems as the stratification effect of the waters in the later period[3, 4]. However, the profile method also has its own limitations in that its measurement error is large in the shallow-sea and turbid waters. Besides, there exists the problem of the self-shadowing correction of the device.

In 1998, the National Ocean Technology Centre imported from the Canada Satlantic Co. a nine-channel optical profiler (SPMR/SMSR), thus making up the lack of the domestic equipment for measuring optical properties in the water. In the same year, this device was used in China's East China

Received on October 28, 2003

Sea area and the high-precision *in-situ* spectral data for the waters were obtained for the first time[5]. We can say that, to a certain extent, the introduction and application of SPMR/SMSR has laid foundation for the development of the *in-situ* observational technologies in marine optics in China in recent years. The fact that many institutions at home have imported high-precision optical profilers in the light of different research objectives also indicates that the high-precision seawater optical parameters have great potential for application in multidisciplinary areas.

At present, many applied algorithms have been studied and developed in view of the profiling method, and the typical ones are S84, P94 and P97 algorithms[6]. Each of these has shown good results of application in the class- I waters, but a poor effect of application in the class- II waters. On the basis of briefly introducing the principles of profile measurement, this paper proposes an applied algorithm in the class- II waters and analyses the effect of application of the profile method in the class- II waters in the light of the data measured by SPMR/SMSR in the Huanghai Sea in 2002.

1 Principles of profile measurement and multi-channel optical profiler

The nine-channel optical profiler is a typical apparatus for measuring the apparent optical parameters (AOP) in the waters by using the profile method. It consists of the profile units that can measure the ascending radiant luminance profile and the descending irradiance depth profile and the surface units that can measure the sea surface incident total irradiance (Fig. 1). In 2000, we added a sensor that can measure the ascending radiant luminance at the depth of 0.75 m onto the surface unit, thus providing a new method for improving our measuring precision in the class- II waters.

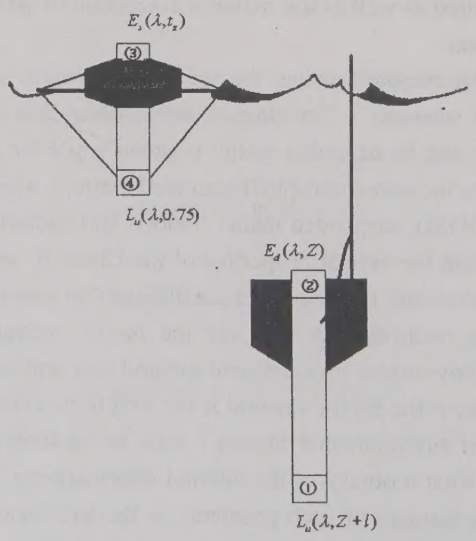

Fig. 1 Profiler (SPMR/SMSR) and principles of profile measurement

① is the sensor for measuring the ascending radiant luminance $L_u(\lambda, Z+l)$ at the depth of $Z+l$, where l is the distance between sensor ① and sensor ②; ② is the sensor for measuring the descending irradiance $E_d(\lambda, Z)$ at the depth of Z; ③ is the sensor for measuring the sea surface incident total irradiance $E_S(\lambda, t_z)$, in which t_z represents the measuring time of the surface unit when the profile unit is at the depth of Z; ④ is the sensor for measuring the ascending radiant luminance $L_u(\lambda, 0.75)$ at the depth of 0.75 m.

According to the principles of profile measurement[3, 4] (as shown in Fig. 1), and by using the ascending radiant luminance $L_u(\lambda, Z_1)$ and $L_u(\lambda, Z_2)$ in the waters at the different depths of (Z_1, Z_2), the diffuse attenuation coefficient $K_L(\lambda)$ of the ascending spectral radiant luminance may be computed by the following formula:

$$K_L(\lambda) = \frac{1}{Z_2 - Z_1} \ln \frac{L_u(\lambda, Z_1) / E_S(\lambda, t_{Z1})}{L_u(\lambda, Z_2) / E_S(\lambda, t_{Z2})} \tag{1}$$

where, t_Z represents the measuring time when the profile unit measures the optical parameters of the daters at the depth of Z. $E_S(\lambda, t_Z)$ in the formula serves to make up for the variations of light conditions in the course of measurement.

After $K_L(\lambda)$ is obtained, the data on the ascending radiant luminance at a given depth may be extrapolated to obtain the ascending radiant luminance just below the water surface:

$$L_u(\lambda, 0^-) = L_u(\lambda, Z_1) e^{K_L(\lambda) Z_1} \tag{2}$$

With $L_u(\lambda, 0^-)$ penetrating the sea surface, we can get the water-leaving radiance we require $L_w(\lambda)$[7]:

$$L_w(\lambda) = \frac{1 - \rho(\lambda)}{n_w^2(\lambda)} L_u(\lambda, 0^-) \tag{3}$$

where, $\rho(\lambda)$ is the Fresnel's reflectance of seawater; $n_w(\lambda)$ is the refraction index of seawater. As at the visible light-near-infrared wave band, $\rho(\lambda)$ and $n_w(\lambda)$ may be regarded as the constants which have nothing to do with the wave length, $(1 - \rho(\lambda)) n_w^{-2}(\lambda) \approx 0.544$ [8].

Lastly, according to definitions[3, 4, 9], the normalized water-learning radiance L_{wn} may be computed and obtained:

$$L_{wn}(\lambda) = \frac{F_0(\lambda)}{E_s(\lambda)} L_w(\lambda) \tag{4}$$

where, $F_0(\lambda)$ is the average solar irradiance outside the atmosphere; $E_S(\lambda)$ is the sea surface incident irradiance.

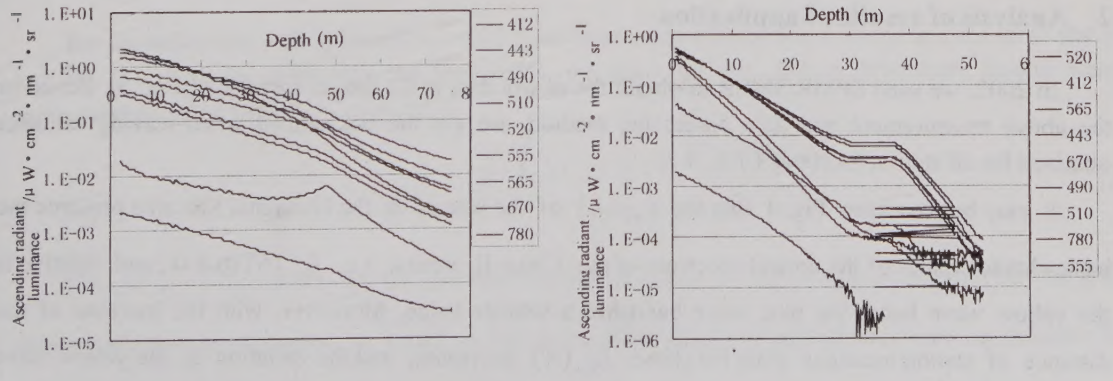

Fig. 2 a) Typical spectral data of the Class-II waters; The optical depths of various wave bands are about 30 ~ 40 m; b) Typical spectral data of the Class-II waters in the Huanghai Sea; The optical depths of various wave bands are around 10 m and below 30 m, the data present obvious bottom effect.

It can be seen from above that the principles of profile measurement assume that the optical properties of the water within the waters at the observational depth are homogeneous and that the diffuse attenuation coefficient $K_L(\lambda)$ of the ascending spectral radiant luminance is smaller, *i.e.*, the equivalent optical depth Z_{90} is greater, so that it is possible to obtain adequate effective data at the greater depths with which to calculate the optical properties of the shallower waters. This is very fit for the Class- I waters in the ocean (Fig. 2a). But in the Class- II waters (Fig. 2b), such as the Huanghai waters of China, although the water body can also be assumed to be horizontally stratified and the optical properties within the upper waters are also homogeneous, the incident radiant luminance attenuates quickly with depth due to the increase of the pigment concentrations in the water, and Z_{90} is smaller, so that the effective data points available for assessing the optical properties of the near-surface waters are very few; Besides, the bottom effect in the shallow waters would result in the failure of the data at great depths. This would require that we extrapolate from the $L_u(\lambda,Z)$ at smaller depths to obtain the ascending radiant luminance $L_u(\lambda,0^-)$ just below the sea surface. However, there exist greater random errors in the near-surface $L_u(\lambda,Z)$ due to wave action so that the precision of the water-leaving radiance obtained from computation is poor.

Fortunately, we can introduce the measured data of $L_u(\lambda,0.75)$. As the radiant luminance sensor at the depth of 0.75 m is able to measure the long time-series ascending spectral radiant luminance, it can provide the near-surface, high-precision ascending radiant luminance datum. It can be seen from Formula (1) that the assessment of $K_L(\lambda)$ reflects the relative change of the ascending radiant luminance. As the effect of sea surface waves in the Class- II waters rapidly declines with depth, the error resulted from the assessment of $K_L(\lambda)$ is smaller. In the meantime, if $L_u(\lambda,0.75)$ is used, the effect of the $K_L(\lambda)$ errors on the calculation of the precision of $L_u(\lambda,0^-)$ is not great. Thus we can get the following formula for calculating $L_u(\lambda,0^-)$:

$$L_u(\lambda,0^-) = L_u(\lambda,0.75)e^{0.75K_L(\lambda)} \tag{5}$$

2 Analysis of results of application

In 2002, we used SPMR/SMSR to obtain the *in-situ* data at 22 station locations (Fig. 3). Based on the above measurement and data processing method, we got the normalized water-leaving radiance obtained for all station locations (Fig. 4).

It may be seen from Fig. 4 that the $L_{wn}(\lambda)$ of the waters in the Huanghai Sea area presents the basic characteristics of the optical spectrum of the Class- II waters, *i.e.*, $L_{wn}(670) \neq 0$, and, relative to the yellow wave band, the blue wave band has a smaller value. Moreover, with the increase of the distance of station locations from the shore, $L_{wn}(\lambda)$ decreases, and the variation at the yellow wave band is larger while that at 412 nm relatively smaller. This suggests that phytoplankton has little effect on the optical properties of the waters in this sea area while suspended sediment and yellow matter play a dominant role.

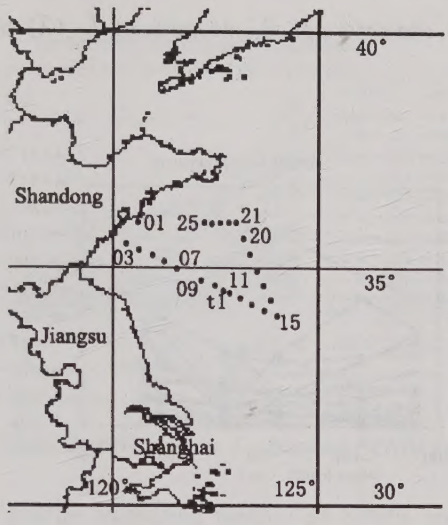

Fig. 3 Locations of Huanghai Sea experimental stations in 2002

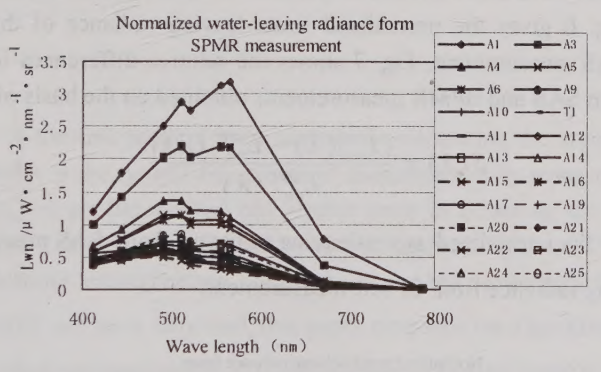

Fig. 4 L_{wn} at 22 station locations in the Huanghai Sea experiment in 2002 by using SPMR/SMSR

Except individual station locations (A25), we have made measurement in one and the same station location 2 ~ 3 times. Following the formula(6), we have got the relative differences among many measurements of SPMR/SMSR (Fig. 5).

$$\delta(\lambda) = \frac{\frac{1}{N}\sum_{i=1}^{N} | L_{wn}(\lambda, i) - \overline{L_{wn}(\lambda)} |}{\overline{L_{wn}(\lambda)}} \tag{6}$$

Where: $L_{wn}(\lambda, i)$ is the normalized water-leaving radiance for the i th measurement; N, the total number of measurement times; $\overline{L_{wn}(\lambda)}$ is the average value of normalized water-leaving radiance for the Nth measurement.

It can be seen from Fig. 5 that the relative difference among the data from many measurements by SPMR/SMSR at the same station location is not greater than 4 %, thus indicating that the profile

algorithm based on $L_u(\lambda,0.75)$ can ensure good uniformity of $L_{wn}(\lambda)$ obtained in the Class-II waters by SPMR/SMSR.

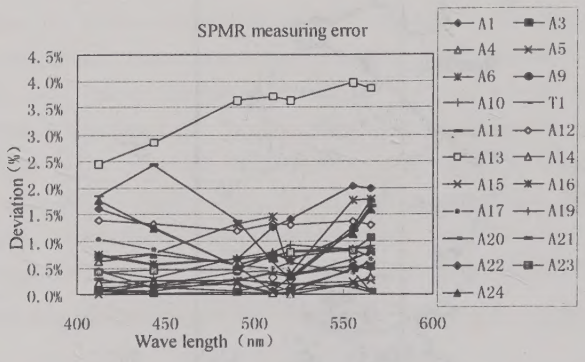

Fig. 5 Relative differences among various measuring results at the same station location

In the experiment, we have also carried out synchronous measurement by using SeaWiFS Simulator (SAS) and profiler. Fig. 6 gives the normalized water-leaving radiance of the above -mentioned 22 station locations for SAS measurement. Fig. 7 shows the relative differences in the normalized water-leaving radiance between SAS and SPMR measurements obtained on the basis of the formula (7).

$$\delta(\lambda) = \frac{|L_{wn}^{sas}(\lambda) - L_{wn}^{spmr}(\lambda)|}{L_{wn}^{spmr}(\lambda)} \tag{7}$$

where: $L_{wn}^{sas}(\lambda)$ is the normalized water-leaving radiance from SAS measurement; $L_{wn}^{spmr}(\lambda)$, the normalized water-leaving radiance from SPMR measurement.

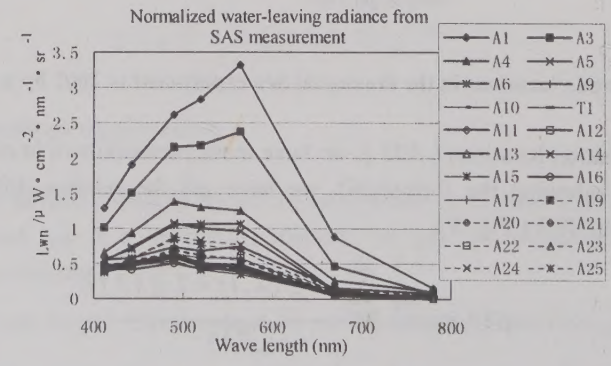

Fig. 6 L_{wn} at 22 station locations from SAS

It can be seen from Fig. 7 that for all the data of 22 station locations, the relative difference in the normalized water-leaving radiance between SAS and SPMR measurements at the wave band of 412 nm ~ 520 nm is not greater than 10 %, and that at the wave band of 565 nm is not greater than 16 %. Owing

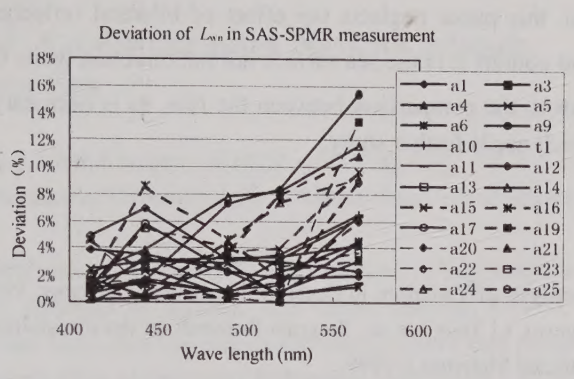

Fig. 7 Relative difference in L_{wn} between SPMR and SAS

to the difference between the profile measuring method of SPMR and the above-water measuring method of SAS, there lacks comparability between the 670 nm and 780 nm wave bands, so these two wave bands are not included in Fig. 7. The data of Fig. 7 show that SPMR and SAS are in good agreement in obtaining the normalized water-leaving radiance.

4 Conclusions

The profile method is the first method to be chosen for measuring the apparent optical parameters of waters and SPMR/SMSR is the typical equipment of measurement by using the profile method. Due to its own characteristics, the profile method has greater error in obtaining the water-leaving radiance from its application in the Class- II waters. Based on the characteristics of China's nearshore waters (*i.e.*, the upper waters is more homogeneous, but its absorbing and scattering effect is great) as well as the features of SPMR/SMSP we have imported, this paper proposes the algorithm based on $L_u(\lambda,0.75)$. It can be seen from the results of application in the Huanghai Sea experiment in 2002 that for the many measurements at one and the same station location, the relative error in the normalized water-leaving radiance between SPMR and SMSR measurements is within 4 %; while that between the profile method and the above-water measuring method is not greater than 10 % at the wave band of 412~520 nm, and not greater than 16 % at the wave band of 565 nm. This shows that SPMR/SMSR is stable in performance and the algorithm based on $L_u(\lambda,0.75)$ which it adopts has good results of application in the experimental waters.

Although this paper suggests that the algorithm has achieved good results of application in the Huanghai Sea experiment in 2002, there are some limitations and problems that need to be further studied.

(1) The algorithm has to a certain extent raised the precision and accuracy of the profile measuring method in obtaining the apparent optical properties of the waters in the Class- II waters, but it requires that the waters be somewhat transparent. For the waters very close to the shore where the light field attenuates very rapidly (the optical depth of some waters is only 0.5~1 m), the error of this method in calculating the water-leaving radiance would still be great.

(2) In comparing the normalized water-leaving radiances between the profile method and the above

-water measuring method, this paper neglects the effect of bilateral reflection of the waters. As the $L_{wn}(\lambda)$ the profile method obtains is in the sea surface normal direction while the $L_{wn}(\lambda)$ got by SAS is in the 45° direction, prior to the comparison between the two, its is necessary to make correction and compensation for this, which needs further study.

References

[1] Morel A Y, Prieur L. Analysis of Variations in Ocean Color. Limnol Oceanogr, 1997, 22, 709-722.

[2] Chen Qinglian, Tang Junwu, Li Tongji *et al.*. Program Research on the Plausibility Test of the Satellite-borne Remote-sensing. (Restricted Materials), 1999.

[3] G S Fargion and J L Muller. Ocean Optics Protocols for Satellite Ocean Color Sensor Validation. Revision 2, NASA/TM-2000-209966, 2000.

[4] J L Muller and G S Fargion. Ocean Optics Protocols for Satellite Ocean Color Sensor Validation. Revision 3, NASA/TM-2002-210004, 2002

[5] Chen Qinglian, Tang Junwu, Wang Xiangnan *et al.*. *In-situ* Measurements and Data Analysis for the Spectral Properties of the Waters in the East China Sea Experimental Zone. Ocean Technology, 1999, 18(3).

[6] S B Hooker, G Lazin *et al.*. 2000: An Evaluation of Above - And In - Water Methods for Determining Water - Leaving Radiances. JGR.

[7] Austin R W. 1974: The Remote Sensing of Spectral Radiance from Below the Ocean surface, In: Optical Aspects of Oceanography. N G Jerlov and E S Nielsen, Eds, Academic Press.

[8] Austin R W. Gulf of Mexico, Ocean Color Surface Truth Measurements Bound. — Layer Meteor, 1980, 18: 269-285.

[9] Gordon H R and D K Clark. Clear Water Radiance for Atmospheric Correction of Coastal Zone Color Scanner Imagery. Applied Optics, 1981, 20: 4 175-4 180.

Characteristics of $K_d(490)$ around Nansha Islands in the South China Sea

Zhang Qingling (张清凌), Chen Chuqun (陈楚群), Shi Ping (施 平), Yin Kedong (殷克东)
LED, South China Sea Institute of Oceanography, Chinese Academy of Sciences, Guangdong 510301

Abstract The diffusion attenuation coefficient for downwelling irradiance, $K_d(490)$, is an important optical parameter of seawater. The optical property, $K_d(490)$, around Nansha Islands in the South China Sea was analyzed based on optical data profiles measured with SPMR (SeaWiFS Profiling Multichannel Radiometer) and SMSR (SeaWiFS Multichannel Surface Reference) instrument in April and May, 1999. The results show that $K_d(490)$ is closely correlated with chlorophyll-a concentration, $C_{chl.a}$, and that the vertical distribution of $K_d(490)$ shows the strong stratification of the water column in this area. $K_d(490)$ has a similar vertical co-variation as $K_L(490)$, the diffusive attenuation coefficient for upwelling radiance. Both coefficients increase with depth in the upper layer, where $K_L(490)$ is greater than $K_d(490)$; and after a depth, approximatively at the chlorophyll maximum, they decrease with depth, with the former being smaller than the latter.

Keywords South China Sea, Nansha Islands; diffusion attenuation coefficient $K_d(490)$, underwater spectral measurement

Introduction

$K_d(\lambda)$, diffusion attenuation coefficient for downwelling irradiance at wavelength λ, is an important optical parameter of seawater. $K_d(490)$ is especially unique in that light beam with a wavelength of 490nm penetrates relatively deeper in the water column of seawater. Research on $K_d(490)$ in most seas around the world has progressed greatly. Austin *et al*[1] reviewed the linear regression relationship between $K_d(490)$ and other $K_d(\lambda)$s. In the South China Sea, Zhong *et al.*[2] studied the vertical distribution of $K_d(\lambda)$ and found that the maximum value of $K_d(\lambda)$ is at the depth where there is the maximum content of dissolved and suspended materials, which has the similar vertical distribution property as $K_d(\lambda)$. Little has been studied on the optical characteristics of $K_d(490)$ of seawater around Nansha Islands in the southern part of South China Sea.

During April to May, 1999, we measured the optical spectrum of seawater in vertical profile around Nansha Islands in the South China Sea and analyzed optical characteristics of $K_d(490)$.

1 Materials and Methods

1.1 Field Survey Data

The Instruments *Sea WiFS Profiling Multichannel Radiometer* — SPMR and *Sea WiFS Multichannel Surface Reference* — SMSR (Satlantic Company) are used to collect data on seawater profile spectrum. SPMR and SMSR are manufactured by Satlantic, Inc. and designed for calibration of

Received on July 16, 2003
This work was jointly supported by project KZCX2-202 from CAS, the project of 818-06-03 from national 863 program and project 97-926-07 of national special program for science and technology.

SeaWiFS data and could have totally up to 13 bands. The instruments, from the National Marine Technical Center of China, are assembled with 9 bands. The central peak wavelengths of these 9 bands are: 412 nm, 443 nm, 490 nm, 510 nm, 520 nm, 555 nm, 565 nm, 670 nm, and 780 nm. SPMR is used to obtain downwelling irradiance (*E*d) and upwelling radiance (*L*u) of these 9 bands, and SMSR is used to obtain sea surface irradiance (*E*s) to monitor change of sea surface irradiance and to provide a reference for adjustment in processing profile spectrum data[3]. Ancillary data such as chlorophyll a (Chl.*a*) and DOC are obtained at the same time at some stations. Spectrum data of totally 63 profiles were obtained at 27 stations during April 1999 (No. 9904 Cruise) around Nansha Islands (Fig. 1).

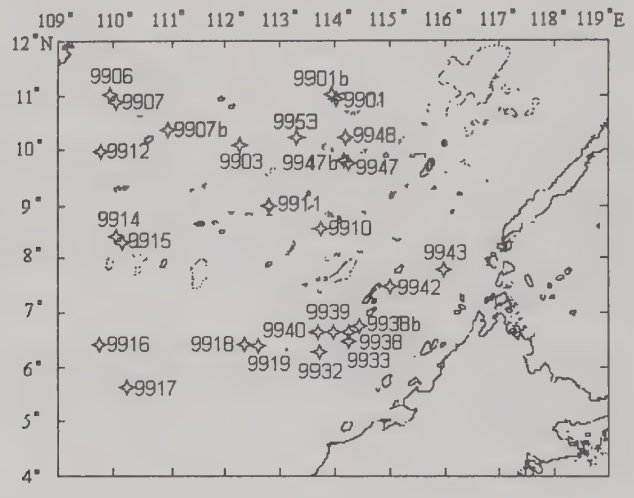

Fig.1 Map of stations during 9904 Cruise in Nansha Islands

1.2 Data Processing

Due to waves of the sea surface, values of E_d and L_u just below the sea surface (depth of 0^-) cannot be measured directly and must be extrapolated using values at a certain depth z or even more generally using values in a certain layer[4]. Data processing is based on the Smith & Baker local linear regression method, in which logarithm transformation on irradiance in the depth range of $z \pm \Delta z$, is performed, and then the logarithmic values are linearly regressed against depths. Thus the slope of the linear regression in a range of $z \pm \Delta z$ is $K_d(\lambda, z)$, where subscript d stands for downwelling irradiance, λ for wavelength, and z for depth[4].

2 Results

2.1 Vertical Distribution Characteristics of $K_d(490)$

Vertical distribution of diffusive attenuation coefficient $K_d(490)$ basically falls into two categories. The first category is that in the upper layer, $K_d(490)$ value increases with depth and reaches a single maximum at a certain depth. Deeper than this depth, $K_d(490)$ decreases with depth. As shown in Figure 2a, most stations belong to this type. The other category is that at some stations, $K_d(490)$ shows

maximums at several different depths. Figure 2b shows that several maximums appear at the station 9906.

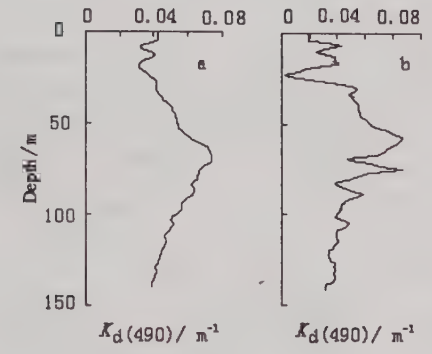

Fig. 2 Vertical distribution of $K_d(490)$ at the station 9910(a) and the station 9906(b)

By comparing the vertical distribution of $K_L(490)$ with $K_d(490)$ at the same station, we have found that they are coincident: in the upper layer, $K_L(490)$ and $K_d(490)$ both increase with depth; at a certain depth(Z_{max}), $K_L(490)$ and $K_d(490)$ almost reach the maximum at the same time; deeper than that depth(Z_{max}), $K_L(490)$ and $K_d(490)$ decrease as the depth increases. However, in the upper layer which is shallower than (Z_{max}), $K_L(490)$ is slightly larger than $K_d(490)$; in the lower layer which is deeper than (Z_{max}), $K_L(490)$ is slightly smaller than $K_d(490)$. Figure 3 shows the relationship between $K_L(490)$ and $K_d(490)$ at the station 9918. According to the obtained spectrum data, a similar phenomenon is also observed at other stations with depths > 70 m.

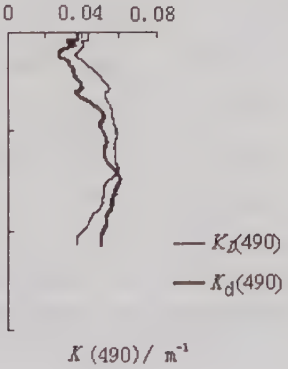

Fig. 3 Vertical distribution of $K_L(490)$ and $K_d(490)$ at the station 9918

Further analysis reveals that at the same station, K_L and K_d of bands 412 nm and 443 nm with wavelength shorter than 490 nm also have the similar relationship. It is even more intensive. While among those bands with wavelength longer than 490 nm, such a kind of relationship tends to recede, and

even to disappear when wavelengths increase. Figure 4 shows such a trend very clearly. In order to quantitatively analyze changes of diffusion attenuation coefficient at different stations, we have averaged values of $K_d(490)$ in different water layers. Results are listed in Table 1.

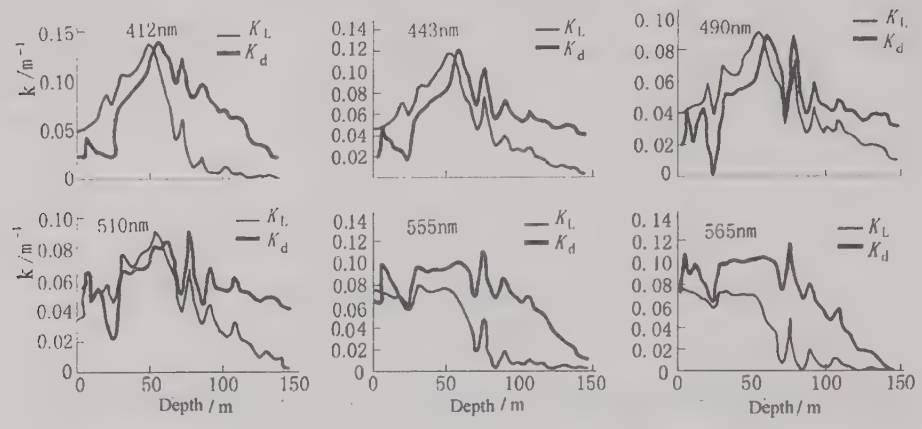

Fig. 4 Vertical distribution of K_L and K_d of some wave bands at the station 9906

Examining average values of $K_d(490)$ in Table 1, we find that in the upper layer (0 ~ 30 m) and the water layer deeper than 100 m, $K_d(490)$ is relatively small. The maximal values of $K_d(490)$ are located at the depth 50 ~ 75 m.

Tab. 1 Average $K_d(490)$ (m^{-1}) of different layers in the water column at some stations near Nansha Islands

	station	9906b	9907nb	9910d	9911b	9912b	9915b	9918b	9938b	9939b	9953b	9953e
	0 ~ 30 m	0.028	0.036	0.038	0.031	0.026	0.034	0.035	0.041	0.036	0.041	0.033
	30 ~ 50 m	0.055	0.047	0.048	0.047	0.047	0.055	0.046	0.061	0.056	0.044	0.038
D	50 ~ 75 m	0.061	0.076	0.066	0.055	0.067	0.062	0.054	0.056	0.061	0.051	0.059
	75 ~ 100 m	0.051	0.054	0.061	0.055	0.050	0.053	0.055	0.050	0.049	0.056	0.058
	>100 m*	0.038	0.040	0.043	0.042	0.040	0.040	0.050	0.046	0.047	0.039	0.043

Note: *Field survey depths (D) at the above stations are different, with the maximum depth being 150 m and the minimum depth being 109 m. Thus, thickness of the layer deeper than 100 m would be different.

2.2 Profile $K_d(490)$ and Profile Chlorophyll a content ($C_{chl.a}$)

The very clear seawater near Nansha Islands is very similar to the oceanic class I water in the optical classification. Water color factors affecting characteristic of class I water are primarily *chlorophyll a* and its biodegradation product — *yellow substance*. The above vertical distribution pattern of $K_d(490)$ in this area is closely related to the differential distribution of $C_{chl.a}$ at different depths. Takahashi *et al.*[5] pointed out that the maximum value of $C_{chl.a}$ exists at the subsurface layer

and the measured value of 50 m layer accounts for about 55 % of the total in the whole water column in North-West Pacific and South China Sea. Huang Liangmin also indicated that the content of *chlorophyll a* is highest at 50 ~ 75 m layer and its vertical distribution exhibits a single maximum pattern. Same features of *chlorophyll a* are found at stations in our cruise. Figure 5 shows the distribution of $C_{chl.a}$ at some stations. We can see that the shape of the vertical distribution of $C_{chl.a}$ is congruous with that of $K_d(490)$. Both of $C_{chl.a}$ and $K_d(490)$ reach their maximum values at the 50 ~ 75 m layer. This indicates they are positively correlated to each other.

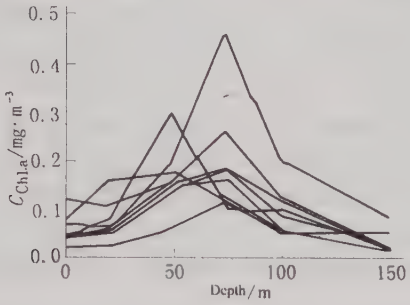

Fig. 5 Vertical distribution of Chl.a of this cruise

After integrating $K_d(490)$ and $C_{chl.a}$ individually vs. depth (down from surface, accumulating values layer by layer) at the station 9910, we have obtained two new series of data. The results after performing regression analysis on these two data sets reveal that the correlation between $K_d(490)$ and $C_{chl.a}$ is very good ($R^2 = 0.9875$), as shown in Figure 6.

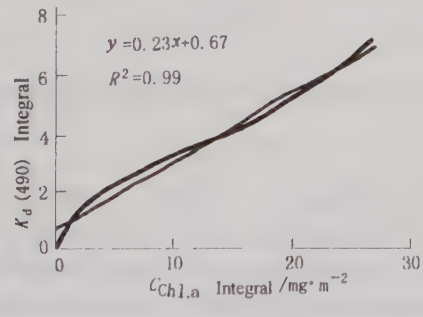

Fig. 6 Linear relationship between integrals of $K_d(490)$ and $C_{chl.a}$ to depth at the station 9910

By linearly fitting $K_d(490)$ and $C_{chl.a}$ at all depths at the same station, a correlative equation is created as the following:

$$y = 0.23\,x + 0.03 \qquad (R^2 = 0.90 \quad x = C_{chl.a};\ y = K_d(490)) \tag{1}$$

Its correlative curve is shown as Figure 7a. As observed, $K_d(490)$ and $C_{chl.a}$ can be fitted quite well. As shown in Figure 7a, the curve is comprised of two clearly separated curve segments. Considering

vertical segmented patterns of the factors at the station 9910 (as Figure 8), we divide the water column into the upper and lower layers at the depth where the maximum $K_d(490)$ occurrs, and then $K_d(490)$ is linearly fitted to $C_{chl.a}$ in the two layers separately. Results are as the following:

$$y = 0.89\,x + 0.03 \quad \text{upper} \quad (R^2 = 0.94) \tag{2}$$

$$y = 0.12\,x + 0.03 \quad \text{lower} \quad (R^2 = 0.95) \tag{3}$$

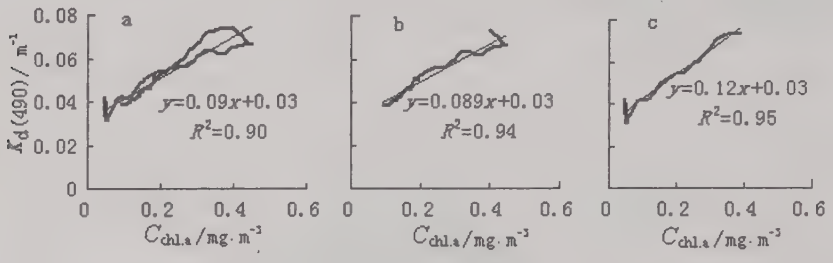

Fig. 7 Linear fitting relation between Chl.a concentration and $K_d(490)$ at the station 9910

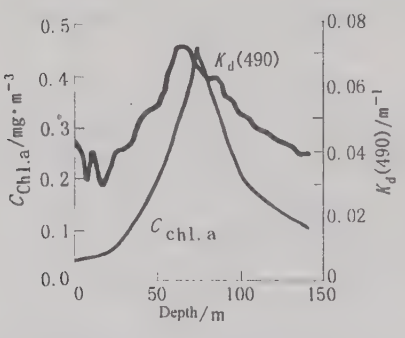

Fig. 8 Vertical distribution of $K_d(490)$ and $C_{chl.a}$ at the station 9910

The fitness curves are shown in Figure 7. It is very clear that the linear fitting relation between $K_d(490)$ and $C_{chl.a}$ is increased ($R2$ increases from 0.90 to 0.94 and 0.95, respectively). During Cruise 9904 there were totally 8 stations where $C_{chl.a}$ data and spectrum data were obtained at the same time. The linear fitting relation of $C_{chl.a}$ and $K_d(490)$ at the other 7 stations are listed in Table 2.

Tab. 2 Linear relation between integrals of $C_{chl.a}$ and $K_d(490)$ of some stations of 9904 Cruise

Station	Linear fitting equations between $C_{chl.a}$ and $K_d(490)$	Station	Linear fitting equations between $C_{chl.a}$ and $K_d(490)$
9906	$y = 1.2445\,x - 0.3401$ ($R^2 = 0.9919$)	9940	$y = 3.3683\,x - 0.4809$ ($R^2 = 0.9935$)
9912	$y = 1.9947\,x + 0.4884$ ($R^2 = 0.9826$)	9942	$y = 1.9362\,x - 0.2275$ ($R^2 = 0.9924$)
9915	$y = 2.8265\,x - 0.6251$ ($R^2 = 0.993$)	9953	$y = 2.9992\,x - 0.0202$ ($R^2 = 0.9982$)
9916	$y = 3.164\,x + 0.6659$ ($R^2 = 0.9718$)	Note: x = integral of $K_d(490)$; y = integral of $C_{chl.a}$	

2.3 K_d(490) and stratification effects of seawater in Nansha Islands

Because phytoplankton photosynthesis occurs only in the euphotic zone and the optical characteristics of seawater which can be detected by underwater optic instruments are limited to this layer, here analysis of stratification effects is limited to the upper layer of seawater less than 200 m and mostly focuses on small/tiny-scale structures of seawater stratification.

A stratification phenomenon of seawater in Nansha Islands is relatively obvious. Analyzing seawaters temperature, salinity, density and $C_{chl.a}$ data of many years and of Cruise 9904 in this sea area, we have found that during spring there is a vertical tri-layer structure existing in the water column which is shallower than 200 m around Nansha Islands: the first upper layer just below sea surface is the Evenly-Mixed Layer where physical and chemical properties of seawater are relatively even; under the Evenly-Mixed Layer is the pycnocline where vertical gradients of temperature, salinity and density are relatively sharp; from the pycnocline to the depth of 200 m is the Gradually-Changed Layer where vertical gradients of temperature, salinity and density still exist but are smaller than those within the pycnocline. The field data at each station of Cruise 9904 reveal that depths where the pycnocline occurs are not always the same at different stations. Basic information of the thermoclines at typical stations is listed in Table 3.

Tab. 3 Basic information of thermocline and the depth of maximum K_d(490) at some stations (m)

Station	9906	9907	9910	9912	9915	9918	9938	9940	9939	9953
Depth of upper boundary of pycnocline	23.0	20.0	40.4	9.0	10.3	26.8	17.0	22.2	19.0	49.0
Depth of lower boundary of pycnoocline	43.2	36.9	46.2	49.7	30.6	32.4	29.4	38.7	35.5	67.2
Thickness of pycnocline	19.7	16.9	5.7	40.7	20.3	5.5	12.1	16.5	16.1	17.5
Depth of the first K_d(490) maximum	59.0	56.8	70.0	59.0	51.1	75.4	35.4	47.9	50.6	77.8
Depth of the second K_d(490) maximum	75.5				63.2				59.3	
Distance between the lower boundary of the pycnocline and the first maximum of K_d(490)	15.7	19.9	23.7	9.2	20.4	42.9	6.0	25.6	15.0	10.6

Note: The least gradient of the pycnocline is 0.2℃/m.

The presence of phytoplankton enforces the stratification effect in the water column. Optical characteristics of chlorophyll a, organic particles and yellow substance reflect the stratification properties of seawater, as shown in the profile curves of K_d(490). This can be reflected more clearly by analyzing the average value of K_d(490) at each layer of seawater (Table 1). At each station the average value of K_d(490) appears to reach the maximum in the layer where the maximum chlorophyll *a* occurrs. In other words, there are obviously differences among different layers.

2.4 Relations between K_d(490) together with $C_{chl.a}$ and environmental factors

The above analysis shows that vertical distribution of $C_{chl.a}$ is the major factor that affects the vertical distribution of K_d(490). As many environmental factors affect major phytoplankton pigment, chlorophyll *a*, environmental factors directly affect K_d(490) through the growth effect of phytoplankton.

The vertical distribution pattern of$C_{chl.a}$ indicates that a concentrated zone of phytoplankton exists in

the subsurface layer (50 ~ 75 m) other than in the surface layer. At least three environmental factors have contributed to the vertical distribution of $C_{chl\,a}$.

(1) As discussed before, an Evenly-Mixed Layer exists in surface layer in the sea area around Nansha Islands. Its thickness is 20 ~ 30 m during summer. Under it there is a strong pycnocline. It is the pycnocline that limits upward infiltration or convection of deep seawater with rich nutrients. As shown in Figure 9b, concentrations of nutrients in the Evenly-Mixed Layer are relatively lower than that in the subsurface layer, and hence, the Evenly-Mixed Layer may not be the suitable layer for phytoplankton to grow even though there is full sunlight. In the pycnocline and subsurface layer, with moderate sunshine condition and sufficient supply of nutrients, phytoplankton reach maximum growth. In the bottom of the euphotic zone, growth of phytoplankton is limited by low light condition[4].

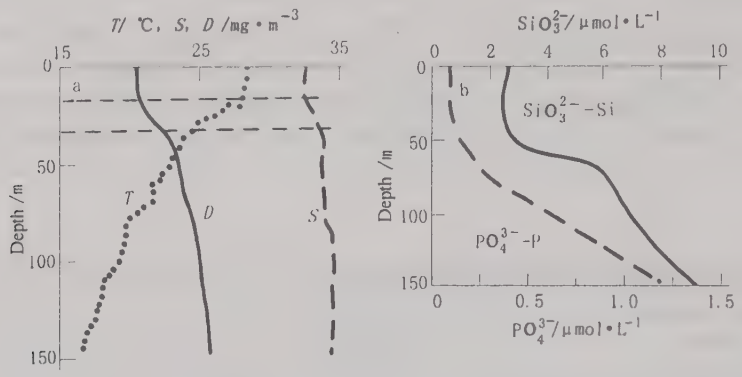

a. Temperature (T), Salinity (S), Density (D) b. Vertical distribution of nutrients[6]

Fig. 9 Vertical distribution of the environmental factors in the Nansha Islands sea area

(2) Phytoplanktons live in a very passive living mode. Smayda[7] found that the sinking rate of phytoplankton cells increases with the cell size in a seawater column with even density. Large phytoplankton cells are hardly to be promoted in this surface mixed layer. In contrast, seawater density starts to increase in the subsurface layer, which allows sinking phytoplankton to accumulate at the pycnocline where nutrients are abundant as well.

After analyzing the stratification characteristics of seawater near Nansha Islands, we have found that the depth, at which maximum value of $C_{chl\,a}$ occurrs, is generally deeper than the lower boundary of the thermocline (refer to Table 3). Some large phytoplankton cells will continue to subside until reaching the depth where the seawater density is equal to its density other than just stopping at the bottom of the pycnocline.

(3) The growth rate of phytoplankton is not only related to the total light energy but also restricted by the intensity of sunshine. Due to the photoinhibition of photosynthesis under strong light, the rate of photosynthesis will decrease in the surface under intensive light. Since the geographic position of Nansha Islands is near the Equator, surface layer of the seawater is under very intensive sunshine and consequently phytoplankton photosynthesis is limited in this layer. Light is attenuated through the surface layer when it reaches the subsurface layer where the rate of photosynthesis increases instead. While in the lowest part of the euphotic zone, sunlight is not adequate enough for photosynthesis and the

growth rate of phytoplankton here is very small.

3 Conclusion

1 In the Nansha Islands sea area the vertical distribution of $K_d(490)$ in the euphotic zone exhibits the maximum value of $K_d(490)$ in the 50 ~ 75 m layer.

2 There is an interesting phenomenon in the profile curve of $K_d(490)$: almost at the same depth both $K_d(490)$ and $K_{l_r}(490)$ reach a peak value; above this depth $K_{l_r}(490)$ is slightly bigger than $K_d(490)$, while beneath this depth $K_{l_r}(490)$ is slightly less than $K_d(490)$. The phenomenon is worth further studying.

3 The vertical distribution of $K_d(490)$ has a strong correlative relation with the vertical distribution of $C_{chl.a}$. $C_{chl.a}$ and $K_d(490)$ could be fitted very well by using a linear equation.

4 The vertical change of $K_d(490)$ is affected by the stratification effect of the seawater in the Nansha Islands sea area.

Acknowledgments

This work was jointly supported by project KZCX2-202 from CAS, the project of 818-06-03 from national 863 program and project 97-926-07 of national special program for science and technology.

References

[1] Austin R W, Petzold T J. Spectral Dependence of the Diffuse Attenuation Coefficient of Light in Ocean Waters. SPIE, Ocean Optics VII, 1984, 489: 168-178.

[2] Zhong Qiying, Fang Yaosheng. Study on Optical Properties of Seawaters in Central Part of Nansha. Research Reports for the Comprehensive Investigation in South China Sea. Beijing: Science Press. 1982, 187-198.

[3] Chen Chuqun, Zhang Qingling. Study on Validation of Radiance of Seawaters in South China Sea. Collection of Reports on Marine Optical Remote Sensing Applications. The second institute of oceanography, SOA. 2000, 1-18.

[4] Smith R C, Baker K S. The Bio-optical State of Ocean Waters and Remote Sensing. Limnology and Oceanography, 1978, 19: 1-12.

[5] Takahashi M, Hori Y. Abundance of Picopgytoplankton in the Subtropical and Tropical Waters, Marine Biology, 1984, 79(2): 177-186.

[6] Huang Liangmin. Preliminary Study on the Distribution of Primary Productivity and Photosynthesis Pigments in the Sea Areas around Nansha Islands. Collection Works on Marine Biology of Sea Areas around Nansha Islands and its Adjacent Areas. Beijing: Ocean Press. 1991, 34-49.

[7] Man K H. Ecology of Coastal Waters. Beijing: Ocean Press. 1989.

Research on the Evaluation of Marine Environmental Quality by Using the GIS Technology

Wang Lihua (王立华), Li Jilong (李继龙), Ge Changshui (葛常水), Li Xiaoshu (李小恕), Jia Jing (贾　静), Huang Qiquan (黄其泉)
Chinese Academy of Fisheries Sciences, Beijing 100039, *China*

Abstract Based on the biological resources surveys in China's exclusive economic zone, the paper discusses the application of the GIS technology in evaluating the marine environmental quality, establishes the basic concept and technological process for evaluating the environmental quality of the habitats of marine living resources, proposes the key points for the establishment of the relevant evaluation attributes database by applying the GIS technology and analyses several typical evaluation models and the data interpolation method for the model in GIS. Results show that the combination of the GIS technology with the quantitative evaluation model can be applied to the fast and accurate evaluation of the marine environmental quality.

Keywords GIS technology; marine biological environment; environmental quality evaluation; database

Ecological environment is closely linked with the biological resources in the ocean. The marine hydrological changes are closely related to the migration and movement of marine life. The chemical elements of seawater are the material base for marine life and phytoplankton, zooplankton and benthos constitute the basic links in the food web of ecosystem. Primary productivity which represents the ability of sea area to produce organic matter is an important parameter for evaluating the biological production level of the sea area and the environment is of great significance to the survival and development of marine living resources[1~5]. The Geographic Information System, as a product of the combination of traditional sciences (geography, cartography and surveying) with modern science and technology (computer science, *etc.*), is gradually evolving into an integrated modern discipline for processing spatial information[6]. GIS is an effective managing tool for the geographical information resource, and its powerful databases and ability of spatial analysis have found more and more applications in the fields of marine resource and environment as well as in the marine fishery research[7~11]. Taking the biological resource area of China's excusive economic zone for example and with the GIS as the supporting tool software, the paper establishes the basic environmental database for the study area, discusses the GIS method and the mathematical model accomplished for the evaluation of marine environmental quality and makes a comprehensive evaluation and quantitative analysis of the water quality, pollution, nutritional status of the studied waters, thus providing scientific basis for analyzing the quality of the living environment of marine biological resources in China.

1 Materials and methods

Received on December 18, 2003

1.1 Preparation and pre-treatment of data

The data for this study come from the biological resource survey in China's special marine survey projects with a time span of 1998 — 2000. Located at 4.5° N ~ 41° N, 107° E ~ 128° E, the survey area covers China's Bohai Sea, Huanghai Sea, East China Sea and South China Sea, East China Sea and South China Sea, totaling 1 280 station sites. The data items extracted include dissolved oxygen, phosphate, nitrate, amino nitrogen, chlorophyll, phytoplankton, zooplankton, benthos, *etc.*.

Data processing: The data are screened by seasons so as to gain consistency in time. For more than two surveys in the same station site within the same season, the means of their data are counted and calculated. The data dimensions are unified, the erroneous station sites are removed and the erroneous data are checked. Longitude and latitude are added into the fields which represent the spatial characteristics of geographical elements according to the station locations so that the data may be directly reflected in the geographical distribution, and, in the meantime, an appropriate relationship is kept with the spatial data and other attribute data of the basic background data.

Preparation of spatial data: The basic geographic electronic maps officially published by the state are adopted, including the lines of administrative zones, continental coastlines of waters, insular coastlines, rivers and water systems, isobaths of sea areas, *etc.*. The mode of projection is Mercator projection and the coordinate system parameters are the projection method, ellipsoid, central meridian line, and transverse shift, adopting Mercator, WGS-84, 117° and 500 km, respectively.

1.2 Research methods and steps

This study adopts the integrated index methods such as the nutritional status quality method[4], the integrated index method for organic pollution[2], the "Seawater Quality Standards of the People's Republic of China" (GB 3097-1997), and models for evaluating the level of bait organisms and the primary productivity[5] to evaluate the sea area biological environmental quality. As the environmental quality index method is characterized by comprehensiveness and generality, being concise and to the point, the objective, quantitative and dimensionless evaluation results and the strong scientific nature and operability in treatment by using GIS, these index method evaluation models may be used in the analysis and application of GIS and the strong ability of the GIS in the database technology and spatial analysis is utilized to analyses the spatial distribution characteristics of the evaluated indicators to generate the qualitative and quantitative analytical results which combine the point and plane, charts and graphs.

The research methods and steps are as follows: (1) The relevant survey data items are extracted. For macroscopic evaluation, the whole surveyed sea area is sampled and the data of the same season are extracted; while for a local area, the data are extracted by the survey cruise so that the data may better reflect the consistency in space and time; (2) Based on the survey station sites, the whole sea area is divided into several basic evaluation units fit for the area's macroscopic and quantitative evaluation, which are in essence the geographic units and are manifested in the basic cartographic units; (3) The environment is factorized to extract the evaluation model and determine the main influential indexes of various factors as the fundamental basis for data analysis; (4) The basic databases for evaluation are established by using GIS and the model calculation is carried out; (5) The spatial interpolation analysis is carried out with the GIS, the coordinate system projection transformation is made for the results of interpolation and the results of evaluation are output so as to realize qualitative and quantitative analysis and evaluation of the biological environmental quality; (6) The GIS, basic evaluation databases and evaluation models are integrated to accomplish the rapid application of the evaluation methods.

The process is as follows:

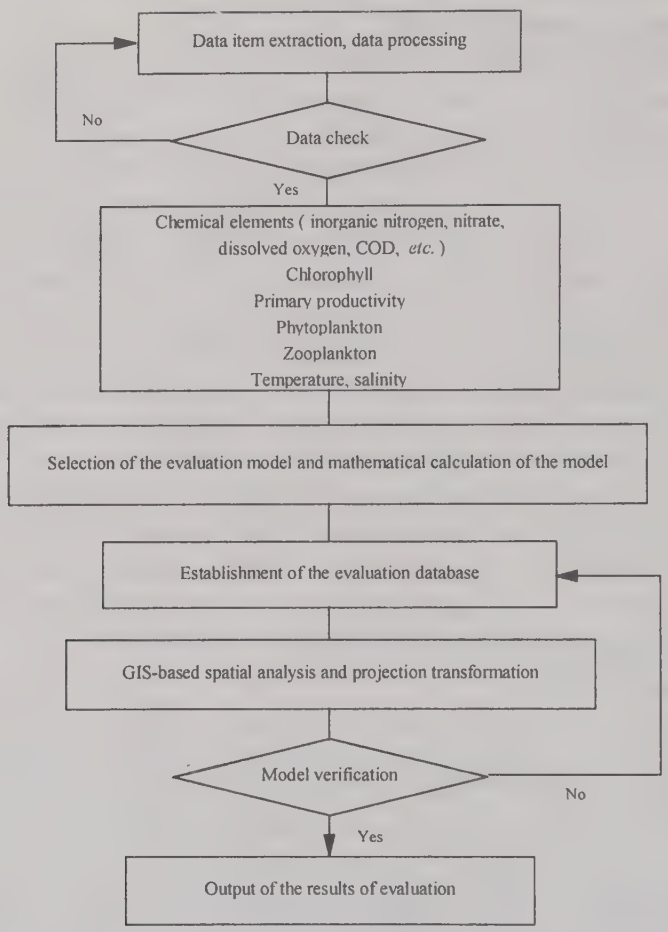

Fig. 1 Flow diagram of GIS-aided water quality evaluation

1.3 Establishment of evaluation databases

The treatment of the evaluation model is divided into two parts. First, the algorithm routine is established according to the model for integrated factor evaluation and the evaluation value of each station site is calculated. Then, the interpolation operation is performed for the values of the known sites and the results of evaluation are treated by using the mathematical model of geographical statistics so that the distribution of points is transformed into the greyscale numerical distribution of plane so as to output the analytical results of evaluation.

Spatial attribute should be assigned to each point, which can be realized by establishing the attribute database. The fields for the spatial characteristics of geographical elements should be established and assignments should be made according to the longitude and latitude of the survey station sites so that the data may be directly reflected in the geographic distribution. The attribute database is evaluated, the major key of the database is the station number and each station site should have the corresponding coordinate field of longitude and latitude. The evaluation field is established to keep various results of evaluation and the evaluation value for each station site is stored in the database.

The attribute database is the data format supported by the GIS to facilitate access and call by the

GIS. This study adopts Arcview as the basic GIS software. VFOX is used to develop the programming module for mode calculation and compute the analytical results, which are stored in the DBF evaluation attribute database. In the GIS system, the evaluation database is loaded in the form of Add Event Theme, which is transformed into the vector theme for use in the spatial analysis of the interpolation.

The evaluation map adopts the grid data structure with grid as unit. The grey scale of each grid is calculated by interpolation operation and the hierarchical threshhold is designed to obtain the results of evaluation in spatial distribution. As the earth is an ellipsoid while the grid images for evaluation take longitude and latitude as units, it is necessary to redefine the coordinate system and carry out equivalent projection transformation. Only by so doing is it possible to accurately count the area, output the statistical charts for the proportion it occupies and get the quantitative results of analysis for the area at the evaluation level.

1.4 Selection, analysis and comparison of the processing algorithm for the spatial data in the GIS

This study makes an analysis and comparison of the spatial interpolation technologies of environmental factors in the light of the spatial variability of marine environmental factors so as to pick out an appropriate interpolation algorithm to process the results of evaluation, minimize the distortion factor of the greyscale value distribution in the output plane and define the interpolation method which fits better.

1.4.1 Introduction to the common interpolation methods

Inverse Distance Weighted Interpolation (IDW): IDW is based on the concept that the farther is the distance, the smaller is the influence on the estimated point and that the weighted value also varies with distance. Interpolation is carried out with the inverse distance power as weight. Therefore, the value of the estimated point F(x, y) is often fitted by the linear weighting of several nearby points as shown in Formula (1). In the DIW weighted method, the influence weighted value of each observation point is expressed by the formula (2).

$$f(x,y)=\sum_{i=1}^{n} w_i f_i \tag{1}$$

$$w_i=\frac{h_i^{-p}}{\sum_{j=1}^{n} h_j^{-p}} \tag{2}$$

$$h_i=\sqrt{(x-x_i)^2+(y-y_i)^2} \tag{3}$$

Where n is the number of observation points within the influence radius; f_i, the value of the observation point; w_i, the weight function; h_i, the distance between the ith observation point and the estimated point; the exponent p, the weight parameter, which is used to control the velocity of the weighted value varying with the distance. When the exponent increases, the weighted value of the observation point which is farther away would decrease.

Spine interpolation: Approximating fully the various observation points with the minimum plane of curvature like a curved rubber sheet passing through all the observation points while making the surface curvature the least. In theory, interpolating estimation may be made by using the higher polynomial to obtain the higher smoothing results. But in the actual research, the second-order polynomial estimated value is often used and its corresponding value is:

$$F(p)=\sum_{i=1}^{n} c_i\left|p-p_i\right|^3+a+b\cdot x+c\cdot y$$

Where, p is the point to be obtained; p_i, the point with the known elevation value. The values of

the coefficients c_i and a, b, c are solved by a linear equation group.

Kriging algorithm: Kriging is a calculation method for optimal prediction, an interpolation algorithm which predicts the values of unknown points from the known sites. Representing the spatial variations and distribution in the form of the variables map, it is one of the methods in the GIS used to calculate the isoclines and equivalent planes[12]. Its determination of the weight of each observation point is obtained from analysis of the semi-variance map, and, based on the requirement for the optimal estimation algorithm, and by using the principle of Lagrange minimization, the relationship between the weight value W and the semi-variance $\tilde{r}$ is proposed[13].

$$\sum_{i=1}^{n} W_j \tilde{r}_{ij} + \mu = \tilde{r}_{i0} \qquad 1 \le i \le n \qquad \text{in which:} \quad \sum_{j=1}^{n} W_j = 1$$

Where, μ is the Lagrangian. After the coefficient of each weight is obtained, the analytical value for the nth point to be interpolated for the evaluated area.

1.4.2 Comparison of interpolation methods

By applying the above-mentioned methods, the results of interpolation are compared and analyzed so as to define the better fitted interpolation method. Specifically, part of the observation value v_i is compared with the divided difference MR or the mean-square deviation MSR of its corresponding fit value $\hat{v}_i$.

$$MR = \frac{1}{n}\sum_{i=1}^{n}(v_i - \hat{v}_i) \qquad MSR = \frac{1}{n}\sum_{i=1}^{n}(v_i - \hat{v}_i)^2$$

Samples of four environmental factors, *i.e.*, phosphate, nitrate, temperature and salinity, are chosen.

Tab. 1 Comparison of three methods of interpolation

Interpolation	Theoretical model	Environmental elements	MR	MSR
Kriging	Linear model	t (℃)	0.813	1.003
		S	0.440	0.540
		Phosphate (μ mol/L)	0.027	0.031 5
		Nitrate (μ mol/L)	1.103	2.256 8
	Exponential model	t (℃)	0.778	0.930
		S	0.383	0.478
		Phosphate (μ mol/L)	0.026 4	0.030 8
		Nitrate (μ mol/L)	1.112 7	2.257 1
	Globular model	t (℃)	0.812	0.956
		S	0.441	0.569
		Phosphate (μ mol/L)	0.025 4	0.029 5
		Nitrate (μ mol/L)	0.914 1	1.436 6
	Universal linearity	t (℃)	0.814	1.005
		S	0.444	0.324
		Phosphate (μ mol/L)	0.026	0.035
		Nitrate (μ mol/L)	0.970	1.621
IDW	Index is one	t (℃)	0.948	1.386
		S	0.418	0.498
		Phosphate (μ mol/L)	0.025 9	0.030 9
		Nitrate (μ mol/L)	1.085 6	2.159 8
Spline	Second-order	t (℃)	0.917	1.774
		S	0.448	0.616
		Phosphate (μ mol/L)	0.034 3	0.044 6
		Nitrate (μ mol/L)	0.876 8	1.323 8

There are 21 sampling points of data and their ranges are respectively: phosphate: 0.061 ~ 0.179 μ mol/L; nitrate: 2.13 ~ 5.13 μ mol/L; temperature t 9.7 ℃~ 25.6 ℃; and salinity S: 28.67 ~ 34.56.

The above-mentioned analytical results indicate that the exponential model of Kriging fits better with temperature and salinity, and that the globular model of Kriging and Spline fit better with the data of nutrient salts. Generally, the universal linear model of Kriging has the best mean fit for the environmental elements measured.

2 Results and discussion

The above-mentioned flow is used to process the integrated evaluation model for the integrated index of organic pollution and trophic status quality and the spatial interpolation algorithm adopts the Kriging interpolation method. The model is Universal Linear; the radius of the data interpolation, 12~15; and the range, the sea area to be evaluated. Statistical calculation of the area: The areas of different grey scale sections are read after the equivalent projection transformation is made by using the coordinate system. The projection mode is Lambert Equal-area Azimuthal, Ellipsoid: sphere, central meridian line: 115° ; Reference latitudinal line: 30° ; The results obtained in the GIS are shown in Figs. 2 and 3.

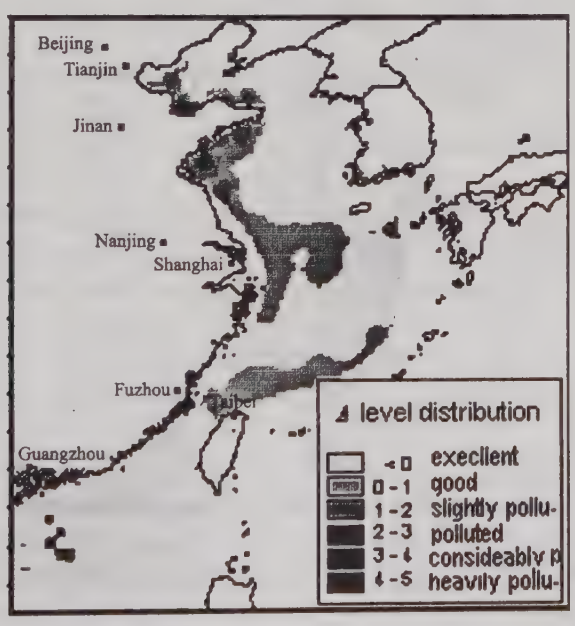

Fig. 2 Map of A levels of seawater assessment results during spring of 1998

Fig. 2 reflects the distribution of A levels of organic pollution indexes of seawater in the Bohai Sea, Huanghai Sea, East China Sea and South China Sea during spring of 1998. It can be seen from the figure that the pollution index in the coastal areas of Bohai Sea, Huanghai Sea and East China Sea is higher than that in the off-sea area of the same latitude, and especially in the inlet of the Huanghe River into the sea, Leizhou Bay and off-sea of Qingdao, the A levels have increased significantly. Near the inlet of the Changjiang River into the sea and the north of Bohai Sea, as the survey stations are farther away and no

data are available for the coastal area, the assessment map fails to reflect the pollution condition in the coastal area, but a water tongue area with higher A levels due to the effect of the Changjiang River water may be clearly identified. Generally speaking, the organic pollution indexes in China's four sea areas of the South China Sea, Huanghai Sea, East China Sea and Bohai Sea are between < 0 and $0 \sim 1$ and the seawater quality is basically good (Tab. 2).

Tab. 2 Comparison of graded areas of organic pollution index A levels

A level	Water quality assessment	Area	Proportion
1 ~ 2	Beginning to be polluted	24 602.10	1.05
2 ~ 3	Light pollution	6 742.36	0.28
3 ~ 4	Medium pollution	2 425.30	0.10
4 ~ 5	Heavy pollution	1 712.54	0.07

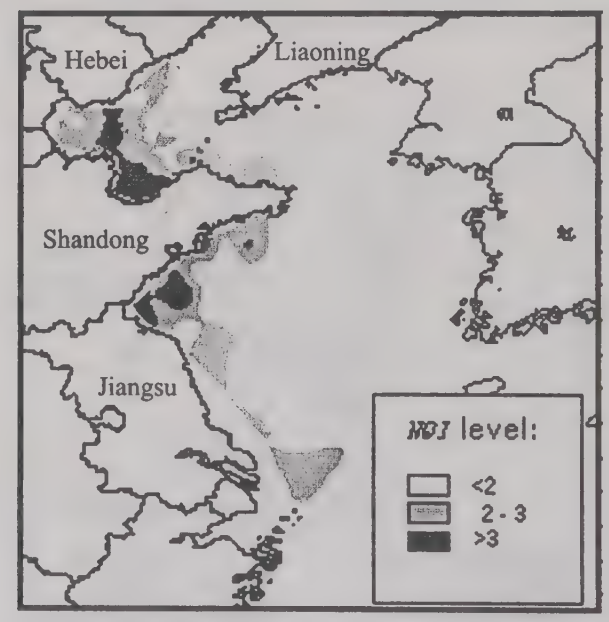

Fig. 3 Map of NQI levels of seawater assessment result during spring of 1998

Fig. 3 indicates that according to the analysis by the NQI method, the sea area with NQI > 3 is under the condition of eutrophication and is mainly distributed in the inlet of Huanghe River into the sea, Leizhou Bay and off-sea of Qingdao. This shows that this sea area begins to be subjected to organic pollution in spring, which accords with the distribution of A levels of organic pollution index. This also indicates that, in the low flow season of spring, the smaller diluting action of the terrigenous water, the delayed dilution and diffusion of nutrients and COD matter after they enter the sea and the poor exchange capability of seawater in spring are also the reason why the water begins to be subjected to organic pollution and seawater eutrophication takes place in spring. The area of the eutrophicated waters calculated in the GIS through equivalent projection transformation is 16 282.17 km^2.

3 Concluding remarks

Analysis is made of the seawater quality in the study areas of China in spring by the above-mentioned evaluation methods. The water quality of the most waters of the South China Sea is good, belonging to the water quality Class 1—2 and that of the Taiwan Straits and its northern waters belongs to Class 3. The pollution indexes in the near shore areas of the Bohai Sea, Huanghai Sea and East China Sea are higher than in the off-sea area of the same latitudes, but the water quality of the off-sea area is good. The local sea area in the Bohai Sea in the inlet of the Huanghe River into the sea and in the Huanghai Sea near the coast are slightly polluted or partly under the condition of eutrophication. But, viewed as a whole, the organic pollution index level is between < 0 and $0-1$ in the four sea areas of China, *i.e.*, the South China Sea, Huanghai Sea, East China Sea and Bohai Sea and the seawater quality of approximately 98.5 % of the study area is basically good.

References

[1] Lin Ronggen. Preliminary Analysis of Assessment Methods for Seawater Eutrophication Levels. Marine Environmental Science, 1996, 15(2): 28-31.

[2] Tian Jiayi, Dong Jingyue. Initial Investigation and Research on the Organic Pollution and Red-tide Organisms in the Sea Area around the Huanghe River Mouth. Marine Environmental Science, 183, 2(1): 46-53.

[3] Zou Jingzhong, Dong Liping, Qin Baoping. Preliminary Discussion on Eutrophication and Red Tides in the Bohai Bay. Marine Environmental Science, 1983, 2(2): 41-55.

[4] Zhang Shuijin, Yang Qingquan, Qiu Huihuang *et al.*. Red Tides and the Countermeasures for Preventing and Controlling Them. Beijing: China Ocean Press, 1994, 211-215.

[5] Jia Xiaoping, Li Chunhou. Integrated Assessment of the Ecological Quality of China's Marine Fishery. Proceedings of the National Marine Special Survey[C]. Beijing: China Ocean Press , 2002, 368-375.

[6] Chen Shupeng, Lu Xuejun, Zhou Chenghu. Introduction to the Geographic Information System. Beijing: Science Press, 2000.

[7] Jeffries-Harries T. GIS Make Inroads into UK Marine Environment. GIS Europe, 1992, 1(8): 36-38.

[8] Green D R, Stockdale A. GIS and Marine Resource Management: A Vocational Approach. In Proceedings of EGIS93. Genoa, Italy: EGIS Foundation, 1993. 1 387-1 396.

[9] Impson J. Remote Sensing and Geographical Information Systems: Their Past, Present and Future Use in Global Marine Fisheries. Fisheries Oceanography, 1992, 1(3): 238-280.

[10] Fang Yinxia. Application of the Geographical Information System in the Marine Fields. Marine Science Bulletin, 2000, 19(3):85-89.

[11] Su Fenzhen, Zhou Chenghu, Shao Quanqin *et al.*. Development, Application and Prospects of Marine Fishery Geographical Information System. Aquatic Products Journal, 2002, 26(2): 169-174.

[12] Oliver M A, Webster R. Kriging: A Method of Interpolation for Geographical Information System. Geographical Information Systems, 1990, 4(3), 313-332.

[13] Isaaks H, Mohan Srivastava R. An Introduction to Applied Geostatistics. London: Oxford University Press, 1989.

Laboratory Simulation on Phosphorus Releasing near the Water/ Sediment Interface in the East China Sea off the Changjiang Estuary

Zheng Libo[1] (郑丽波), Zhou Huaiyang[2] (周怀阳), Ye Ying[3] (叶 瑛)

1 *Geographical Department, East China Normal University, Shanghai* 200062, *China*;

2 *Second Institute of Oceanography, SOA, Hangzhou* 310012, *Zhejiang, China*

3 *Department of Earth Sciences, Zhejiang University, Hangzhou* 310027, *Zhejiang, China*

Abstract Surface sediment samples taken from the East China Sea off the Changjiang estuary are used as raw materials for phosphorus releasing experiment. It is found that after being thoroughly mixed with seawater for about 10 minutes, phosphorus released from the sediments reaches its maximum value. Adsorption kinetics can be fitted with both Elovich equation and two-constant rate equation. The releasing amount is closely related to the composition of the sediments. Phosphorus release from silty and muddy sediment is higher than from that dominated by sandy composition. For the desorption reaction, iron-phosphorus (Fe-P) is the most active one, with a releasing ratio higher than other phosphorus forms, followed by absorbed-phosphorus (Ad-P) and organic bound phosphorus (OP). All of them can be referred to as bio-available phosphorus. The results demonstrate that phosphorus in sediments can be released into seawater under suitable hydrodynamic conditions, and have a great impact on the nutrition state and primary productivity of marine biosphere.

Keywords off Changjiang estuary, East China Sea, sediments, phosphorus release, simulating experiment

Introduction

The factors affecting phosphorus transportation at the water/sediment interface include the chemical -physical conditions of the sedimentary environment, sediment composition and hydro-dynamic conditions[1~4]. Previous studies on phosphorus release and adsorption occurring at the water/sediment interface consider mostly the change of environmental factor. Daqing Yin *et al.*. studied phosphorus release of the sediments taken from the Wuli Lake through altering the environmental factor[5]. Hong Chen *et al.* emphasized the influence of environmental factors like temperature, dissolved oxygen, pH, *etc.*. on phosphorus release of the sediments from the South Lake[6]. This study designs the experiment of phosphorus release of surface sediment samples collected from the East China Sea off the Changjiang estuary by the Second Institute of Oceanography on Oct. 1997 and May 1998, respectively, in a mimic marine environment. The experiment stresses the influence of hydro-dynamic conditions and the characteristic of the sediments (e.g. physical composition and different forms of phosphorus) on phosphorus release.

2 Sample and method

2.1 Sample

Received on October 29, 2003

Sediments have been collected by the multi-corer device (diameter of 7.1 cm) from four areas in the East China Sea, *i.e.*, A1 (32° N, 122.5° E, 20 m water depth), B5 (31.5° N, 124° E, 41 m water depth), C1 (31.5° N, 122.5° E, 21 m water depth), and Meso (30.84° N, 122.61° E, 18 m water depth). Sediments are dried at 60 ℃ and their particle compositions are indicated in Table 1. The salinity of the man-made seawater is 35 per thousand, and the pH is adjusted to 8.0 by NaOH.

Tab. 1 Composition of the sediment

Site	Composition of the sediment (%)		
	Sand	Silt	Mud
A1	65.98	22.17	11.85
B5	94.05	4.36	1.59
C1	15.15	54.01	30.84
Meso	1.72	60.75	37.53

2.2 Method

Ten grams of sediment sample is weighted into jars, each containing 5 L man-made seawater. The jars are capped with stopples and shaken for 10 minutes, then leave them at rest. Sampling is carried out at selected time intervals (as shown in Tab. 2). Each solution of 5 mL is sampled at five layers, which results in 25 mL in total. The combined solution is diluted to 50 mL, which is then divided into two parts. Only the mixed reagent, not the ascorbic acid, is added to one of the colorimetric tubes to measure the turbidity. Sample absorbances and P concentrations are determined using a Shimadzu UV-1202 Spectrophotometer with 5 cm cell.

Solid particles are filtrated through the 0.45 μm fiber and dried at 600 ℃. Then, these 4 solid residues and their corresponding 4 original sediment samples are ground, passing through 200 meshes, and analyzed for total phosphorus as well as its different forms. The method can be found in the reference [7].

3 Results and discussion

3.1 Relationship between phosphorus release and particle size composition

The experiment is designed to mimic marine environment in the study area, with emphasis on physical release and chemical release. As shown in Tables 2, 3, the amount of phosphorus released from the sediments in the study area is quite large, especially those consisting mainly of silty and muddy components like Meso and C1which reach up to 62 μg/g. As to the coarse sediment at B5, phosphorus release is insignificant and below the detection limit (0.02 μmol/L in solution). The maximum quantity of phosphorus release is negatively correlated with the sand content of the sediments (R^2 = 0.8457), but positively with the silt and mud content (R^2 = 0.8012). As shown in Tab. 1, the sand contents of these 4 sediments are in the order of B5>A1>C1>Meso. Sediment at B5 is mainly composed of sand, that at A1 is sand-silt, and those at C1 and Meso are silt-mud (Tab. 1). Generally, phosphorus in fine-grained sediments is higher than in coarse sediments. On the other hand, the mechanisms of phosphorus release in the experiment are mainly phosphorus diffusion through concentration difference, which is caused by the difference in the physical-chemical characteristics of sediments and water. Therefore, the smaller the

sediment size, the larger the surface of the sediments per unit weight. As a result, the contact of sediments with seawater will be more fully, and the possibility of phosphorus exchange would be greater, which results in a greater amount of phosphorus release.

Tab. 2 Variation of phosphorus release with time

t / h	P / ($\times 10^{-6}$)			
	A1	B5	C1	Meso
0.10	22.58	2.88	47.93	36.64
0.25	19.81	3.19	60.25	64.36
0.42	9.65	1.65	43.83	37.67
0.75	7.5	2.11	26.89	26.38
1.25	6.88	1.95	18.58	21.66
2.25	7.8	1.34	14.58	16.42
3.25	6.73	1.34	14.89	17.96
4.25	8.11	1.8	13.65	13.65
6.25	6.26	1.49	13.04	13.65
8.25	5.8	1.34	12.11	12.73
11.25	6.11	1.34	12.11	11.5
23.25	4.57	1.34	11.81	10.57
24.25	4.57	1.34	11.65	10.73

Tab. 3 Changes of phosphorus forms after the phosphorus releasing experiment

Site	TP / ($\times 10^{-6}$)	P released /(%)	OP / ($\times 10^{-6}$)	P released /(%)	Ad-P / ($\times 10^{-6}$)	P released /(%)	Fe-P / ($\times 10^{-6}$)	P released /(%)	Ca-P / ($\times 10^{-6}$)	P released /(%)	De-P / ($\times 10^{-6}$)	P released /(%)
A1	502.4		74.08		9.81		31.12		25.79		361.6	
		1.6		4.5		4.9		20.3		1.4		-----
A1	494.3		70.79		9.33		24.8		25.44		364.9	
C1	462.0		74.56		16.05		46.68		25.02		299.7	
		4.7		9.9		13.6		35.9		0.4		-----
C1	440.3		67.19		19.78		29.93		24.92		304.4	
Meso	558.8		92.47		11.02		70.6		37.32		347.5	
		4.9		10.2		20.0		26.1		10.0		------
Meso	531.6		83.08		8.82		52.16		33.59		354.0	

Notes: A1, B5, C1 and Meso represent the original sediments, and A1, B5, C1 and Meso represent the sediments after the experiment.

3.2 Change of phosphorus forms after the phosphorus releasing experiment

As shown in Tab. 3, Fe-P, OP and Ad-P can be released from the sediments, especially Fe-P with a maximum value of 35 % , and they tend to transform into detritus-phosphorus (De-P). The change of total phosphorus (TP) is a bit higher than the quantity of phosphorus released . Its because that part of phosphorus is released from the sediments again during the process of filtration. It is shown that OP and calcium-phosphorus (Ca-P) change significantly at B5, probably it's because the shell content of the

sediments is higher at B5, and the large shell is picked out when the sediments are ground after the experiment. Therefore, the content of OP and Ca-P changes a lot, and so does the content of TP. In view of the content change of Fe-P and Ad-P, it corresponds to the phosphorus release very well. In general, the change of phosphorus forms and the quantity of phosphorus released into water is in accord with the mass balance principle.

Our results demonstrate that Fe-P, OP and Ad-P can be released from the sediments to seawater, and these three phosphorus forms tend to transform into De-P, which is in accord with the results of many previous works[8~10]. The feature of phosphorus release is closely related to the physical-chemical characteristics of all phosphorus forms. Many researchers[8~10] proposed that phosphorus release at the water-sediment interface is mainly due to two processes, firstly the mineralization and decomposion of organic matter and early digenesis, and secondly the adsorption/desorption of dissoluble reactive phosphorus, especially Fe-P and Ad-P. Fe-P extracted by $NaOH\text{-}Na_2CO_3$ solution is known as the potential available component in sedimentary phosphorus[11]. Ad-P in sediments is one of the important forms of inorganic phosphorus and can be easily released to water and uptaken by phytoplankton. Both Ad-P and Fe-P are reactive phosphorus forms. Organic phosphorus includes refractory OP and leachable OP, and leachable OP can be easily released from sediments[8]. Therefore, these forms of phosphorus can be easily released into seawater. De-P in this paper represents the apatite of igneous or metamorphic origin as well as other non-dissolved inorganic phosphorus, and its chemical characteristics is stable. So, even re-adsorption occurs after phosphorus release, part of phosphorus can be transformed into De-P.

The phosphorus exchanged at the water/sediment interface is closely related to bioavailable phosphorus, which includes those released from the sediments and can be re-cycled[12]. Bioavailable phosphorus has a great impact on the nutrition state and primary productivity of marine biosphere. It has important environmental and biological significance.

3.3 The relation between the quantity of phosphorus released and time

Tab. 2 shows that after being thoroughly mixed with seawater for about 10 minutes, phosphorus released from the sediments reachs its maximum value. After 3 hours, it reaches a dynamic equilibrium state. Elovich equation and two-constant rate equation are chosen to model the data of this experiment. Tab. 4 shows that these two equations, especially the two-constant rate equation, can describe the kinetics of phosphorus release. There are adsorption and desorption reactions in the course of phosphorus release, and desorption reaction has the same mechanism as that of adsorption. Both include fast and slow stages[13]. Lagging status happens during the desorption process, that is to say, adsorption reaction lags behind desorption reaction. The mechanism of phosphorus release in this experiment is due to the diffusion caused by the concentration difference between sediment and water. Therefore, desorption reaction is very quick at the beginning, and adsorption reaction is minor. As the experiment

Tab. 4 Comparison of kinetics equations in the phosphorus releasing experiment

Site	R^2	
	Elovich equation: $Q = a + b \ln t$	Two-constant rate equation: $Q = K_0 C_0 t^{1/m}$
A1	0.6628	0.7937
B5	0.6621	0.6979
C1	0.7683	0.8675
Meso	0.7139	0.8961

goes on, the concentration of phosphorus in seawater is increased , desorption reaction is gradually weakened, while adsorption reaction becomes more important. The result shows that phosphorus released from the sediments reaches its peak value quickly (in 10 minutes in this experiment). After that, adsorption reaction become more and more obvious and it reaches equilibrium after 3 h.

4 Conclusion

It is found that after being thoroughly mixed with seawater, phosphorus released from the sediments reaches its maximum value in about 10 minutes. This experiment indicates that the maximum amount of phosphorus release is negatively correlated with the sand content, but positively with the silt and mud content of the sediments.

Fe-P, Ad-P and a small portion of OP can be released from the sediments, especially Fe-P with a maximum value of 35 % . Fe-P, O-P and Ad-P tend to transform into De-P after re-adsorption. This feature of phosphorus release correlates closely with the physical-chemical characteristics of all phosphorus forms.

After being thoroughly mixed with seawater for about 10 minutes, phosphorus released from the sediments reached its peak value. After 3 hours, it reaches a dynamic equilibrium. Elovich equation and two-constant rate equation are chosen to model the dynamic condition of phosphorus release.

Fe-P, Ad-p and OP released from the sediments in this experiment are the bioavailable phosphorus. Bioavailable phosphorus has a great impact on the nutrition state and primary productivity of marine biosphere. The study indicates that the phosphorus exchange at the water/sediment interface in the East China Sea off the Changjiang estuary is the potential source of bioavailable phosphorus. Phosphorus in sediments can be released into seawater under suitable hydrodynamic conditions to amortize the phosphorus concentration. Fe-P released from the sediment is especially the important source of endogenesis phosphorus. It indicates that this experiment has a great environmental and ecological significance.

References

[1] Zable M, Dahme A, Schulz H D. Regional Distribution of Diffusive Phosphate and Silicate Fluxes through the Sediment-water Interface: The Eastern South Atlantic. Deep-Sea Research I, 1998, 45: 277-300.

[2] Cowan J L W, Pennock J R, Boynton W R. Seasonal and Inter-annual Patterns of Sediment-water Nutrient and Oxygen Gluxes in Mobile Bay, Alabama (USA): Regulating Factors and Ecological Significance. Mar Ecol Prog Ser, 1996, 141: 229 245.

[3] Emsley J, The Phosphorus Cycle. Handbook of Environmental Chemistry, 1980, 1(part A): 147-167.

[4] Krom M D, Berner R A. Adsorption of Phosphate in Anotic Marine Sediments. Limnol Oceanogr, 1980, 25(5): 787-806.

[5] Daqing Yin, Qiurong Qin, Hang Yan. Effects of Environmental Factors on Release of Phosphorus from Sediments in WULI Lake. Journal of Lake Sciences, 1994, 6(3): 240-244.

[6] Hong Chen, Jiabao Chen, Wenwei Liu *et al.* The Study on Phosphorus Release from Sediments of Nanhu Lake of Nanning. Journal of Guangxi University (Nat Sci Ed), 1998, 23(3): 269-273.

[7] Huaiyang Zhou, Libo Zheng, Huaizhao Wang *et al.* Distribution of Different forms of Phosphorus in A Sediment Core from the Sea Outside Huaniaoshan Island and Its Environmental Significance. Donghai Marine Science, 2000, 18(4): 9-15.

[8] Jensen H S, Mortensen P B, Andersen F *et al.*. Phosphorus Cycling in A Coastal Marine Sediment, Aarhus Bay, Denmark. Limnol Oceanogr, 1995, 40(5): 908-916.

[9] Song Chen, Wenzhuo Liao, Bingkun Luo *et al.*. Release of Phosphorus in Wastewater Particle-seawater System. Journal of Oceanography in Taiwan Strait, 1996, 15(1):36-40.

[10] Song Chen, Rujian Lin, Wenzhuo Liao, et al. Adsorption-release Experiment of Phosphorus on Particles in Seawater-effluents Mixture. Journal of Oceanography in Taiwan Strait, 1991, 10(1): 1-6.

[11] Huanxin Weng. Different Phosphorus Forms in River Sediments and Their Environmental Geochemical Significance. Science Gazette, 1993, 38(13): 1 219-1 222.

[12] Sumei Liu, Jin Zhang. Chemical Extraction of Phosphorus in Sediments. Marine Science, 2001, 25(1): 22-25.

[13] Jianlin Wang, Jiafang Chen, Meizhi Zhao. Kinetics of Adsorption and Desorption of Phosphate on the Variable Charge Surface. Acta Scientiae Circumstantiae, 1989, 9(4): 437-445.

Distribution of Dissolved Inorganic Phosphate in Nansha Islands Sea Area, Southern South China Sea

Cheng Saiwei (程塞伟), Lin Hongying (林洪瑛)
South China Sea Institute of Oceanography, Chinese Academy of Sciences, Guangzhou 510301, *Guangdong, China*

Abstract Based on the survey data from the program Multidisciplinary Expedition to Nansha Islands Sea Area, the distribution of dissolved inorganic phosphate (PO_4^{3-}-P) in the sea water of Nansha Islands Sea Area is comprehensively analyzed in this paper. The results show that PO_4^{3-}-P concentration in the sea water of southeastern Nansha Islands Sea Area is commonly higher than that in the other sea areas; the vertical distribution of PO_4^{3-}-P concentration varies inconspicuously in different seasons; the concentration of PO_4^{3-}-P increases with water depth and changes most greatly in the layer of 50 ~ 100 m. The diurnal variation of PO_4^{3-}-P concentration differs in different seasons and at different observation stations. The distribution and variation of PO_4^{3-}-P concentration result from the physical and biological processes together.

Keywords Nansha Islands sea area; dissolved inorganic phosphate; distribution

Introduction

Phosphorous is an essential nutrient for the growth of marine plankton. The distribution of dissolved inorganic phosphate (PO_4^{3-}-P) has an important effect on the biological source and environment. Therefore, the distribution and variation of phosphorous has intrigued scientists for decades[1~4]. It has been suggested that the factors controlling distribution of PO_4^{3-}-P are different between tropic region and temperate region. Although PO_4^{3-}-P is measured routinely during every survey in the Nansha Islands Sea Area, complete analysis for PO_4^{3-}-P is needed all the same. Based on the survey data from the program "Multidisciplinary Expedition to Nansha Islands Sea Area", PO_4^{3-}-P is analysed in this paper, providing basis for the further research on nutrient and primary productivity.

1 Sampling and methods

The cruises were made in May ~ June 1990, December 1993, September ~ October 1994, and July 1999. Samples were collected on Ship "Shiyan 3" by using Rossette Autosampler System. PO_4^{3-}-P, water temperature, salinity, and depth were measured *in situ*. The sampling sites are showed in Fig. 1.

2 Results and discussion

2.1 Distribution and seasonal variation

The distribution of PO_4^{3-}-P is shown in Fig. 2. In the spring of 1990, PO_4^{3-}-P concentration in the southeast was lower than other parts of Nansha Islands Sea Area. In 1993, PO_4^{3-}-P concentration was

Received on April 28, 2003

relatively homogeneous. In the autumn of 1994, PO_4^{3-}-P concentration was higher in the north at surface layer and lower in the west at 75 m depth. In the summer of 1999, high values appeared in the east, near the Barake Strait.

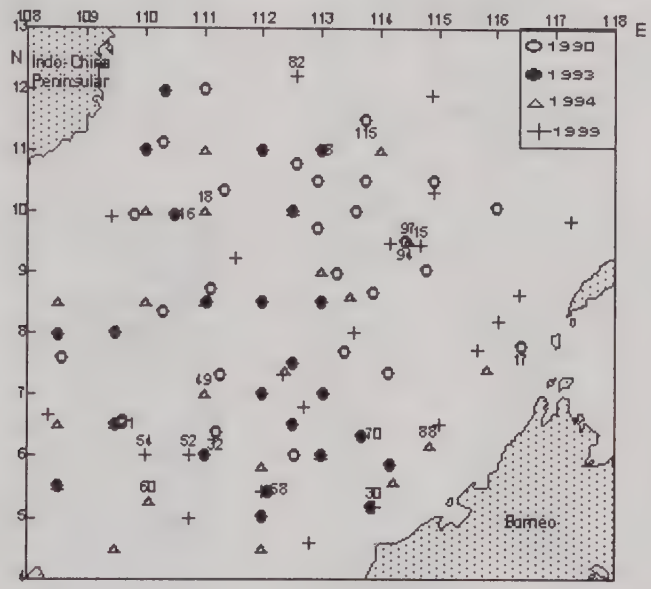

Fig. 1 Sampling stations

Controlled by monsoon, the physical condition is different in different regions. In order to understand PO_4^{3-}-P distribution in different regions, we divide the Nansha Islands Sea Area into four districts by Longitude 113° E and Latitude 8° N. The results are shown in Table 1.

The PO_4^{3-}-P concentration on average at 75 m deep was high in the spring of 1990, and at surface layer was high in the autumn of 1993, relatively. Although there are no data for the northeast, we can make estimation by the data from three other parts. Northeaster prevailed in the winter and a strong cyclone eddy occurred[5] in the northwest of Nansha Islands Sea Area which increased PO_4^{3-}-P value in the southwest. At the same time, there were eastern coastal current and western coastal current in the Nansha Islands Sea Area. Terrigeneous nutrients enriched PO_4^{3-}-P in the surface layer. The value on average in the autumn of 1994 was lower than in other seasons, which is in agreement with the conclusion that PO_4^{3-}-P is the limiting factor for photoplankton[6]. The PO_4^{3-}-P values varied a lot between east and west in the summer of 1999. During the season, the maximum data appearing in the southeast may be contributed to the exchanging water from the Balake Strait. The low value in other regions was probably due to the large-scale anticyclone eddy in the Nansha Islands Sea Area in the summer of 1999[5].

Being a tropic region, the Nansha Islands Sea Area characterized by relatively invariable water temperature and thermocline never disappears in different seasons. Thus, seasonal variation of nutrients in Nansha Islands Sea Area could not be explained by the variation of thermocline as in the temperate zone. Furthermore, it is also suggested that circumfluence and biology have jointly influenced the PO_4^{3-}-P concentration in the Nansha Islands Sea Area.

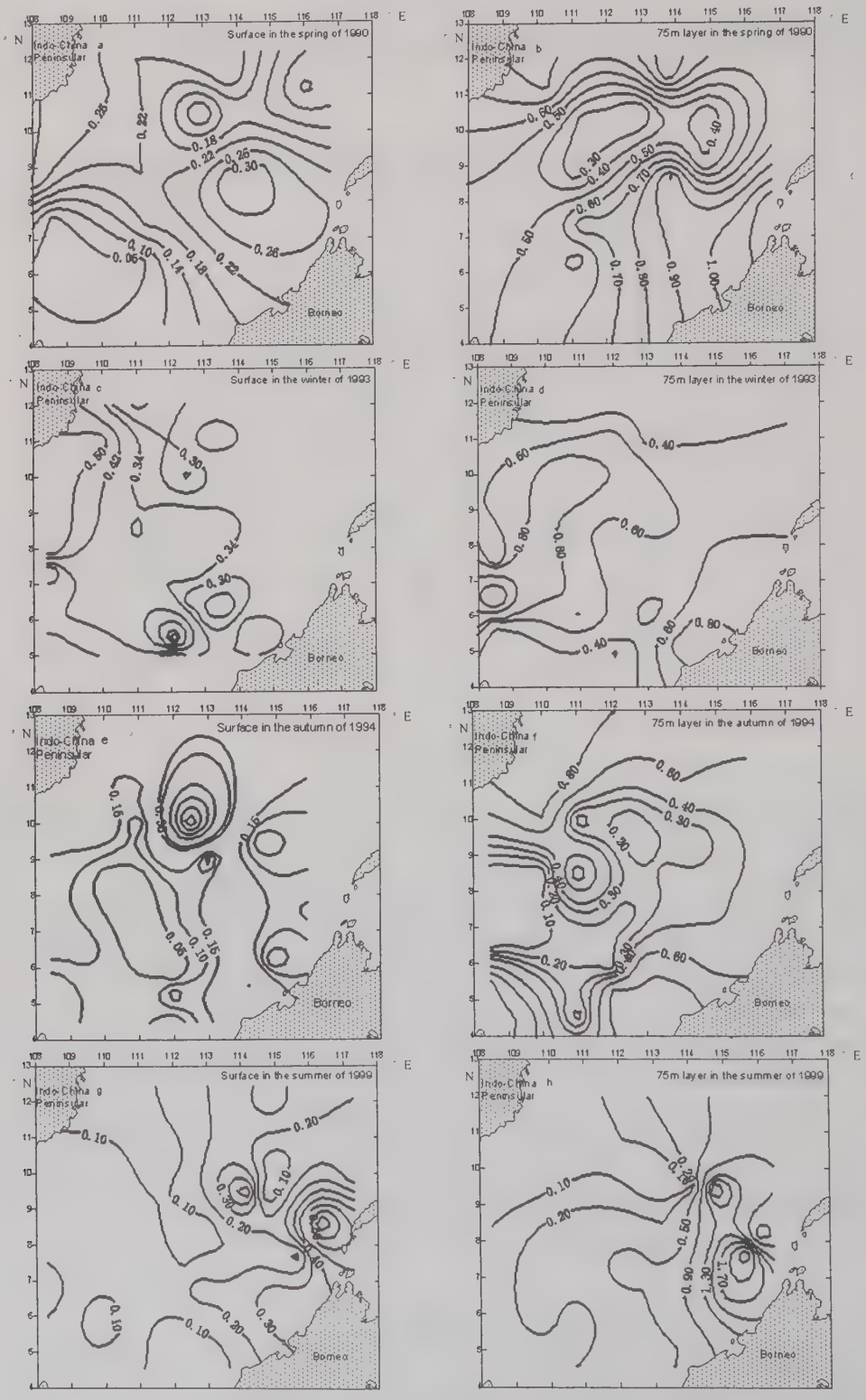
Surface in the spring of 1990
75m layer in the spring of 1990
Surface in the winter of 1993
75m layer in the winter of 1993
Surface in the autumn of 1994
75m layer in the autumn of 1994
Surface in the summer of 1999
75m layer in the summer of 1999
Indo-China Peninsular
Borneo

Fig. 2 Distribution of PO_4^{3-}-P concentration in Nansha Islands sea area

Tab. 1 Concentration of PO_4^{3-}-P in the seawater of Nansha Islands Sea Area

Time	Depth/m	PO_4^{3-}-P (mmol/m^3)			
		Northeast	Northwest	Southeast	Southwest
1990-05	0	0.22±0.12	0.22±0.08	0.26±0.00	0.11±0.09
	50	0.42±0.29	0.51±0.73	0.34±0.00	0.27±0.10
	75	0.67±0.31	0.80±0.07	1.18±0.00	0.46±0.20
	100	1.15±0.29	0.98±0.85	1.18±0.00	0.89±0.16
1993-12	0		0.35±0.09	0.30±0.05	0.32±0.06
	50		0.39±0.14	0.32±0.04	0.41±0.15
	75		0.55±0.27	0.58±0.24	0.92±0.88
	100		0.76±0.38	0.74±0.28	0.95±0.20
1994-10	0	0.14±0.17	0.11±0.08	0.16±0.13	0.07±0.06
	50	0.38±0.29	0.37±0.25	0.26±0.16	0.09±0.08
	75	0.39±0.19	0.57±0.44	0.56±0.18	0.43±0.43
	100	0.58±0.46	0.94±0.60	0.87±0.25	0.29±0.18
1999-07	0	0.35±0.22	0.07±0.04	0.66±0.67	0.14±0.10
	50	0.48±0.23	0.16±0.12	0.66±0.50	0.19±0.16
	70	0.70±0.81	0.16±0.04	1.41±0.76	0.36±0.20
	100	1.16±0.78	0.56±0.19	1.94±0.83	0.81±0.27

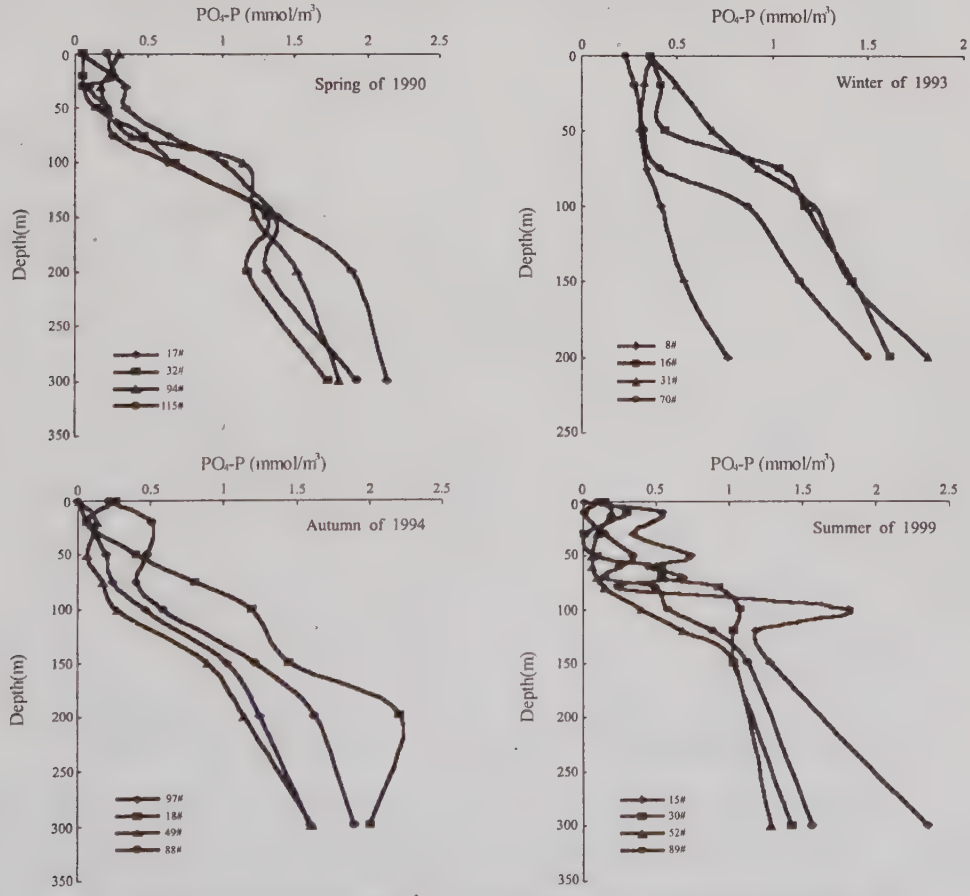

Fig. 3 Vertical variation of PO_4^{3-}-P concentration in the Nansha Islands sea area

2.2 Vertical Distribution

PO_4^{3-}-P concentration increases with the water depth in the Nansha Islands Sea Area. Plankton cells subside into deeper water column after death and PO_4^{3-}-P is released by bacterial action, which enriches PO_4^{3-}-P concentration in deep water. The upper layer is difficult to be renewed by deep water for it is obstructed by thermocline. Therefore, PO_4^{3-}-P value is low and varies slowly in 0 ~ 50 m (0.002 mmol • m^{-3}). Fig. 3 shows that the maximum variation rate is found in 50 ~ 100 m (0.011 mmol • m^{-3}), which suggests that the process of PO_4^{3-}-P releasing from settling particles occurs mainly in this layer. The variation rate decreases in 100 ~ 200 m (0.006 mmol • m^{-3}) and decreases to the surface level in 200 ~ 300 m (0.003mmol • m^{-3}).

2.3 Diurnal variation

The diurnal variation of PO_4^{3-}-P in the Nansha Islands Sea Area varies with different seasons and different stations. Fig.4 is made by the data from winter of 1993, autumn of 1994, summer of 1999. Diurnal sampling stations are all in the southeast. Fig.4 shows that there was no maximum value in the

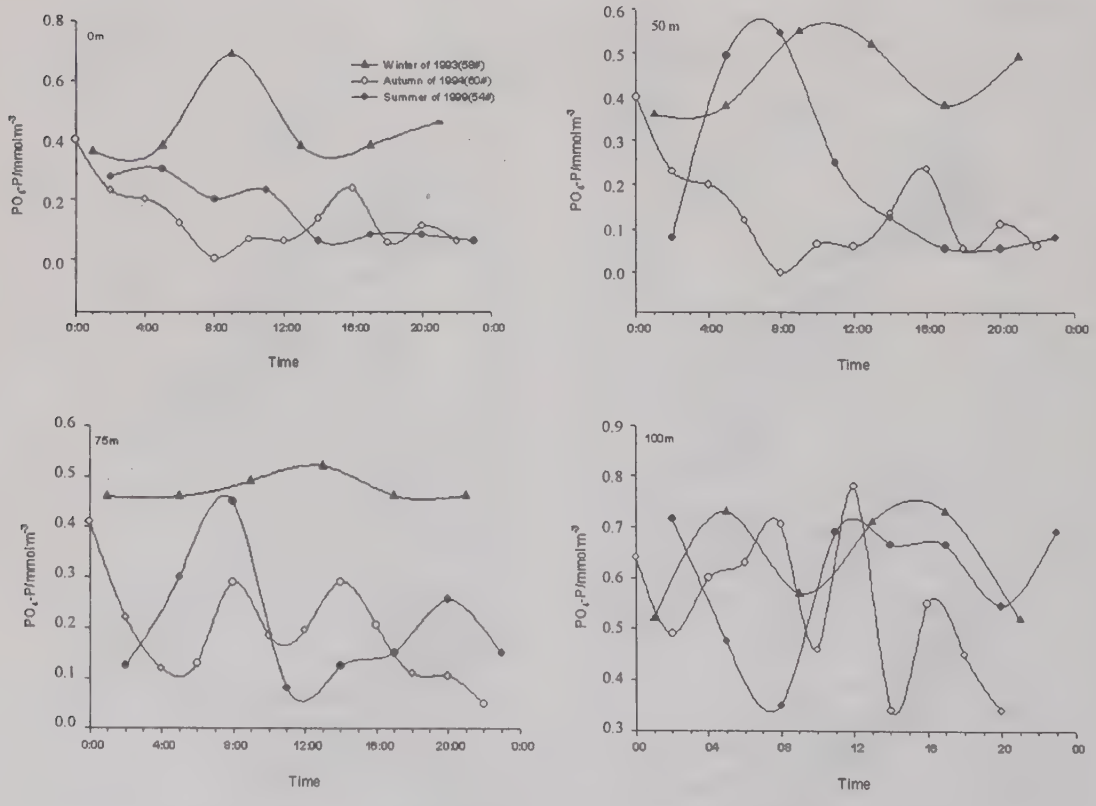

Fig. 4 Diurnal variation of PO_4^{3-}-P concentration in the Nansha Islands sea area

relatively complicated figures of 1994. In the winter of 1993, the maximum value appeared approximately at 9:00 am in the surface layer, at 12:00 at the water depths of 50 m and 70 m. In the summer of 1999, no apparent maximum value occurred in the surface layer. However, at the water depths of 50 m and 70 m, the maximum value appeared about at 6:00 and 8:00, respectively. Two

maximum values appeared at 100 m deep. In the Nansha Islands Sea Area, waves occur at the boundary of thermocline, which are called "internal waves". The diurnal variation of PO_4^{3-}-P maybe contributes to such waves. Tritium data suggest that the maximum diffusing factor is at the water depth of 100 m, which indicates the fastest water mixing here. The existence of internal waves makes it possible for the water to mix well, enhances the supply of nutrient, and is beneficial to plankton growing and mustering in the subsurface layer.

3 Conclusion

(1) The distribution of PO_4^{3-}-P in the Nansha Islands Sea Area has its rules: the PO_4^{3-}-P concentration on average in surface was highest in the winter of 1993 and lowest in the autumn of 1994; at 75 m depth, it was highest in the spring of 1990. PO_4^{3-}-P concentration in the southeast was higher than in other regions. This must be due to the terrigeneous input, coastal currents and exchanging with other seas, and cyclone eddy in the monsoon.

(2) PO_4^{3-}-P concentration increases with water depth. The minimum variation rate occurs in 0 ~ 50 m depth. And the maximum variation rate occurs at 50 ~ 100 m depth, which suggests that the process of PO_4^{3-}-P releasing from settling particles occurs mainly in 50 ~ 100 m depth.

(3) The diurnal variation of PO_4^{3-}-P in the Nansha Islands Sea Area is a bit complicated and it is different in different seasons and different sites. The distribution of PO_4^{3-}-P results from the physical and biological processes together.

References

[1] He Qingxi, Zhang Sui, Fang Zhengxin *et al.* Distribution Characteristics of the Environmental Geochemical forms for Nitrogen and Phosphorus in the Sediments of DAYA Bay. Tropic Oceanology, 1992, 11(2): 38-45.

[2] Yang Meilan, Quan Zhongyan, Lin Yantang. Characteristics of Nitrogen and Phosphorus Contents in NANAO Waters of Dapeng Bay. Tropic Oceanology, 1998, 17(2): 74-79.

[3] Peng Yunhui, Wang Zhaoding. Speciation and Distribution Characteristics of Phosphorus in Waters of Dapeng Bight. Tropic Oceanology, 1996, 15(2): 28-35.

[4] Han Wuying, Wu Linxing, Lin Hongying. Marine Chemistry in South China Sea. Beijing: Science Press, 1998.

[5] Fang Wendong, Fang Guohong. The Recent Progress in the Study of the Southern South China Sea Circulation. Advance in Earth Science, 1998, 13: 166-172.

[6] Lin Hongying, Han Wuying. Distribution of Nutrients in the Nansha Islands Waters. Marine Sciences, 2001, 25(10): 12-14.

[7] J. P. Riley, G. Skirrow. Chemical Oceanography (Vol.2). Translated by: Cui Qingchen. Beijing: Marine Press, 1982.

[8] Lin Hongying, Han Wuying. Vertical Characteristics for the Physical and Chemical Parameters and A Viewpoint of the Thermocline Ecosystem in the Nansha Islands. Acta Oceanologica Sinica, 2001, 23(1): 48-56.

Application of SAR Imagery in Submarine Topography Surveys

Zhang Ningchuan (张宁川), Liang Kailong (梁开龙), Gui Limin (桂力民)
Department of Hydrography and Cartography, Dalian Naval Academy, Dalian 116018, *Liaonin, China*

Abstract An important research area in oceanographic surveying and mapping is to obtain submarine topography by remote sensing technique, especially by SAR imagery. In this article, problems related to SAR imagery are analyzed to provide references for the further research.

Keywords SAR Imagery, Submarine Topography Surveys, Image Processing

Introduction

Since the 1960's, space science has been developing rapidly. The remote sensing technique, especially the spaceborne remote sensing technique, has brought about a revolution in the field of oceanographic observation. As a major component of this technique, the synthetic aperture radar (SAR) has arrested more and more attention from the marine researchers. This technology is capable of detecting objectives under all weathers, at all times, through multiple frequency bands and polarities, from various perspectives and at different angles of depression. Consequently, the images so obtained provide rich information, distinct profiles and sharp contrasts. Therefore, in comparison with the optical sensors, SAR images present more details of the targets and better discrimination of features between close-by targets. Since the space-borne SAR is based on a special working and imaging mechanism, it naturally has developed its own series of submarine mapping methods.

1 SAR imaging mechanism of submarine topography

The extraction mechanism of bathymetric information from SAR sounding data is different from that of the optical ones. SAR is an active remote sensor working in the microwave band. Because of the dielectric constant of sea water, EM wave attenuates very quickly and does not penetrate to any considerable depth in the sea water, making it impossible to directly reach the bottom terrain. Therefore, bottom topography cannot be viewed directly by SAR, and the image is actually formed via Bragg wave resonant backscattering from the sea surface roughness. As shown on SAR imagery, the variation of radar backscattering energy density correlates closely with water depth. This correlation can help us to obtain the information of underwater topography quantitatively (see Fig. 1.). The adlittoral features of SAR imagery appear in the form of alternating white and dark stripes, corresponding to depths of no more than 50 m. These are the signatures of underwater sandbanks, sand-ridges and sand waves. In deep water background, the undulating texture of SAR images is associated with depth variations at 100 m, 1 000 m, or even greater depths. Their *wavelengths* usually extend to several kilometers.

It is known that microwave cannot penetrate any more than several centimeters through surface

Received on May 12, 2003

water. Then what makes it possible to go through the surface to *detect* the shallow water bottom topography and obtain the sounding data? With the continuous enrichment and in-depth study of satellite data, associated theories are continuously emerging, among which the model of Alpers and Hennings (1984) is the most representative one.

General speaking, the SAR imaging mechanism of submarine topography consists of three steps[2]:

1) The interaction between the current and the sea bottom topography leads to the variations in the current velocity at the surface.

2) The variation in the surface current velocity modulates the short-scale surface roughness, of which the process can be described by the weak hydrodynamic interaction theory in terms of relaxation time approximation.

3) The modulation of the sea wave spectrum gives rise to changes in radar backscatter cross-section.

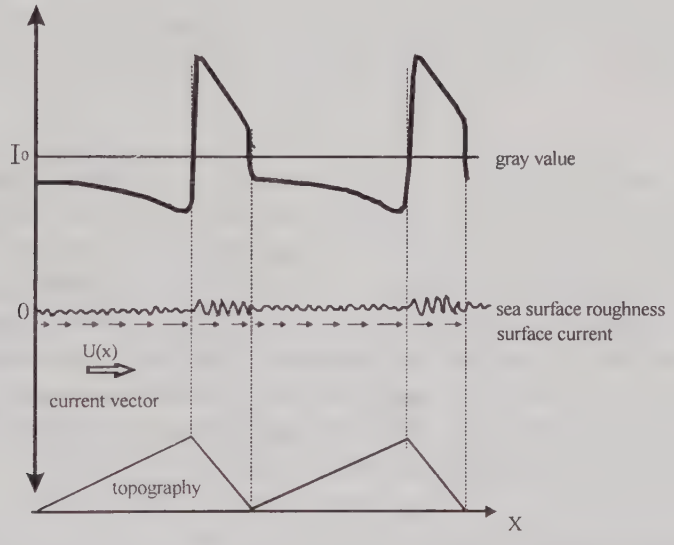

Fig. 1 Physical model of SAR imaging mechanism of submarine topography

To describe the above three stages, sufficient effort has been made worldwide to establish a variety of numerical models[3]. One especially noteworthy model is founded by Volgezang *et al* in the Netherlands, which is a bathymetry assessment system (BAS) based on ERS-1/2 SAR. This system combines satellite ERS-1/2 SAR images with a limited amount of actual echo-sounding data to invert the water depths in a vast shallow water area, limiting the rms error to 30 cm in the testing zone. Many Chinese scholars have also conducted in-situ experiments, and accomplished theoretical researches that lead to promising results[4~8].

The SAR marine imagery is a planar distribution of the backscatter cross-section of surface micro-scale waves, which represents its sensitivity to the rough surface backscattering. However, in the disquiet ocean, there simultaneously exist multi-scale dynamic processes which actuate and modulate the micro-scale surface waves. Therefore SAR imagery is a concentrative representation of motions at various scales included in these *coexistent* dynamical processes. In this sense, the interpretation of radar imagery is subject to its own particularity and complexity. Now the main aspect of the adlittoral topography or

the study of shallow water sounding is to improve the present models, so as to reduce to the minimum the quantity of on-spot data obtained by traditional means of measurement and, at the same time, to enhance the inversion precision.

2 Resolution of SAR imagery, mapping scale, and projection selection

In the case of remote sensing systems, a clear understanding of system resolution is the basis of SAR imagery interpretation. In order to assess the feasibility of the sensors in use, we have to take into consideration our knowledge of system resolution and the range of resolution variables. The concept of resolution is used to describe the minimal distance of two adjacent objects in space that can be distinguished by radar. It is defined in two dimensions azimuth resolution, which parallels the heading of the radar-carrying vehicle, and range resolution, which is perpendicular to the heading.

Considering the fact that remote sensing data have to be integrated with GIS, the keynote in information conversion lies in a correct understanding of the relationship between resolution and mapping scale. Generally, we can establish this kind of relation with a simple expression as follows:

$$S = 1 : \frac{R_r \times R_s}{0.0254}$$

where S is the local scale, R_r is the resolution of radar, and R_s is the resolution of the output equipment.

While extracting information from SAR imagery, the total request is to express information in a certain stated frame of projection reference, so as to carry out some manipulations such as geometrical measurement, comparison and complex analysis. At the same time this is also the basis to establish corrective function in geometrical correction. Generally, projection selection is mainly concerned with the scale of the output imagery and the projection mode of imagery submitted for comparison. For example, large scale mapping commonly selects Gausss Projection or Plane Projection, while small scale mapping may select Mercators Projection. And, if the map is projected by means of isometric cónical projection, corresponding conversion will be necessary.

3 Satellite SAR image processing technique[9]

3.1 Geometric correction of SAR image

Satellites travel along certain orbit in the outer space. After digital processing, the imaging radars product is transformed to SAR digital imagery composed of a two-dimensional matrix. Every pixel of the imagery corresponds to a certain ground geographical target. However, under the influence of some unfavorable factors, such as the satellite orbit, earth rotation, earth curvature and inconsistent mapping scales, the asymmetrical movement and unstable posture of radar antenna, as well as radars clinographic projection (see Fig. 2), a problem called *geometrical distortion* will emerge, which is because of the incoherence between the actual ground objects and those found in the SAR images in terms of position, shape, size, azimuth and other features. That is why geometric correction of SAR images is indispensable. Accurate ground object location can be achieved by establishing the precise mathematic relation (*i.e.* correcting the conversion function) based on the SAR imagery coordinates and map coordinates, both of which are two-dimensional plane coordinates systems (see Fig. 3)[10].

Normally, geometric correction of SAR image can be classified into ortho-correction and geo-reference correction. The ortho-correction includes corrections of earths rotation, curvature, satellite

posture, slant to ground range conversion, and a simple correction by fitting a transform formula based on ground control points. The geo-reference correction makes use of SAR imaging models or DEM to ulteriorly eliminate the geometrical errors caused by landform for the generation of a geo-reference orthograph[11, 12].

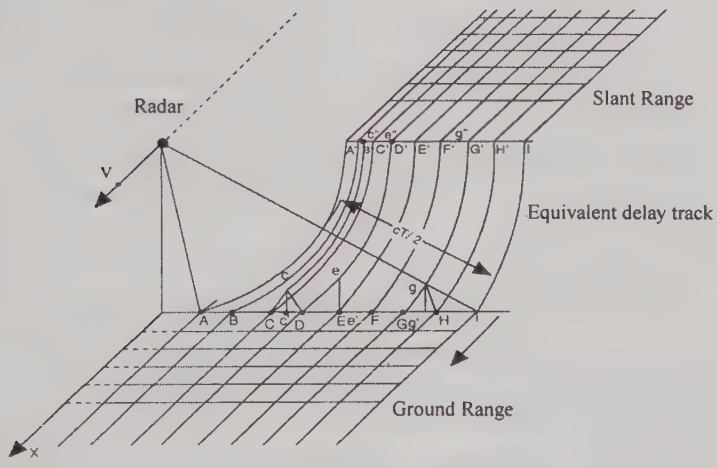

Fig. 2 Slant Range and Ground Range of an SAR image

Imaging radars illuminate the scene from an oblique point of view. The resulting imagery exhibits inherent geometric characteristics and distortions quite different from those in the case of vertical optical sensors. Since the incidence angle varies only several degrees, SAR produces a symmetrical geometry in the whole swath. According to the SAR imaging mechanism of submarine topography, the surface feature is relatively flat. What we are concerned about is the variation of short-scale surface wave backscattering cross sections. There is no need to consider the aberrant influence generated by the fluctuant landforms that frequently occur on land. On the other hand SAR imaging geometry is very complicated and the DEM information of seabed is difficult to acquire. So in general marine application we always adopt some simple method to revise SAR imagery. There is obviously a pressing need for the marine remote sensing scientists to break these limits for the maximum improvement of location accuracy.

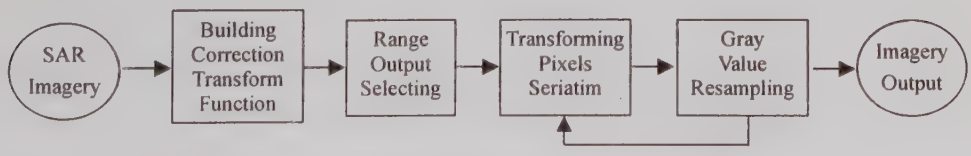

Fig. 3 Procedures for geometric correction of SAR imagery

Piecewise polynomial correction is a kind of general method in practice. Firstly, we divide SAR imagery into several pieces. Secondly, we take the given ground control point (GCP) or data of the imagery as reference point to figure out the control point coordinates on map with projection

transformation, setting up the polynomial relation of the control points coordinates on SAR image and map. We use least-squares fit to work out the coordinates of other points so as to revise the imagery of every piece. Finally, we join the pieces. The precision of this method correlates with the GCPs precision, distribution, quantity and range of correction. The more precise the GCP is, the more accurate the correction will be. However, the polynomial correction is largely limited by the fact that certain quantity of GCPs should be evenly distributed in the map. Yet it is very difficult to find these given GCPs in the ocean. Besides this there are other limitations too. For example, while the result of correction fits the point fairly well where the transform coefficients are confirmed, at other points the inserted values may show obvious deviation that mis-coordinate with the adjacent GCPs, i.e. oscillation may occur at some points. In addition, to avoid ill-conditioned matrix caused by possible linear correlation between some lines or rows in the normal matrix ($A^T PA$), Logendre polynomial is used sometimes in lieu of general polynomial during geometric correction.

3.2 Radiometric correction and enhancement of SAR images

Information extraction from SAR imagery has a series of processing methods of its own, such as, antenna pattern correction, speckle reduction filters, change detection using speckle de-correction *etc.*, which are quite different from those in the case of vertical optical sensors.

3.2.1 Antenna pattern correction

According to the SAR imaging mechanism, the illumination energy is not symmetrical in the range direction, which is derived from the antenna pattern. So the antenna pattern correction is necessary to compensate the energy asymmetry of SAR image. We generally carry out the correction based on the antenna pattern or antenna gain revision system promulgated and updated periodically by the SAR Data Processing Center. If there are no such data available, Polynomial Fit should be adopted to calculate the modulation coefficient for each line. The method is described as follows:

a) Additive Function: $D(x) = D_0(x) + M - P(x)$

b) Multiplicative Function: $D(x) = (D_0(x) - Min) \cdot M / (P(x) - Min)$

where $D(x)$ is the gray value corrected, $D(x)$ is the original gray value, M is the mean value of the whole image, and Min is the minimum gray value of the whole image. $P(x)$ is a function fitted by the mean values per line.

3.2.2 SAR image ratio transform and contrast adjustment

The output data provided by the Data Processing Center has two record formats: 8 bit and 16 bit. Since the displays gray level is only 256, the 16 bit data must be transformed into the 8 bit data through Scaling Transform. Suppose D is one pixels gray value on a 16 bit imagery and D' is the value transformed. A commonly used and effective method is to calculate the Mean Value and Standard Deviation of the 16 bit imagery firstly, and then, do the transform as follows:

a) Conventional Transform

i) $A - 2S > 0$

$$D' = \begin{cases} 0 & D < A - 2S \\ (D - A + 2S) \times 255 / 4S & A - 2S \le D \le A + 2S \\ 0 & D > A + 2S \end{cases}$$

where the input range is $[A - 2S, A + 2S]$.

ii) $A-2S \le 0$

$$D' = \begin{cases} D \times 255/(A+2S) & D \times 255/(A+2S) \\ 0 & D > A+2S \end{cases}$$

where the input range is $[0, A+2S]$.

b) Exponential Conventional Transform

i) $A-2S > 0$

$$D' = \begin{cases} 0 & D < A-2S \\ [(D-A+2S)/4S]^{\alpha} \times 255 & A-2S \le D \le A+2S \\ 0 & D > A+2S \end{cases}$$

ii) $A-2S \le 0$

$$D' = \begin{cases} [(D-A+2S)]^{\alpha} \times 255 & D \le A+2S \\ 0 & D > A+2S \end{cases}$$

When $\alpha = 1/2$, the transform is identical to Square Root Stretching, which is applicable in the case of left deviation from the crest. When $\alpha = 2$, it is identical to Square Stretching, which is applicable in the case of right deviation from the crest. Users could adjust the exponent to get the most satisfactory results for contrast adjustment. It is also possible, in practice, to adjust the range of input before doing anything to the exponent. Such a sequence will most effectively reinforce the target information observed.

3.2.3 Speckle reduction filters

Speckles are intrinsic in SAR imagery. They bring negative effects on the interpretation of SAR images. Speckles are formed because of the echo vector change (fading) at each scatter point due to the movement of sensors and the coherent superposition at such points inside each ground surface unit illuminated by radar pulses. This vector change will lead to the brightness change between two adjacent observed units of the same backscatter cross-section, which, in turn, brings about a speckle.

There are two ways to suppress the speckle noise. One is the multi-looking processing, managed at the expense of spacial resolution loss. The other is by way of smoothing filters, which goes without any resolution loss. Presently, the most popular noise suppression filter is built up around the local area statistic adaptive filter. In view of the asymmetry of SAR imagery, points in the neighborhood and their weight factors are determined on the basis of a local gray value plot. Several allied types of filters are: the Kuan filter, the Enhanced Lee filter, and the Enhanced Frost filter. The sight number is used to determine the noise intensity of imagery. This method has the merit that it can adjust the balance of effects between smoothing and fringe-keeping. Besides these methods, Geometry filter (e.g. Gamma MAP filter) and Classification filter can reduce the speckle noise successfully as well.

4 SAR data analytical technique

SAR image interpretation indicators include tinge, texture, shape, size, model and shadow. These characteristics depend on two groups of parameters. One is the parameters of radar system, and the other is object parameters, including complex dielectric constant, surface roughness, geometry, surface scattering and its directionality[9, 13].

In the course of observation on marine landform, we are mainly concerned about the planar targets, which, in the case of lower resolution imagery, will be regarded as point targets. The interpretation may be based on the images texture, which refers to the roughness or consistency within an area on the SAR imagery. This implies that texture is connected with sea surface roughness. Although texture is not a precisely quantified object characteristic, medium texture and macroscopical texture are important factors for object identification. Medium texture is developed either by the asymmetrical permutation of a number of resolution units in the same kind of objects or by the fine textures of different objects that occupy several resolution units, that is, the variation of spatial hue is represented by the scales of several resolution units. The macroscopical texture is the characteristics of sea bottom feature in nature. This texture is resulted because the variation of radar echoes along terrain features has changed the incident angle as well as the geometrical relationship between beam and target.

Texture analysis can be used not only directly as a method for image processing or information extraction but also in combination with GIS. It includes two parts: the first is the traditional visual interpretation, and the second is to use a special cyber-software for quantitative analysis[9].

The Second Institute of Oceanography has performed some research on the SAR detection of shallow water bottom features and depths within the project 863-818-06-02. Figure 4 shows the image of *Xiaoyinsha*, which is one of the underwater sand ridges making up the Subei radialized sand ridges. The data were received at 10:34 on July 8, 1995. We can see a relatively bright striation in the middle part of the calculating area. Judging from the brightness variation and its extension, we can conclude that the direction of topography change goes from south to north. The brightest part of the stripe should be the crest of the *Xiaoyinsha*sand ridge. Having been filtered, the characteristic becomes even more evident. As shown in Figure 5, the depth at the crest is 2 m, that at the bottom is 7.5 m, and the deepest part of the area nearly reaches 11 m. Compared with the real chart, the rms difference is 0.42 m. The whole job has

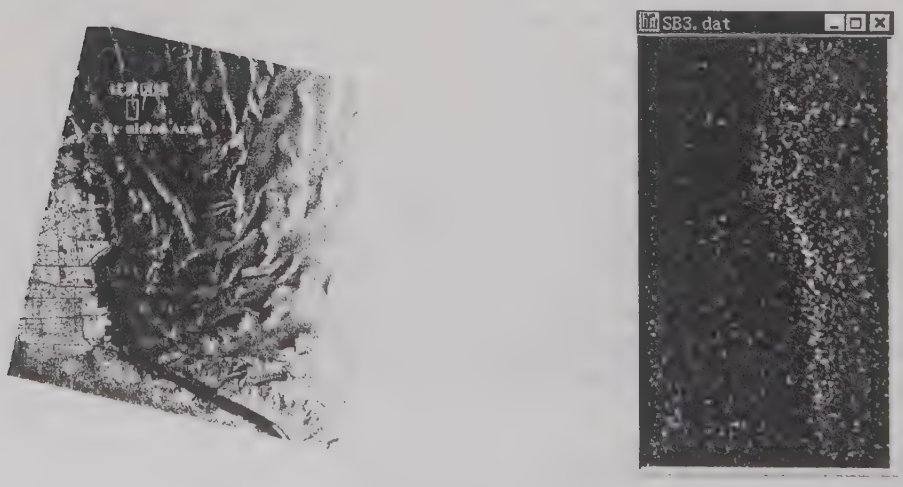

(a) (b)

Fig. 4 SAR image of sand ridges

(a. Subei radialized sand ridges b. *Xiaoyinsha*)

been accomplished with the support of the software developed by the investigators.

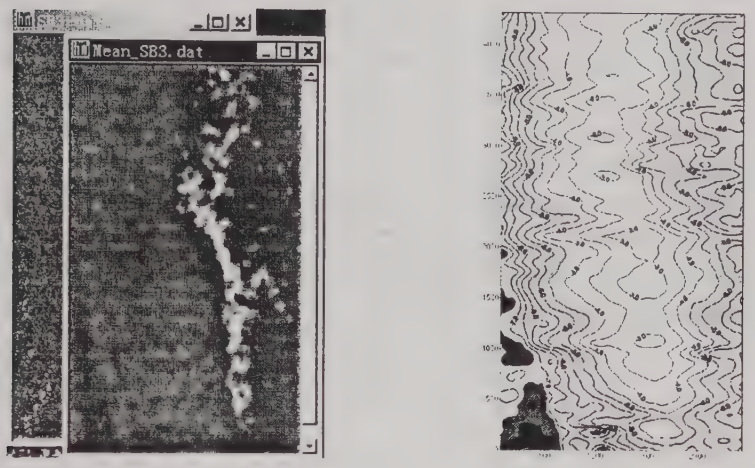

Fig. 5 Image filtered and water depth (in meters) of *Xiaoyinsha* calculated from Fig. 4

5 Conclusion

Spaceborne SAR imagery can be applied both qualitatively and quantitatively to the description of bathymetric surveys in shallow coastal waters. Convergence of the technique is to be suggested by good comprehension on SAR imaging mechanism and proper using or processing of imageries.

Acknowledgements

We wish to thank the Statellite Oceanic Administration of Second Institute of Oceanography, headed by Weigen Huang, for providing the SAR imagery and all kinds of references.

References

[1] Shi Maochong *et al.*. Oceanic Investigation Method. Qingdao: Ocean University of Qingdao Press. 2000.

[2] W Alpers and I Hennings. A Theory of the Imaging Mechanism of Underwater Bottom Topography by Real and Synthetic Aperture Radar. Int. J. Geophys. Res., 1984, 89: 10 529-10 546.

[3] I Hennings. An Historical Overview of Radar Imagery of Sea Bottom Topography. Int. J. Remote Sensing, 1998, 19: 1 447-1 454.

[4] Wei-gen Huang, Man-na Gao, Chang-bao Zhou *et al.*. Spaceborne SAR Observations of Underwater Bottom Topography off the North Coast of Penglai. Donghai Marine Science, 1996, 14 (1): 52-57.

[5] Huang Weigen, Fu Bin, Zhou Changbao *et al.*. Simulation of Optimal Synthetic Aperture Radar (SAR) Parameters for Mapping Underwater Topography. Journal of Remote Sensing, 2000, 4(3): 172-177.

[6] Fu Bin , Huang Weigen, Zhou Changbao *et al.*. Simulation Study of Sea Bottom Topography Mapping by Spaceborne SAR-Relationship between Topographic Parameters and Measurement of Water Depth. ACTA

Oceanologica SINICA, 2001, vol. 23(1): 35-42.

[7] He Yuhua and Wang Yong-jiang.Remote Sensing Application on the Investigation of Island, Reef, Beach and Sands Resources Distribution Actual State. China Geology, 1998, 8: 43-46.

[8] Shao Jiebo, Ma Yi, Liu Baoyin *et al.*. The SAR Imaging of Nansha Isles Submerged Reef. Journal of Oceanography of Huanghai and Bohai seas, 1999, 17(4): 66-70.

[9] Guo Huadong *et al.* Theories and Applications of Radar for Earth Obervation. Science Press. 2000.

[10] Zhang Yongsheng. Remote Sensing Imagery Information Systems. Science Press. 2000.

[11] Liu Yuxian Geo-reference Correction of Spaceborne SAR Image Using DEM, Developments of Topography Science and Technology, 1994, 14-17.

[12] Wang Guodong and Zhou Yinqing. An Algorithm Improving Geometric Calibration of Spaceborne SAR Image. Remote Sensing and Remote Control, 1999, 21 (3): 16-18.

[13] Wu Jun and Zhao Zhongming. Scale Co-occurrence Matrix for Texture Analysis Using Wavelet Transform. Journal of Remote Sensing, 2001, 5(2): 100-103.

Thermodynamic Analysis of Heavy Metals Biosorption by Two Macroalgae

Chen Lidan (陈丽丹), Wang Xian (王 宪), Xu Lurong (徐鲁荣), Qian Aihong (钱爱红)
College of Oceanography and Environmental Science, Xiamen University, Xiamen 361005, *Fujian China*

Abstract The thermodynamic process of two macroalgae, *Sargassum fusiforme* and *Lamin aria japonica*, absorbing heavy metal ions Cu^{2+}, Pb^{2+}, Cd^{2+} and Ni^{2+}, has been studied. The result indicates that the absorption isotherms of these two macroalgae clearly accord with the Landmuir adsorption model. The absorptive processes of *S. fusiforme* and *L. japonica* for Cu^{2+} are endothermal, and at 35 ℃, the adsorption heat of these two algae is 59.5 kJ/mol and 76.8 kJ/mol respectively. Temperature could affect the algae's adsorption capacity. Their adsorption capacity increases with temperature (25 ℃ and 35 ℃).

Keywords thermodynamics of biosorption, adsorption capacity, heavy metal, macroalgae

In order to identify the essential physical-chemical character of heavy metal biosorption by algae, it is necessary to research the thermodynamic process. Preliminary work has showed that the adsorption capacity varies with the kinds of alage, for example, the macroalgaes adsorption capacity is markedly more than microalgae, and it is also determined by some environmental factors[1~4]. This study focuses on the thermodynamic process of heavy metal biosorption. The bioaccumlation of Cu^{2+}, Pb^{2+}, Cd^{2+} and Ni^{2+} by two macroalgae, *S. fusiforme* and *L. japonica* has been examined. The aim of this work is to improve the adsorption capacity of algae adsorbent to the utmost, ascertain its feasibility of being used in industrial waster water treatment, and finally provide experience and mechanism for the application of algal adsorbent.

1 Materials and method

1.1 Biomass and adsorbent preparation

The biomass samples *S. fusiforme* and *L. japonica* are obtained from the coast of Xiamen and the Yellow Sea in Qingdao respectively. These two macroalgae are pre-treated by $CaCl_2$, and the fraction of 80~120 mesh is chosen as adsorbent for later use.

1.2 Test chemicals

The metal ions studied are Cu^{2+}, Pb^{2+}, Cd^{2+} and Ni^{2+}. Metal solutions of desired concentration are prepared from $CuSO_4$, $Pb(NO_3)_2$, $CdCl_2$ and $NiSO_4$, by dissolving the exact quantities of metal salts in deionized water. All the reagents used are of analytical reagent grade and the deionized water is used for all experiments.

1.3 Method

0.5 g dried algal powder is added into flasks, in which we have already added 200 mL of initial metal solution (10 ~ 100 mg/L, pH=5.0). The flasks are shaken for 4 h, and each solution is exacted by

Received on October 9, 2003

centrifugation for 5 mL clear. The clear and initial metal salt solutions are analyzed for metal ions concentration with the aid of a Hitachi Z8000 atomic absorption spectrophotometer(AAS).

2 Results and Discussion

2.1 Absorption capacity of these two macroalgae in individual metal ion system

Thermodynamic absorptive equilibrium parameter is defined to describe the basic parameter of absorptive process of system. As a classical thermodynamic absorptive model, Langmuir equation which has been widely used in waste water treatment, expresses the relationship between the specific metal uptake q_e (mg/g biomass) and the equilibrium metal concentrationC_e (mg/L) at a certain temperature. It is suitable for monolayer adsorption, and can be expressed as:

$$q_{eq} = \frac{Q^0 bC_e}{1 + bC_e}$$

Where Q^0 is the maximum uptake capacity by biomass and b is a variable connected with the affinity of heavy metal ions to absorptive sites. Theoretically speaking, an efficient absorbent need to have a bigger value of Q^0 and a smaller value of b. We can attain the value of Q^0 and b through extrapolation from the relation curve of $C_e/q_e \sim C_e$.

The specific metal uptake q_e (mg/g biomass) by *L. japonica* and *S. fusiforme* for Cu^{2+}, Pb^{2+}, Cd^{2+} a nd Ni^{2+} has been investigated in each individual metal ion system while the absorptive process attained equilibrium, and the relation curves of $q_e \sim C_e$ are presented in Fig. 1 and 2 respectively. The result indicates that the absorption isotherms of these two macroalgae clearly accord with the Landmuir adsorption model. They all have a rapid increase at first, and then tend to balance. According to the Landmuir model, the high degree of the steady part of the curves presents the maximal adsorptive capacity. It is obvious that the maximal adsorption capacity of these two macroalgae to the four metal ions obeys the rule: $Pb^{2+} > Cd^{2+} > Cu^{2+} > Ni^{2+}$. The rapid increase of the curves at first implies that both *L. japonica* and *S. fusiforme* display high affinity to Pb^{2+}, while the affinity of *S. fusiforme* to Ni^{2+} is so poor that its absorption capacity to Ni^{2+} is markedly lower than other metal ions.

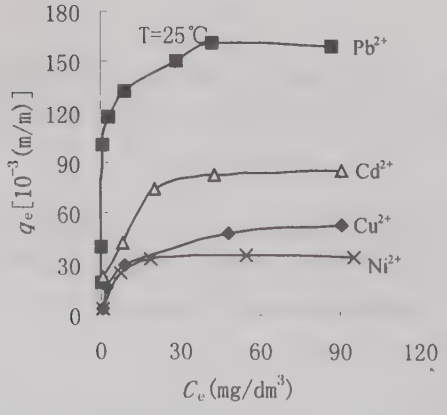

Fig. 1 Adsorptive isotherm of *L. japonica* for heavy mental ions

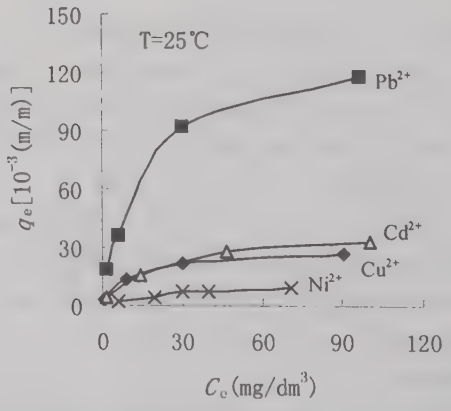

Fig. 2 Adsorb isotherm of *S. fusiforme* for heavy mental ions

There is just the qualitative analysis above, but the thermodynamic process of heavy metal biosorption by algae need to be further discussed. So we transform the Langmuir equation into:

$$(C_e / q_e) = (C_e / Q^0) + (1 / Q^0 \cdot b)$$

The curves of $C_e/q_e \sim C_e/q_e$ are shown in Figs. 3 and 4. It is readily apparent that C_e/q_e and C_e/q_e are linearly correlative. From Figs. 3 and 4, we can calculate the thermodynamic constant of Landmuir adsorption equation: Q^0=1/k, b=k/a, where k and a are slope and intercept of beeline respectively. The thermodynamic constants of these two macroalgae absorbing each heavy metal ions are presented in Tab. 1. From the results we can see that the maximum uptakes of *L. japonica* for each heavy metal ions

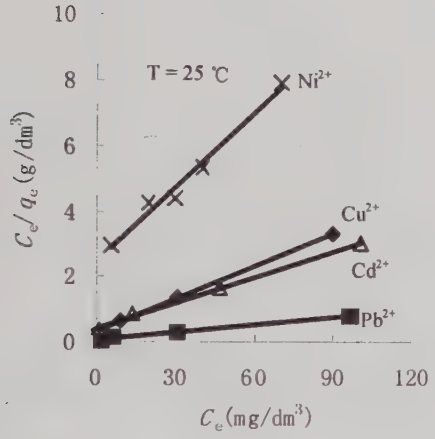

Fig. 3 The (*Ce/qe*) ~ *Ce* curve of metal biosorption by *S. fusiforme*

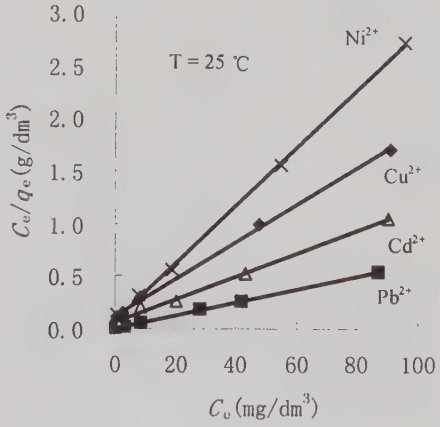

Fig. 4 The (*Ce/qe*) ~ *Ce* curve of metal biosorption by *L. japonica*

are much greater than *S. fusiformes*. The difference in adsorption capacity may be determined by the difference in the chemical composition and structure of these two macroalage. Algin, sodium alginate and mannitol are often extracted from *L. japonica* which has a very thick texture, and is abundant in algae colloid and sodium alginate. While algae are ground into pieces, the cell wall is spoiled and more functional groups are exposed. Adsorptive sites increase and the adsorption capability to metal ions enhances, which leads to the increase in the metal uptake of algae.

Tab. 1 Constants of adsorption thermodynamics to the heavy mental ions

Algae	Metal ion											
	Cu^{2+}			Pb^{2+}			Cd^{2+}			Ni^{2+}		
	Q^0	b	R^2	Q^0	b	R^2	Q^0	b	R^2	Q^0	b	R^2
S. fusiforme	54.35	0.56	0.99	135.14	0.07	0.98	38.46	0.06	0.98	13.19	0.03	0.98
L. japonic	64.94	1.56	0.99	161.30	0.91	0.99	91.74	0.17	0.98	36.50	0.31	0.99

In Tab. 1, the unit of Q^0 is 10^{-3}(m/m), b is dm^3/mg, and R^2 is standard variance(n=5).

Furthermore, the adsorption capacities of *S. fusiforme* and *L. japonica* for these metal ions follow the rule: $Pb^{2+} > Cd^{2+} > Cu^{2+} > Ni^{2+}$, which is not just opportune, but there must be an intrinsic relation to the structure and chemical character of each element. It is reported that with the ionic radius increasing the metal uptake of *Rhizopus arrihizus* also increases[1]. There is still another opinion focusing on the effect of ionic potential on biosorption. Ionic charge associated with ionic radius affects the process of metal ions adsorption and ion exchange. Different ions are diverse in the affinity to absorbent which may be decided by the ionic potential, higher ionic potential, and stronger affinity to organism[2]. Ionic potential can be defined as: $\phi = Z/r$, where Z is the ionic charge, and r is the ionic radius. According to this opinion, there is a contradiction that if the metal ions have a same charge their adsorption capacity need to decrease with the increase of the ionic radius. Nonetheless, in fact the result of our study agrees with neither of these two opinions. In this study, it is implied that the adsorption capacity of these two macroalgae powder for Pb^{2+}, Cd^{2+} and Cu^{2+} decreases with the decrease of the ionic radius, while Ni^{2+} is distinctive, and on this point there have been some reports in some other articles about the particularity: compared with other heavy metal ions, Ni^{2+} is a more resistant infectant, and combines microalgae quite infirmly though they can adsorb other heavy metal ions strongly[3]. Chan *et al.* (1991) found that the % metal uptake of Cu^{2+} in plating wastewater can reach 90 %, but for Ni^{2+} the absorptive ability of *chlrella* can not satisfy anyone[4]. Tsezos *et al.* (1995) also found that the adsorptive ability of a series of micro-algae to heavy metal ions is rather better than Ni^{2+} [5]. This may be the connatural chemical character of Ni^{2+} that makes it form an ion-structure space block in the process of biologic adsorption[6].

2.2 Effect of temperature on the absorption capacity

Figs. 5 and 6 show the biosorption balance curves of *S. fusiforme* and *L. japonica* to Cu^{2+} under different temperatures respectively. According to the Langmuir equation we plot the regression line in Figs. 7 and 8, and list the modulus of Langmuir equation under 35 ℃ in Tab. 2.

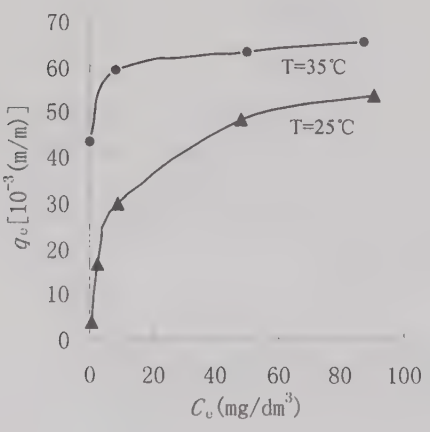

Fig. 5 The adsorption curve of *L. japonica* to Cu^{2+} at different temperatures

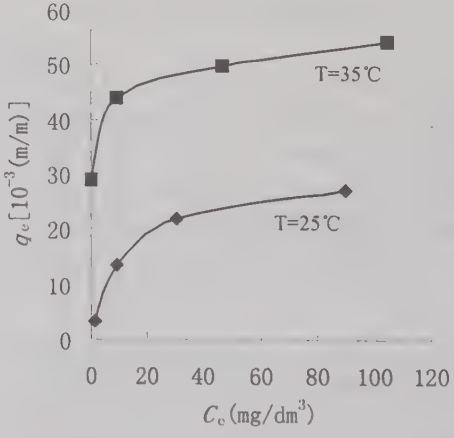

Fig.6 The adsorption curve of *S. fusiforme* to Cu^{2+} at different temperatures

From Fig. 2, we can conclude that with rising of temperature the adsorptive capability of the two algae for Cu^{2+} increases obviously. This changing trend shows that the absorptive process of the two

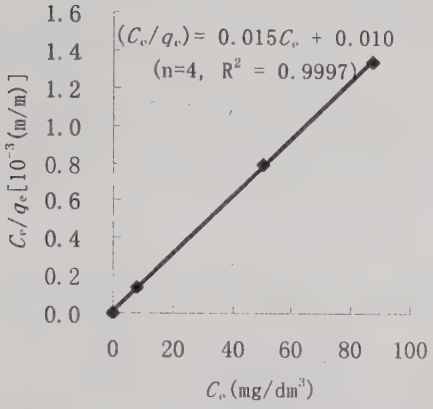

Fig. 7 The adsorption thermodynamic curve of *L. japonica* to Cu^{2+}

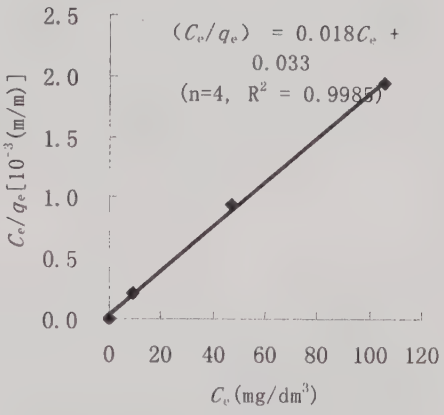

Fig. 8 The adsorption thermodynamic curve of *S. fusiforme* to Cu^{2+}

algae for Cu^{2+} are both endothermic. Based on:

$$b = b_0 \exp(-\Delta H / RT)$$

Where ΔH is the enthalpy variety in the process of adsorption and according to it we can determine the radiative process; b_0 is value of b under 0 K. The adsorption heat of these two algae is 59.5 kJ/mol and 76.8 kJ/mol respectively at 35 ℃. Temperature could affect the algae's adsorption capacity by some factors:

(1) Stability of metal ions in the solution;

(2) Stability of ion complexation between metal ions and alage;

(3) The effect of temperture on the structure of cell wall;

(4) Chemical content on the cell wall partly ionized.

Tab. 2 Some parameters about adsorption equilibrium of *S. fusiforme* and *L. japonica* for Cu^{2+} at 35 ℃

S. fusiforme				*L. japonica*			
C_i	C_e	q_e	C_e/q_e	C_i	C_e	q_e	C_e/q_e
72.6	0.09	29.0	0.003	108.1	0.12	43.2	0.003
118.6	8.90	43.9	0.203	155.5	7.97	59.0	0.135
171.5	47.0	49.8	0.944	207.6	50.1	63.0	0.795
240.3	105.3	54.0	1.950	249.8	87.3	65.0	1.343

The unit of C_i and C_e is mg/dm^3, and C_i is the initial concentration of metal ion. And the unit of q_e and C_e/q_e are 10^{-3} (m/m) and g/dm^3 respectively.

At present, little study has focused on enthalpy variety in the biosorption process. The process of *S. Viridochromogenes* and *C. regularis* fixed by polyacrylate amine absorb the U^{3+} is regarded as a endothermal process, because the adsorptive capacity increases with the rising of temperature[17]; the adsorption capacity of *Z.rumigera* and *R. arrhizus* for Cr^{3+}, Pb^{2+} also increases with the rising of

temperature (0 ~ 45 ℃), and is considered as endothermal reaction[8]; the adsorption for Cu^{2+}, Ni^{2+} reaches maximum at 25 ℃, and when the temperature rises from 25 ℃ to 45 ℃, the adsorption capacity decreases quickly, which is regarded as exothermic reaction; the adsorption capacity of *C. pyrenoidosa* and *S. platensis* for Cu^{2+}, Zn^{2+}, Cd^{2+} and Ni^{2+} increases by a quantity level in the range of 0~60 ℃. Generally, the combination of metal ions and carboxyl is endothermic, and the combination to amido is radiative[9].

3 Result

(1) The adsorption capacity of *S. fusiforme* and *L. japonica* for the four heavy metal ions follow the rule: $Pb^{2+} > Cd^{2+} > Cu^{2+} > Ni^{2+}$;

(2) Temperature influences the adsorption capacity, the biosorption of *S. fusiforme* and *L. japonica* for Cu^{2+} is both endothermic, and the adsorption capacity increases with the rising of temperature (25 ℃, 35 ℃), and the absorptive heat is 59.9 kJ/mol and 76.8 kJ/mol respectively.

(3) Adsorptive capacity of *S. fusiforme* for the four heavy metals Pb^{2+}, Cd^{2+}, Cu^{2+} and Ni^{2+} is all smaller than *L. japonica* when the thermodynamic process of biosorption reaches a balance.

Acknowledgements

We gratefully acknowledge the financial support for this project from the Advanced Technology Fund of Xiamen.

References

[1] Tobin J M, Copprt D J, Neufeld R J *et al.* Uptake of Metal ions by *Rhizopus Arrihizus* Biomass. Environ Microbiol, 1984,47: 821-824.

[2] Mattuschka B, Straube G. Biosorption of Metals by Waste Biomass. J Chem Tech Biotechnol, 1993, 58: 57-63.

[3] Wong J P K, Wong Y S, Tam N F Y *et al.* Nickel biosorption by Two Chlorella Specices. *C.Vulgaris* (A Commercial Species) and *C. Miniata* (A Local Isolate). Bioresource Technology, 2000, 73: 133-137.

[4] Chan S S, Chow H, Wong M H, *et al.* Microalgae as Biosorbents for Treating Mixture of Electroplating and Sewage Effluent. Biomed Environ Sci., 1991, 4: 250-261.

[5] Tsezos M, Remoudaki E, Angelatou V *et al.* A Study of the Effects of Competing Ions on the Biosorption of Metals. Int Biodeter Biodeg, 1996, 38: 19-29.

[6] Tsezos M, Remoudaki E, Angelatou V *et al.* A Systematic Study on Equilibrium and Kinetics of Biosorptive Accumulation.- the Case of Ag and Ni. Int Biodeter Biodeg, 1995, 35: 129-153.

[7] Nakajima A, Horikoshi T, Sakaguchi T *et al.* Recovery of Uranium by Immobilized Microorganism. Eur J Appl Microbiol Biotechnol, 1982, 16: 88-94.

[8] Sag Y, Kutsal T. Determination of the Biosorption Heats of Heavy Metal Ions on *Zoogloea Ramigera* and *Rhizopus Arrhizus*. Biochemical Engineering Joural, 2000, 6: 145-151.

[9] Bedell G W, Darnall D W. Immobilizaion Biosorbent of Nonviable Algal Biomass for the Recovery of Metal Ions. Boea Raton, CRC Press, 1990, 314-326.

Calculation of Environmental Capacity of Petroleum Hydrocarbon in Jiaozhou Bay*

Li Keqiang (李克强), Wang Xiulin (王修林), Deng Ningning (邓宁宁), Shi Xiaoyong (石晓勇), Zhu Chenjian (祝陈坚), Han Xiurong (韩秀荣), Hu Haiyan (胡海燕)
College of Chem. & Chem. Engineering, Ocean University of China, Qingdao 266003, *Shandong, China*

Abstract The method has been established to calculate the environmental capacity (EC_0), surplus environment capacity (SEC_0) of water with respect to marine petroleum hydrocarbons associated with oil (PHAOs) and the self-purification capacity (SPC_0) of main self-purification process to PHAOs in the Jiaozhou Bay, China, according to the dynamic model for distribution of marine PHAOs among multiphase environments. The variation of concentration of PHAOs in the Jiaozhou Bay is well simulated by the dynamic model. Based on the model, the EC_0, SEC_0 of water with respect to PHAOs in the Jiaozhou Bay were calculated during the last 10 years under the first-class and second-class quality standard requirement, according to SPC_0 of main self-purification process to PHAOs. The results show that about 200 tons of PHAOs could be discharged into the Jiaozhou Bay for maintaining the first class seawater quality standard, and about 600 tons of PHAOs for the second class seawater quality standard later.

Keywords petroleum-hydrocarbon; Jiaozhou Bay; environmental capacity; self-purification capacity; kinetic model

Although marine environmental capacity has been studied by many scholars[1~3] in different countries, no published reports on the calculation method have been mentioned. Actually, the environmental capacity is subjected to the self-purification processes in the coastal area, such as physical processes, volatilization processes, biological processes, and geo-chemical processes. The environmental capacity with respect to petroleum hydrocarbon associate with oil (PHAOs) is only discussed in theory for Chinas coastal area[4]. Up to now there is no published report on the calculation of environmental capacity with respect to PHAOs and covering all the self-purification processes for Chinas coastal area. Thus, the national department of marine environment management subjectively constitutes the total discharge project of PHAOs to the sea, only based on the seawater quality standards and the measured data of PHAOs concentration in the seawater. Therefore, the method has been established to calculate the environmental capacity (EC_0) of water with respect to petroleum hydrocarbon associated with oil in the Jiaozhou Bay, China, according to the basic principle[5~7] of dynamic model for distribution of marine contamination among multiphase environments.

1 Dynamic model for distribution of marine PHAOs among multiphase environments in the Jiaozhou Bay

The environmental capacity (EC_0) of water with respect to marine PHAOs could be defined,

Received on December 18, 2003
* Supported by: the National Natural Science Foundation of China projects (NSFC-40136020, NSFC-40376033); the National Basic Research Priorities Programme (2001CB409703); the Key Project of Chinese Ministry of Education (No.01110); Shandong Nature Science Foundation projects (L2000E01); and Qingdao Green Olympic Games Project.

according to the basic concept of environmental capacity[6], *i.e.*, the discharged amount of PHAOs in a period of time, when PHAOs concentration in seawater reaches certain quality standard (such as the national seawater quality standards of China) without any marine ecological disaster. When the PHAOs is transported to the sea by rivers, ships and atmospheric sedimentation[8], it is subjected to a variety of physical, geo-chemical, chemical and biological processes of self-purification of water with respect to the PHAOs, including processes that may be the physical self-purification process such as transport to the out sea by the water flow and volatilization from water to atmosphere, the biological self-purification process such as biodegradation by microorganism and bio-concentration by phytoplankton and other aquatic organisms as well as transfer from lower to higher trophic levels in food-webs, the chemical self-purification process such as photolysis and chemical oxidation, and the geo-chemical self-purification process such as adsorption by suspended and bottom sediments[9]. Therefore, a dynamic model for distribution of marine PHAOs among multiphase environments in the Jiaozhou Bay (Figure 1) is proposed, according to the basic principle[5~7] of dynamic model for distribution of marine contamination among multiphase environments, which is made up of 6 compartments, including those of phytoplankton bioconcentration (PPT), suspended sediment adsorption(SS), microorganism biodegradation (MO), atmospheric volatilization (ATM), PHAOs input (Oil Input) and transport to the out sea by the water flow (Oil Output).

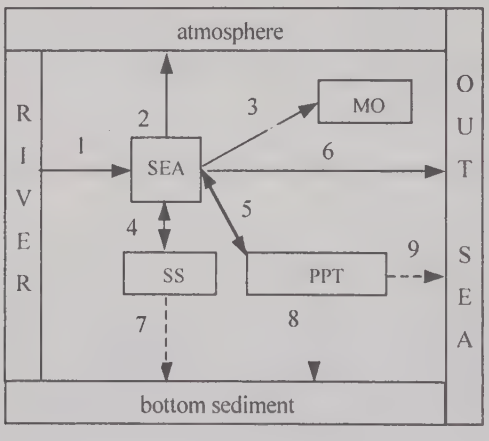

Fig. 1 Dynamic conception model for distribution of petroleum hydrocarbon among seawater, plankton, suspended particles and bottom sediment, animalcule, atmosphere in the Jiaozhou Bay

Where, "1" represents input of PHAOs, "2" represents volatilization processes, "3" represents degregation biodegradation, "4" represents sorption, "5" represents bioconcentration, "6","9" represent transport to the out sea by the water flow, "7" represents sedimentation, and "8" represents decease.

The self-purification capacity (SPC_O) of PHAOs can be calculated first, based on the dynamic model, where the self-purification capacity is the removal amount of PHAOs from certain water area in a fixed period by physical, chemical, biological, geochemical, and other self-purification processes.

$$\dot{SPC}_O = \frac{A^0 - A}{t - t_0} \tag{1}$$

Where, A^0 represents the initial total amount of PHAOs in the study sea area, A represents the final

total amount of PHAOs in the study sea area, t_0 and t represent the initial and final time. The degree of PHAOs removed is subjected to the self-purification processes, thus:

$$SPC_O = SPC_{phy} + SPC_{geochem} + SPC_{chem} + SPC_{bio} \quad (2)$$

$$SPC_{phy} = SPC_{outw} + SPC_{atm} \quad (3)$$

$$SPC_{bio} = SPC_{bd} + SPC_{pp} \quad (4)$$

Where SPC_{phy} represents the physical self-purification capacity, including self-purification capacity such as transport to the out sea by the water flow (SPC_{outw}) and volatilization from water to atmosphere (SPC_{atm}); $SPC_{geochem}$ represents the geo-chemical self-purification capacity, including adsorption by suspended and bottom sediments (SPC_{ss}); SPC_{chem} represents the chemical self-purification capacity, and SPC_{bio} represents the biological self-purification capacity, including biodegradation self-purification capacity (SPC_{bd}) and bio-concentration self-purification capacity by phytoplankton (SPC_{pp}). When SPC_O is larger than zero, the PHAOs is removed from the study water area, and vice versa. Furthermore, to assess the contribution of the processes to the self-purification of water with respect to PHAOs in a certain period of time, the relative self-purification capacity, SPC_O %, is defined as follows:

$$SPC_{geochem}\% = \frac{SPC_{geochem}}{SPC_O} \times 100\% = \frac{SPC_{ss}}{SPC_O} \times 100\% \quad (5)$$

$$SPC_{bio}\% = \frac{SPC_{bd} + SPC_{pp}}{SPC_O} \times 100\% \quad (6)$$

$$SPC_{phy}\% = \frac{SPC_{atm} + SPC_{outw}}{SPC_O} \times 100\% \quad (7)$$

$$SPC_{atm}\% = \frac{SPC_{atm}}{SPC_O} \times 100\% \quad (8)$$

$$SPC_{outw}\% = \frac{SPC_{outw}}{SPC_O} \times 100\% \quad (9)$$

$$SPC_{bd}\% = \frac{SPC_{bd}}{SPC_O} \times 100\% \quad (10)$$

$$SPC_{pp}\% = \frac{SPC_{pp}}{SPC_O} \times 100\% \quad (11)$$

$$SPC_{ss}\% = \frac{SPC_{ss}}{SPC_O} \times 100\% \quad (12)$$

So that a higher value of SPC_O % indicates a greater contribution of the processes to self-purification at that time, and vice versa.

Based on the conceptual model (Fig. 1), PHAOs removed from a certain sea area by different self-purification processes results in the environmental capacity (EC_O). Thus, the standard self-purification capacity, SPC_O (s) can be defined as the SPC when pollutant concentration in seawater reaches certain quality standard without any marine ecological disaster. Accordingly, EC_O is the input amount of

PHAOs to the targeted water area in the corresponding SPC(s) condition. Based on this, the surplus environmental capacity (SEC_O) can be calculated, which is the differences between marine EC_O and the actual input amount of PHAOs under given conditions:

$$SEC_O = EC_O - Q_O \quad (13)$$

Where Q_O represents the actual input amount of PHAOs per year and SEC_O represents the surplus capacity of PHAOs in the study water area under given conditions. When the SEC_O value is larger than zero, it means that more PHAOs can be accepted in the study sea area, and vice versa.

2 Results and discussion

2.1 Model simulation result

As shown in Figure 2, the PHAOs concentration was higher than 50 mg/m^3 from 1991 to 1995, then decreased gradually annually to about 20 mg/m^3. Based on the conceptual model (Figure 1), it was simulated with Modelmaker 4.0 software. And model simulation is in good agreement with the measured data on the annual variation of PHAOs mean concentrations in water in the Jiaozhou Bay from 1991 to 1999 (Figure 2). Thus, based on the equations (1) ~ (12), SPC_O, SPC% and SPC_O(s) for different seawater quality standards could be calculated respectively. Then, EC_O, and later SEC_O could be calculated based on the equation (13).

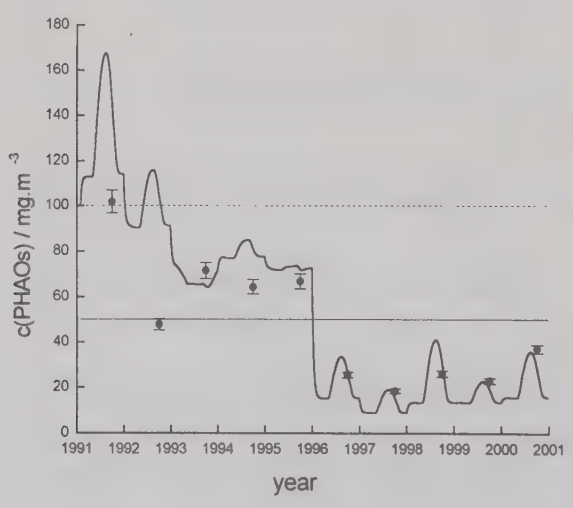

Fig. 2 Annual Variation of Petroleum Hydrocarbon Concentration (●)in the Jiaozhou Bay in 1991—2000 and the Simulation Result of the Model (—)

Where, "-" represents the first Class Seawater Quality Standard," --- " represents the second Class Seawater Quality Standard

2.2 Self-purification capacity (SPC_O) and relative self-purification capacity (SPC_O%)

Annual variation of SPC_O of PHAOs in the Jiaozhou Bay from 1991 to 1999 is described in Figure 3, and the result indicates that SPC_O was generally higher than 500 t/a from 1991 to 1995, then

decreased gradually annually to 180 t/a, which confirms to the variation trend of PHAOs concentration in the Jiaozhou Bay.

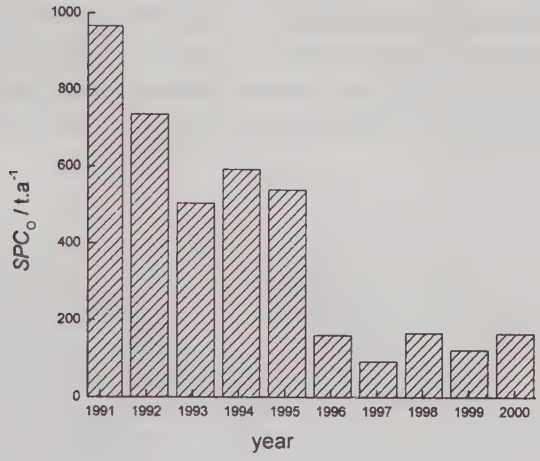

Fig. 3 Annual Variation of Self-purification Capacity (SPC_o) of Petroleum Hydrocarbon in the Jiaozhou Bay in 1991—2000

Based on the model, the physical, chemical, biological and geo-chemical relative self-purification capacities of PHAOs in the Jiaozhou Bay are calculated, and the result shows that the relative self-purification capacity for volatilization to the atmosphere, the biodegradation and transport to the out sea by the water flow are 40, 32 and 25 % respectively, totaling up to 97 %. It can be concluded from the results that these three processes are the main ways of self-purification for PHAOs in the Jiaozhou Bay. By contrast, the relative self-purification capacity of bioconcentration is only 3 %, and the relative geo-chemical and chemical self-purification capacity nearly reaches zero. So the contribution of the processes of bioconcentration to the self-purification of PHAOs in the Jiaozhou Bay by PPT, geo-chemical and chemical self-purification capacities can be neglected.

2.3 Standard self-purification capacity (SPC_o(S)), environmental capacity (EC_o) and surplus environmental capacity (SEC_o)

Based on the model, the standard self-purification capacity such as SPC_o (s) I , SPC_o(S) II and SPC_o(S)III and environmental capacity such as EC_o I , EC_o II and EC_oIII of PHAOs in the Jiaozhou Bay are calculated under the condition of first, second and third class national seawater quality standard requirement. The result indicates that EC_o I is 432 t/a, EC_o II is 864 t/a, and EC_oIII is 3 420 t/a. And SPC_o(s) is somewhat lower than EC_o at that time, for the self-purification of PHAOs was mainly dependent on the processes of volatilization, biodegradation and transport to the out sea by the water flow, while little is released by organisms, suspended matter and other processes.

Annual variations of SEC_o of PHAOs under the condition of different seawater quality standards in the Jiaozhou Bay from 1991 to 1999 are showed in Figure 4. The result indicates that $SEC_o < 0$ in most years from 1991 to 1995 for the first class seawater quality standard requirement, which means the actual PHAOs input amounts exceeds the environmental capacity, while $SEC_o > 0$ since 1995, which is under the environmental capacity. Based on the second class quality standard, $SEC_o > 0$ indicates that the

actual PHAOs input amounts were under the environmental capacity from 1991 to 1999 except 1991. Thus we can conclude that the first class seawater quality standard could be satisfied and more PHAOs can be accepted in the Jiaozhou Bay. Furthermore, about 200 tons of PHAOs could be discharged into the Jiaozhou Bay for the first class seawater quality standard requirement, and about 600 tons of PHAOs for the second class seawater quality standard later. It should be pointed out that the results have been calculated regarding the Jiaozhou Bay as a whole. Seawater quality of some area might be over range according to the standards, such as the east area of Jiaozhou Bay. Mainly the third class national seawater quality standard of China is executed in the east area of Jiaozhou Bay based on the marine functional zoning in Qingdao.

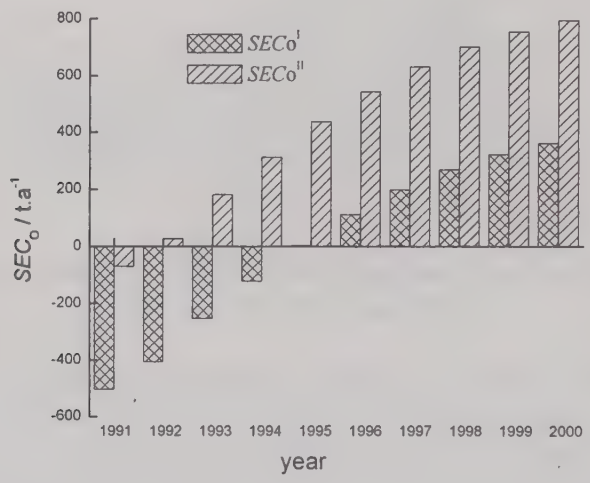

Fig. 4 Surplus Environmental Capacity (SEC_o)of Petroleum Hydrocarbon in the Jiaozhou Bay from 1991 to 2000 relative to the first and second Class Seawater Quality Standards

3 Conclusion

The calculation method has been established for the self-purification capacity (SPC_o) of main self-purification process to PHAOs in the Jiaozhou Bay, China, according to the dynamic model for distribution of marine PHAOs among multiphase environments. Model simulation is in good agreement with the measured data on the annual variation of PHAOs average concentration in water in the Jiaozhou Bay. Then, the self-purification capacity (SPC_o) and the standard self-purification capacity (SPC_o (S)), the environmental capacity (EC_o), surplus environment capacity (SEC_o) of PHAOs under different seawater quality requirements are calculated for the Jiaozhou Bay during the last 10 years. The result shows that the self-purification of water for PHAOs is mainly due to the processes of volatilization, biodegradation and water transportation, the relative self-purification capacities of which are respectively 40 %, 32 % and 25 %. However, the relative PPT, geo-chemical and chemical self-purification capacities of bioconcentration are less than 3 %, whose contribution to the self-purification of PHAOs in the Jiaozhou Bay could be neglected. The environmental capacities of PHAOs are 432, 864 and 3420 t/a separately for the quality requirements of first, second and third class national seawater

quality standards of China. The result indicates that $SEC_O < 0$ in most years from 1991 to 1995 for the first class seawater quality standard requirement, which means the actual PHAOs input amounts exceed the environmental capacity, while $SEC_O > 0$ since 1995, which is under the environmental capacity. From 1991 to 1999 except 1991, $SEC_O > 0$ for the requirement of second class quality standard, which indicates that the actual PHAOs input amounts are under the environmental capacity. About 200 tons of PHAOs could be discharged into the Jiaozhou Bay for maintaining the first class seawater quality standard, and about 600 tons of PHAOs for the second class seawater quality standard later.

References

[1] HORYIA K. Evaluating Method of the Marine Environmental Capacity for Coastal Fisheries and Its Application to Osaka Bay. Marine Pollution Bulletin, 1991, 23: 253-257.

[2] TERTTU M. Regional Marine Environmental Management and the GPA-LBA: Perspectives and the Need for Scientific Purpose. Marine and Coastal Management, 2000, 43(8-9): 713-724.

[3] CHUA Thia-eng. Marine Pollution Prevention and Management in the East Asia Seas: A paradigm Shift in Concept, Approach and Methodology. Marine Pollution Bulletin, 1999, 39(1-12): 80-88.

[4] Ren Xuhe. Evaluating Method of the Environmental Capacity of Petroleum Hydrocarbon. China Offshore Oil and Gas (Engineering), 1994, 6(1): 41-44.

[5] Ye Changming Conception of Multimedia Environment. Advances in Environmental Science, 1995, 3(2): 1-9.

[6] Ye Chang-ming, Lei Zhi-fang, Yan Hai. Dynamic Model of N-(2,4-dimethylphenyl)-N Methyl Formamidine and Other Organic Pollutants in Multimedia Environment. Journal of Environmental Sciences, 1997, 15(2): 1 93-197.

[7] JERTTU L S. Environmental Modeling. New York: John & Sons Inc., 1996, 185-229.

[8] Pu Jiabin. Advances in the Sources of Hydrocarbon in Marine Environment. Marine Environmental Science. 1991, 10(2): 69-73.

[9] WANG Xiulin, AN Yu, ZHANG Jun. Contribution of Biological Processes to Self-purification of Water with Respect to Petroleum Hydrocarbon Associated with No.0 Diesel in Changjiang Estuary and Jiaozhou Bay, China]. Hydrobiologia, 2002, 469: 179-191.

Studies on Biquaternary Ammonium Salt Algaecide for Removing Red Tide Algae*

Liu Jiesheng (刘洁生), Zhang Heng (张 珩), Yang Weidong (杨维东),
Gao Jie (高 洁), Ke Qiong (柯 琼)
Department of Biotechnology, Jinan University, Guangzhou 510632, *Guangdong, China*

Abstract The paper deals with the removal and control of red tide algae, *Phaeocystis globosa* and *Alexandrium tamarense* by biquaternary ammonium salt algaecide. The results show that the efficient concentration of biquaternary ammonium salt to control the two algaes in 96 h is 0.8 mg • L^{-1} and 0.4 mg • L^{-1}, respectively. It is found that biquaternary ammonium salt has high efficiency and longer duration of action in the removal and control of algae. Biquaternary ammonium salt might be an excellent algaecide to control HAB.

Keywords biquaternary ammonium salt, *Phaeocystis globosa*; *Alexandrium tamarense*, red tide

Phaeocystis globosa, one of the most widespread marine Haptophytes, is a newly discovered species of algae in China. During the period from the autumn of 1997 to the spring of 1998, a heavy har mful algal bloom (HAB) of *P. globosal* first occurred in the coastal waters of East China Sea and South China Sea, which caused a great impact on the local aquiculture industry[1, 2]. Since then, this HAB has frequently attacked this area. *Alexandrium tamarense* can produce paralytic shellfish poisoning (PSP) that is dangerous to human beings and mariculture. It is reported that this alga had ever killed a considerable amount of fish and shrimps, even made people poisoned or dead[3, 4]. Its negative impact is growing more and more serious in recent years throughout the world[5, 6]. Therefore, it is very important to find an economical, effective and less eco-impacting method of controlling *P. globosa* and *A. tamarense.*

Quaternary ammonium salts, as disinfecting agents, are widely used in clinic, sanitation, common life, circulating water and so on, due to their eminent characteristics such as stabilization, innocuity, no accumulated effect, and high algaecidal activity in weak alkaline condition[7]. Compared with the routine quaternary ammonium salts, such as monquaternary ammonium salt dodecyl demethyl benzyl ammonium chloride and bactericide isothiozolone[8], biquaternary ammonium salt is more efficient in killing algae, but produces less bubbles. However, so far there seems to be no report about the impact of biquaternary ammonium salt on algae in the literature. The main objective of this study is to gain the information that biquaternary ammonium salt might use as an algaecide to control HAB, through the investigation of the removal of *P. globosa* and *A. tamarense* by the algaecide.

1 Materials and method

1.1 Materials and Reagents

P. globosa (Shantou stain) is provided by the Institute of Hydrobiology of Jinan University in

Received on October 10, 2003

*Supported by grants from the National "973" Program (2001CB409710), Key Project of Nature Science Foundation of Gangdong Province (021168) and Project of Science and Technology of Guangzhou(2002J1-C0011)

Guangzhou, China. *A. tamarense* (HK strain) is obtained from the Environmental Science Research Centre, Xiamen University, China. Biquaternary ammonium salt 2 - (2-phenoxyl ethoxyl) ethyltrimethyl ammonium chloride is purchased from the Wujin Water Stabilizer Factory in Nanjing University of Chemical Engineering.

1.2 Method

1.2.1 Algae culture

The algae cultures are incubated at (21±1) ℃ with a 12: 12 h cycle at an illuminating incubator, in f/2 medium for *P. globosa* and in k media for *A. tamarense*, prepared with the sterile-filtered man-made seawater (salinity 33) with 0.2 μ m filter[9]. All the flasks containing algae are shaken twice everyday. Algal cells are counted using a 0.1 mL counting chamber under an inverted microscope.

1.2.2 Removal effect of biquaternary ammonium salt

To a series of conical flasks containing 100 mL of alga in exponential phase, quaternary ammonium salts of different concentrations are added. The flasks are incubated as mentioned above and agitated daily. Optical density (OD) of cultures is measured after 24, 48, 72, 96 and 120 h, respectively at 680 nm while changes in algal morphology are observed and cell density is counted to learn the removal mechanism of biquaternary ammonium salt on algae cells[10]. The tests are carried out in triplicate, and the culture without treatment is used as control.

2 Results and Discussion

2.1 Removal effect of biquaternary ammonium salt on *P. globosa*

2.1.1 Removal effect of the biquaternary ammonium salt of different concentration on *P. globosa*

To the flasks containing 100 mL of *P. globosa*, 2.0, 1.5, 1.0, 0.9, 0.8, 0.7, 0.6, 0.4 and 0.2 mg • L^{-1} of biquaternary ammonium salt are added when theinitialcelldensityof *P. globosa* is 5.8×10^{8} cells • L^{-1}. The effect of biquaternary ammonium salt on *P. globosal* after three days is showed in Fig. 1.

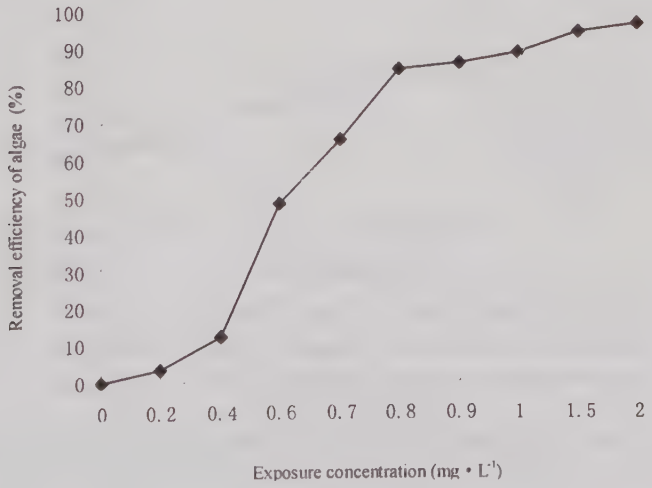

Fig. 1 Removal efficiency of *Phaeocystis globosa* at different biquaternary ammonium salt concentrations

There is a marked correlation between the removal efficiency on *P. globosa* and the concentration of biquaternary ammonium salt. The higher the concentration of biquaternary ammonium salt is, the better the removal efficiency on *P. globosa* is. When the concentration of biquaternary ammonium salt is less than 0.8 mg • L^{-1}, the removal efficiency of algae is low after three days. However, when the concentration is higher than 0.9 mg • L^{-1}, the removal efficiency of algae is up to 80 %.

During the experiment, the change in the shape of alga was observed under an inverted microscope. When the concentrations of algaecide were higher than 1.5 mg • L^{-1}, the cultures turned colorless after 1 d; when the concentrations were 1.0, 0.9 and 0.8 mg • L^{-1} respectively, the cultures became nearly achromatous; and when the concentrations were 0.7, 0.6 and 0.4 mg • L^{-1} respectively, the cultures were light filemot with some floccules at the bottom. Some of the algal cells flocculated into conglomeration and deposited in all the treatments, which might be a cause of removal effect of biquaternary ammonium salts on alga. Many papers showed[7, 8] that the biquaternary ammonium salt carried positive charges, but algae cells had negative charges. It could be predicted that the charge attraction and surfactivity might be responsible for the conglomeration.

2.1.2 Removal effect of biquaternary ammonium salt at different time

From Fig. 2, it can be seen that the removal effect on algae is weak and temporary, the most removal efficiency is only 72 %, and, what's more, the efficiency drops in 3 days when algaecide concentration is less than 0.8 mg • L^{-1}. However, when the concentration is above 0.8 mg • L^{-1}, the removal effect is strong and persistent. The results show that the efficient concentration of biquaternary ammonium salt to control *P. globosa* in 96 h is 0.8 mg • L^{-1}.

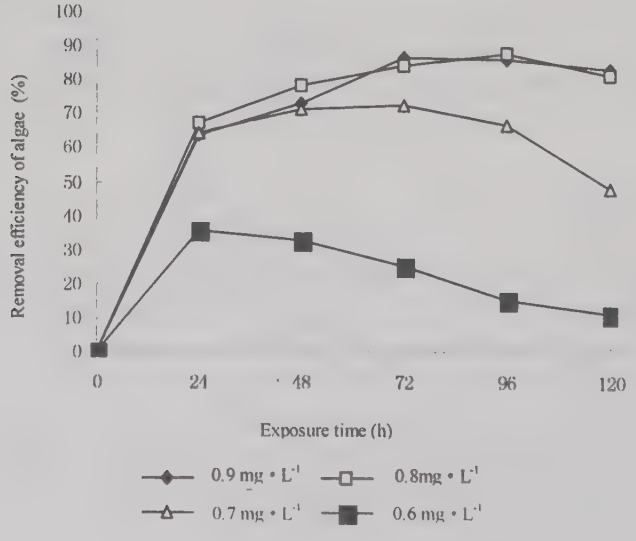

Fig. 2 Removal efficiency of biquaternary ammonium salt at different time

2.2 Removal effect of biquaternary ammonium salt on *A. tamarense*

2.2.1 Removal effect of the biquaternary ammonium salt of different concentrations on *A. tamarense*

To the flasks containing 100 mL of *A. tamarense*, 2.0, 1.0, 0.8, 0.7, 0.6, 0.5, 0.4, 0.3, 0.2 mg • L^{-1}, are added when the initial cell density is 7.0×10^6 cells • L^{-1}. The efficiency of biquaternary ammonium salt on *A. tamarense* 3 days after the treatment is demonstrated in Fig. 3.

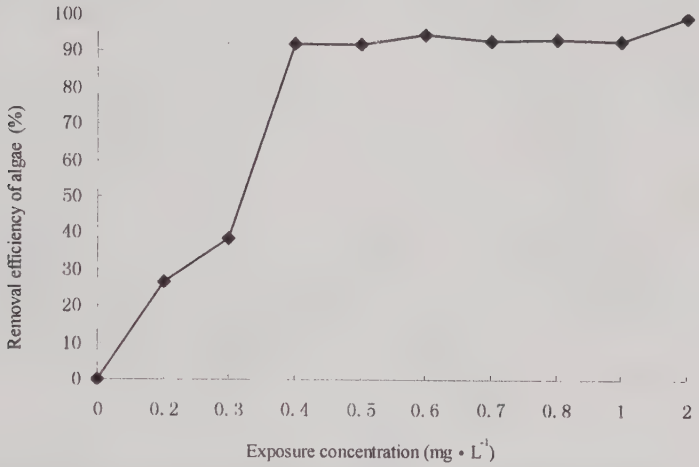

Fig. 3 Removal efficiency of *Alexandrium tamarense* at different biquaternary ammonium salt concentrations

In Fig. 3, removal efficiencies of biquaternary ammonium salt on *A. tamarense* are demonstrated. Similar to *P. globosa*, *A. tamarense* can be removed by the alagecide. When the concentration of biquaternary ammonium salt is higher than 0.4 mg • L^{-1}, the removal efficiency on alga is up to 80 % after 72 h. In contrast, when the concentration is 0.3 mg • L^{-1}, the removal efficiency of alga is only 38.5 %. The changes in color of the cultures occur in all the treatments. When the concentration of algaecide is higher than 0.6 mg • L^{-1}, the solution turns colorless and flocculated deposition appears at the bottom. When the concentration of algaecide is 0.4 mg • L^{-1}, the cultures are lightened and the living cell disappears, but conglomeration emerges. The algal cells in conglomeration are turgor and ruptured finally.

2.2.2 Removal effect of biquaternary ammonium salt at different time

It can be seen from Fig. 4 that when algaecide concentration is 0.3 mg • L^{-1}, the removal effect on algae is weak, the most removal rate is less than 60 % and the removal effect lasts only for 72 h. However, when the concentration is above 0.4 mg • L^{-1}, the removal efficiency is about 80 % in 96 h. The algae cells are replaced by some white spherules after 120 h. Living algae cells do not emerge even when the cultures have been incubated for a few days. In contrast, when the concentration is less than 0.4 mg • L^{-1}, the color of algae gradually renews and the number of cell increases. The results show that the efficient concentration of biquaternary ammonium salt to control *A. tamarense* in 96 h is 0.4 mg • L^{-1}.

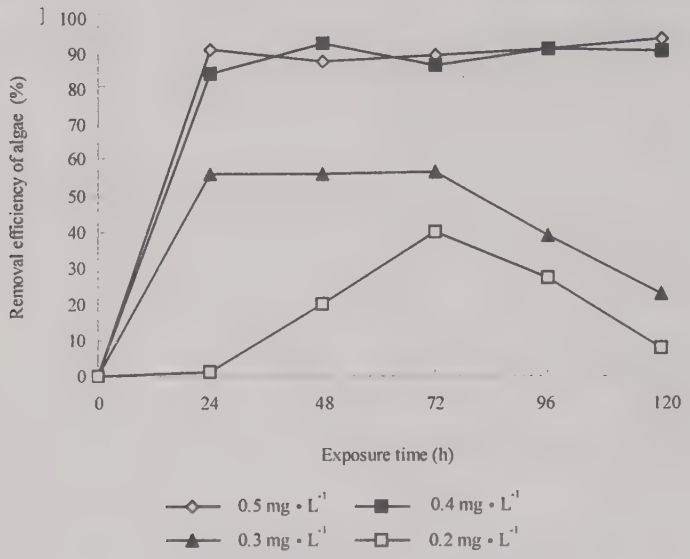

Fig. 4 Removal efficiency of biquaternary ammonium salt at different time

3 Conclusions

1) The efficient concentration of biquaternary ammonium salt to control *P. globosal* in 96 h is 0.8 mg • L^{-1}.

2) The efficient concentration of biquaternary ammonium salt to control *A. tamarense* in 96 h is 0.4 mg • L^{-1}.

3) The mechanism of algae removal of monquaternary ammonium salt could be attributed to the charge attraction and surfactivity. Quaternary ammonium salts carry positive charge in the water, so they have a tendency to cohere on the surface of algal cells with negative charges. The algaecide coheres on the algal cell wall filtered gradually into phospholipid bimolecular layer. As a result, membrane permeability increases, which causes exosmosis of cell contents, concreting of protein, denaturation of enzyme and structural protein, destruction of metabolism, and ultimately, death of cells[7]. The removal effect of biquaternary ammonium salt is stronger than that of monquaternary ammonium salt due to the synergic effect of two quaternary ammonium ions in biquaternary ammonium salt[8].

4) Biquaternary ammonium salt has high efficiency, longer duration of action in the removal and control of algae, and might be an excellent algaecide to control HAB.

References

[1] Cheng J F, Xu N, Jiang T J, *et al.*. A Report of *Phaeocystis globosa* Bloom in the Coastal Waters of Southeast China. *J Jinan Univ* (Nat Sci), 1999, 20(3): 124-129.

[2] Chen Y Q, Wang N, Zhang P, *et al.*. Molecula Evidence Identifies Bloom-forming *Phaeocystis* (Prymnesiophyta) from Coastal Waters of Southeast China as *Phaeocystis globosa*. *Biochem Systematics and Ecology*, 2002, 30 (1): 15-22.

[3] Jiang T J, Yin Y W, Lou Y M, *et al.*. Paralytic Shellfish Toxins in Shellfish from Daya Bay and Dapeng Bay. *Mar Environm Sci*, 2001, 19(2): 1-5.

[4] Lin Y S. Red Tide Caused by a Marine Toxic Dinoflagellate, *Alexandrium Tamarensis*(Lebour) Baleon, in Shrimp Ponds in Xiamen. *J Oceanography in the Taiwan Straits*, 1996, 15(1): 16-18.

[5] Dale B, Yentach C M. Red tide and Palalytic Shellfish Poisoning. *Oceanus*, 1998, 21: 41-49.

[6] Hallegraeff G M. A View of Harmful Algal Blooms and Their Apparent Global Increase. *Phycologia*, 1993, 32: 75-79.

[7] Xue W Q, Xue G B. Progress of Studies on Quaternary Ammonium Cationic Surfactant Disinfector. *Chin J nosocomiol*, 2002, 12(8): 634-636.

[8] Wang C. A Sterilization Test for the Bactericide of Biquaternary Ammonium Salt. *Ind Water Wastewater*. 2000, 31(6): 23-24.

[9] Yan T, Zhou M J, Qian P Y. Study on the Combined Effect of Temperature, Salinity and Irradiance on the Growth of Dinoflagellate *Alexandrium Tamarense*. *Acta Oceanol Sin*, 2002, 24(2): 114-120.

[10] Shen P P, Wang ZH, Qi Y Z, *et al.*. An Optical Density Method for Determination of Microalgal Biomass. *J Jinan Univ* (Nat Sci), 2001, 33(3): 115-119.

Statistical Study of Trace Elemental Concentrations in Major Types of Organisms from Typical Chinese Coastal Waters

Guo Weidong (郭卫东)[1,2] Hu Minghui (胡明辉)[1] Shi Qian (石 谦)[1] Yang Yiping (杨逸萍)[1]
1 *Department of Oceanography, Xiamen University, Xiamen 361005, Fujian, China*
2 *Key Laboratory for Marine Environmental Science of Ministry of Education, Xiamen 361005, Fujian, China*

Abstract Frequency distribution characteristics of trace elements Fe, Mn, Zn, Cu, Sr and Ba are studied for the marine organisms collected from typical Chinese coastal waters and compared with those of major elements Ca and Mg. Nearly all the distributions for trace elements in macroalgae, benthic molluscs, crustaceans, cephalopods and different tissues of fish (muscle, liver and bone) are found to show some degree of positive skewness, indicating a relatively large number of marine organisms with low concentrations for a particular element and only a few organisms with disproportionately high concentrations. Their distribution types are generally logarithmic normal distribution or nearly logarithmic normal distribution. Distribution of Ca is similar to that of trace elements, while Mg shows normal distribution. Average elemental concentrations of major types of organisms are calculated based on their frequency distributions.

Keywords Marine organisms, trace elements, frequency distribution, Chinese coastal waters

Introduction

Trace elements are the key constituents of enzyme and other proteins in marine organisms and play a significant role in life process. However, the distribution of trace elements in marine organisms shows considerable variability due to the influence of biological factors such as taxonomic differences, size, sex, growth period and environment factors such as season cycles and microhabitat[1~3]. In addition, randomicity in sample collection is also an important factor which cannot be ignored. As a result, the frequency distribution of the concentrations of a particular element in certain tissues of organisms are rarely normal and the degree of variability for a distribution may vary from case to case[4]. Hence the study on frequency distribution of the concentrations of trace elements will help to delineate a general distribution characteristics of these elements in marine organisms.

The goal of the present study is to present the frequency distribution of trace elements Fe, Mn, Zn, Cu, Sr, Ba and major elements Ca, Mg in the major types of organisms collected from the temperate (Dalian and Qingdao), the subtropical (Xiamen) and the tropical sea areas along Chinese coastal waters. In order to understand the general levels of trace elements concentrations in marine organisms from Chinese coastal waters, basic statistical parameters such as average value, standard deviation and coefficient of variation (*Cv*) of these elements in each type of organisms are calculated based on their frequency distribution characteristics.

Received on June 5, 2003
Foundation: Special Doctoral Research Foundation of the Ministry of Education (No. 96038412)

1 Materials and methods

1.1 Sample collection and pre-treatment

The samples were collected from four typical places along Chinese coastal waters: Dalian (~39° N) and Qingdao (~36° N) in August 1997, Xiamen (~24° 30′ N) in May 1998 , and Sanya (~18° N) in November 1998. The samples collected from each place are as follows: Dalian: 6 macroalgae species (*Porphyra* sp., *Sargassum* sp., *etc.*), 7 benthic molluscs species (*Patinopecten yessoensis, etc.*), 3 cephalopods species (*Todarodes pacificus, etc.*), 5 crustaceans species (*Portunus trituberculatus* , *etc.*), 32 fish species (*Scomberomorus niphonius, etc.*); Qingdao: 6 macroalgae species (*Laminaria japonica Areseh., etc.*), 5 benthic molluscs species (*Chlamys farreri, etc.*), 2 cephalopods species (*Todarodes pacificus, etc.*), 2 crustaceans species (*Portunus trituberculatus, etc.*), 16 fish species (*Scomberomorus niphonius, etc.*); Xiamen: 3 macroalgae species (*Porphyra sp., etc.*), 2 benthic molluscs species (*Atrina pectinata, etc.*), 3 cephalopods species (*Loligo chinensis, etc.*), 2 crustaceans species (*Portunus pelagicus, etc.*), 24 fish species (*Formio niger, etc.*); Sanya: 1 macroalgae species (*Sargassum* sp., *etc.*), 9 benthic molluscs species (*Perna viridis, etc.*), 4 cephalopods species (*Ommastrephes bartrami, etc.*), 5 crustaceans species (*Portunus pelagicus, etc.*), 33 fish species (*Alectis indica, etc.*).

The macrophyte samples are washed with de-ionized water to clear away any material absorbed onto the surface. The animal samples are dissected into several tissues and organs with plastic knife and tweezers which have been soaked in nitric acid (suprapur grade) leaching solution (1:4) for at least 7 days and washed three times with double-distilled water before use. Muscle, liver and bone tissue from fish, body muscle from cephalopods and soft tissue from benthic molluscs and back muscle of crustaceans are taken and washed with double distilled water immediately. All tissues are dried at 60°C for 48 h to obtain a constant weight.

1.2 Sample digestion and analysis

0.2 ~ 0.3 g of each sample is weighed into a Teflon digestion vessel. After 4 mL nitric acid (suprapur grade) and 2 mL hydrogen peroxide (analytical grade) are added, the Teflon vessel is sealed and then heated in an oven at 150℃ for about 5 h. When the sample is cooled to room temperature, the sample liquid is transferred and diluted into 25 mL with double distilled water.

Trace element concentrations are determined with the inductively coupled plasma atomic emission spectrometry (ICP-AES, E984, Hilger Corp., England). The optimized operation conditions are as follows: incident power, 1.1 kw; carrier, plasma and auxiliary gas, 14.0, 0.8, and 0.4 L/min, respectively. The relative standard deviation of each sample is < 5 %. Two certified reference materials of P. R. China, mussel (GBW08571) and pork liver (GBW08551), are analyzed to determine the accuracy of the methods.

1.3 Classification of statistical units

The samples can be classified into 5 types: macroalgae, benthic molluscs, cephalopods, crustaceans and fish, while fish can be further classified into different tissues — muscle, liver and bone. Accordingly, there are 7 statistical units, as showed in Table 1.

Tab. 1 Skewness of frequency distribution of element concentrations in marine organisms

Statistical Units	n	Fe	Mn	Zn	Cu	Sr	Ba	Ca	Mg
macroalgae	16	0.55	0.26	1.21	0.77	-	0.79	-	-
benthic molluscs	25	1.56	1.34	1.29	3.84	1.25	-	1.42	-
cephalopods	15	1.32	0.83	0.86	1.44	1.19	-	1.41	-
crustaceans	10	0.87	1.39	0.68	0.84	0.72	-	-	-
fish muscle	105	5.28	-	1.84	-	5.56	-	3.89	-0.50
Fish liver	28	3.17	1.81	0.39	2.65	3.12	-	2.54	0.75
fish bone	76	3.40	2.55	3.20	-	-	-	-	

2 Results and discussion

2.1 Skewness of probability distribution of trace element concentrations

Skewness value (*Cs*) reflects degree of deviation from normal distribution of probability distribution of element concentrations. *Cs* equals zero for normal distribution. The bigger the *Cs* is, the greater the degree of deviation from normal distribution will be. It can be calculated from the following expression[5]:

$$Cs = \sum (X_i - AM)^3 / (n \times s^3)$$

where: AM is arithmetic average value; *s* is standard deviation; *n* is number of samples.

The *Cs* values of all trace elements for 7 statistical units are grater than zero (Table 2), *i.e.*, the probability distribution of element concentrations in these types of marine organisms shows some degree of positive skewness rather than normal distribution, indicating that the concentrations of certain trace elements are low in most organisms and only a few organisms have disproportionately high concentrations. This trend is consistent with the observations reported by Lobel *et al.* (1992)[4]. They have studied probability distribution of 27 elements in 11 different types of biological tissues from several hundred samples collected from unpolluted waters and concluded that all elements show a certain degree of positive skewness except the element selenium.

The *Cs* values show a large difference in different types of organisms. The highest *Cs* value is found in the elements of crustaceans and fish tissues, followed by benthic molluscs, while macroalgae have the lowest *Cs* value. This may reflect obvious differences in absorption, accumulation and excretion of elements for different types of organisms during their metabolic process. In addition, even for the same type of organisms, significant variations of the *Cs* value still occur for different elements.

The variation tendency of *Cs* value of the major element Ca is very similar to that of the trace element Sr. Linear regression analysis indicates that the correlation is significant between *Cs* values of Ca and Sr ($r = 0.999$, $p < 0.001$), suggesting the similarity of these two elements in biological process. On the contrary, the *Cs* value of Mg is smaller than that of Ca and Sr, although they belong to the same II_A group in the periodic table of elements, indicating that physiological function of Mg in organisms is distinct from those of Ca and Sr.

Tab. 2 Statistical parameters of element concentrations in major types of organisms from Chinese coastal waters

Statistical units	Element	*n*	Concentration range	Average	*S. D.*	*Cv*	80 % confidence interva
macroalgae	Fe	16	209-2210	597	2.48	1.13	187-1910
	Mn		9.94-151	67.1	44.9	0.67	9.59-125
	Zn		10.4-260	57.6	2.37	1.05	19.1-174
	Cu		1.59-28.5	7.77	2.36	1.04	2.59-23.3
	Sr		ND-598	101*	-	-	-
	Ba		1.63-67.7	13.7	3.34	1.81	2.93-64.0
benthic molluscs	Fe	25	8.29-214	44.5	2.31	1.00	15.3-130
	Mn		0.24-23.1	3.55	3.00	1.53	0.87-14.5
	Zn		22.6-155	61.7	1.48	0.41	37.3-102
	Cu		0.13-72.1	3.11	3.27	1.75	0.68-14.2
	Sr		3.73-32.4	9.88	1.80	0.64	4.65-21.0
	Ba		ND-5.00	0.25*	-	-	-
	Ca		300-3800	934	2.01	0.79	382-2280
crustaceans	Fe	10	8.52-71.5	17.8	3.25	0.77	7.45-42.4
	Mn		0.76-59.6	3.10	3.35	1.82	0.66-14.6
	Zn		99.0-276	141	1.41	0.36	90.4-219
	Cu		6.19-132	26.1	2.39	1.07	8.54-79.7
	Sr		7.86-136	31.8	2.34	1.03	10.7-94.2
	Ba		ND-3.45	0.31*	-	-	-
cephalopods	Fe	15	5.59-128	21.1	2.83	1.40	5.57-80.1
	Mn		0.86-13.9	3.34	2.64	1.25	0.96-11.6
	Zn		19.9-163	63.3	1.79	0.64	30.0-133
	Cu		2.45-48.6	10.7	2.28	0.99	3.73-30.8
	Sr		3.91-28.6	10.8	1.63	0.52	5.76-20.2
	Ba		ND-10.7	0.71*	-	-	-
	Ca		269-2520	838	1.72	0.59	418-1680
fish muscle	Fe	105	0.71- 80.1	11.4	2.48	1.13	3.56 36.5
	Mn		ND-13.2	0.97*	-	-	-
	Zn		5.04-62.2	17.0	1.56	0.47	9.61-29.9
	Cu		ND-12.4	2.00*	-	-	-
	Sr		0.22-9.12	1.59	2.33	1.02	0.54 4.68
	Ba		ND-4.65	0.28*	-	-	-
	Ca		151-1880	456	1.71	0.58	229 908
	Mg		499-1890	1260	264.9	0.21	917-1600

Note: *n* — number of samples, *S. D.* — standard deviation, * — median, units: mg / kg.

2.2 Types of probability distribution of trace element concentrations

Shapiro-Wilk ($3 < n < 50$) and DAgostino ($50 < n < 1000$) normality test methods[5] are applied to examine the types of probability distribution of trace element concentrations in each statistical unit. Normal and logarithmic normal distribution are hypothesized. Any type of probability distribution is thought to be significant when $P < 0.05$. It is found that distribution types of most elements are logarithmic normal distribution or nearly logarithmic normal distribution, except the normal distribution for Mn in macroalgae and Zn in fish liver tissues, and skewness distribution for Zn in fish bone tissues.

Xu Xiaoqing *et al.* (1990) found that the type of probability distribution of As, Cd, Zn in carp from Dongting Lake, Central China was skewness distribution while that of Fe, Cu, Hg, Pb was logarithmic normal distribution[6], suggesting that the type of probability distribution of trace elements in freshwater fish is similar to that of marine organisms, *i.e.* generally not normal distribution. The study on the environmental background level of elements in rivers[7] and soil[8] also reveals that the type of probability distribution of trace elements in river water and soil is generally logarithmic normal distribution or nearly logarithmic normal distribution. These similarities indicate that logarithmic normal distribution or nearly logarithmic normal distribution may be the general characteristic of trace elements in nature.

The probability distributions of major elements Ca and Mg are also different. The type of probability distribution of Mg in fish muscle and liver tissues is normal distribution, as is the case for Mg in freshwater carp[6]. On the contrary, the type of probability distribution of Ca in benthic molluscs, cephalopods, fish muscle and liver tissues is normal distribution. Just like the *Cs* value, the difference in the type of probability distribution for Ca and Mg may be related to the difference of physiological function for these two elements in organisms.

2.3 Statistical parameters of trace element concentrations

The expression of element concentrations in marine organisms should include the central tendency and degree of variation. The statistical methods are different for different probability distributions. The central tendency and degree of variation for logarithmic normal distribution are geometric average and geometric standard deviation and arithmetic average and arithmetic standard deviation, while for skewness distribution, the median is used to express the central tendency. Table 2 lists the calculated basic statistical parameters of trace element concentrations in each statistical group based on the above-mentioned rules. It can reflect the general levels of these elements in marine organisms of Chinese coastal waters since they are collected from the typical Chinese coastal waters.

2.4 Some distribution characteristics of trace element concentrations

2.4.1 Comparison between different taxonomic groups

The variation tendencies of Fe and Mn, Zn and Cu, Sr and Ba are very similar in five taxonomic groups(Table 2), indicating that the distribution of trace elements in marine organisms may be controlled by the intrinsic physico-chemical properties of these elements, since the nature and structure of the 3 pairs of elemental ions are very similar. In addition, the concentrations of Fe, Zn and Sr are generally higher than those of Mn, Cu and Ba, as is the case in seawater. This follows well the abundance law, *i.e.*, for the elements which are similar in physico-chemical properties, organisms will prefer to assimilate those with higher background concentrations.

The decreasing order of Fe and Mn concentrations in different taxonomic groups is macroalgae > benthic molluscs > crustaceans $\approx$ cephalopods > fish muscle. Sr and Ba show a similar order, indicating that enrichment of macroalgae for these elements is very high. Contrary to Fe, Mn, Sr and Ba, the highest Zn and Cu concentrations are found in crustaceans, and the order is crustaceans >

cephalopods > benthic molluscs > macroalgae > fish muscle. The reason is that the respiratory pigment in the blood of shrimps and crabs is Cu-containing haemocyanin[9]. The element concentrations in fish muscle tissues are generally lower than those of the other four groups.

2.4.2 Comparison between different elements in the same group

The concentration order of elements is different for different taxonomic groups. We may take essential elements Fe, Mn, Zn and Cu for example. The Fe concentration is the highest in macroalgae, followed by Zn, Mn and Cu, while the highest concentration is Zn and the order is Zn > Fe > Cu > Mn. Contrary to fish muscle tissue, the Fe concentration is much higher than that of Zn and the order is Fe >> Zn > Cu > Mn.

3 Conclusions

3.1 The frequency distribution curve of trace elements Fe, Mn, Zn, Cu, Sr and Ba in macroalgae, benthic molluscs, crustaceans, cephalopods and different tissues of fish (muscle, liver and bone) from typical Chinese coastal waters is found to show some degree of positive skewness, and their distribution types are generally logarithmic normal distribution or nearly logarithmic normal distribution, indicating a relatively large number of marine organisms with low concentrations for a particular element and only a few organisms with disproportionately high concentrations.

3.2 The distribution of trace elements in marine organisms may be controlled by the intrinsic physico-chemical properties of these elements. The assimilation of trace elements by marine organisms follows the abundance law.

3.3 The highest concentrations of Fe, Mn, Sr and Ba are found in macroalgae, while crustaceans have the highest Zn and Cu concentrations. The element concentrations in fish muscle tissues are generally the lowest.

References

[1] Wu Yulin, Cui Keduo, Zhao Hongru *et al.*. Studies on Trace Metal Concentrations in Invertebrate from Bohai Sea. Oceanologia et Limnologia Sinica, 1986, 17(6): 539-547.

[2] Lee B G, Wallace W G, Luoma S N. Uptake and Loss Kinetics of Cd, Cr and Zn in the Bivalves*Potamocorbula Amurensis* and*Macoma Balthica*: Effects of Size and Salinity. Mar. Ecol. Prog. Ser., 1998, 175: 177-189.

[3] Rainbow P S. Trace Metal Accumulation in Marine Invertebrates: Marine Biology or Marine Chemistry? J. Mar. Biol. Ass. U. K., 1997, 77: 195-210.

[4] Lobel P B, Belkhode S P, Bajdik C *et al.*. General Characteristics of the Frequency Distributions of Element Concentrations and of Interelemental Correlations in Aquatic Organisms. Mar. Environ. Res., 1992, 33: 111-126.

[5] Wu Yi, Li Yongle, Hu Qingju. Applied mathematics statistics. Changsha: National University of Defence Technology Press, 1995, 123-127.

[6] Xu Xiaoqing, Deng Guanqiang, Hui Jiayu *et al.*. A study on relationship between trace element content in fish and its growth. In: Study on the Water Environmental Background Values of Chemical Elements: Geochemical, Biogeochemical Study and Its Analytical Methods in Changjiang River System (Zhang Shen et al eds.). Beijing: Mapping Press, 1990, 132-139.

[7] Yang Jizhong, Xiong Dingguo, Wen Yufang *et al.*. The Primary Research of the Water Environmental Background Values and the Feature of Twelve Metals Elements in the Minjiang-Tuojiang River. In: Study on

the Water Environmental Background Values of Chemical Elements: Geochemical, Biogeochemical Study and Its Analytical Methods in Changjiang River System (Zhang Shen *et al.* eds.). Beijing: Mapping Press, 1990, 25-43.

[8] Wang Yun, Wei Fusheng. Elemental Chemistry of Soil Environment. Beijing: China Environmental Science Press, 1995, 289-318.

[9] Du Lanshan, Lai Wei, Deng Xuehuai *et al.*. Invertebrate Zoology. Shanghai: East China Normal University Press, 1989, 262.

Harmful Ciliates and Dominant Genus in Culture Ponds of Young Abalone

Huang Jianrong (黄建荣), Xu Runlin (徐润林), Liao Jiayi (廖家遗)
School of Life Sciences, Zhongshan University, Guangzhou 510275, *Guangdong, China*

Abstract By using the methods of qualitative and quantitative analysis, the species composition and dominant genus of harmful ciliates in young abalone culture ponds are studied. Totally 68 species of ciliates, belonging to 3 classes, 16 orders and 46 genus, are found. The dominant ciliate species are *Aspidisca leptaspis, Vorticella* sp. and *Euplotes rariseta*. During the young abalone cultivation, the numbers of young abalones increase first, and then show a trend of decreasing. The relationship between the density and composition of ciliates and the density of algae in the young abalone culture ponds is also discussed.

Keywords Ciliate; Young abalone culture ponds; Species composition

Introduction

Artificial abalone culture has a long history in China. It has high economic benefit. In recent years, with the cultivation technologies being continuously perfected, the numbers of abalone culture areas have increased rapidly, and its culture scales are becoming larger.

Though the water of culture has been filtrated by sand, the diatom needs to be cultured in advance, and the process is half open, and therefore there are a lot of small-sized invertebrates in the culture water and on the polyethylene film. Those invertebrates dispute the abalones foodstuff and the board; ectoparasite or commensal on the abalone branchia and body surface, so the growth of abalone is affected; they also spread and cause disease, and then cause economic loss in mariculture. So all those small-sized invertebrates in the culture pool are regarded as harmful biological species[1, 2].

Ciliate is one of this kind of harmful unicellular organism. In China, the studies on the harmful ciliates in mariculture environment are mostly concentrated on morphology description, and few reports on ecology have been published[3, 4].

In this paper, by using the methods of qualitative and quantitative analysis, the species composition and dominant genus of harmful ciliates in young abalone culture ponds are studied, and the relationship between the density, composition of ciliates and the density of diatom in the ponds are also discussed.

1 Material and method

1.1 Culturing water column

Samples have been collected from Hongteng Abalones Culture Company Ltd., Jieshi Town, Lufeng City, Guangdong Province, China. The pond is overshadowed, the water volume is 13.6 m^3 per pond, the water has been filtrated by sand, the temperature is 27~30 ℃, and the salinity is 30~32 during the research. Every polyethylene film for culture is 1.5 m^2. The test is carried out in two ponds respectively.

Received on June 20, 2003

1.2 Samples collecting

Samples are collected each 3 d three days after the larva are inserted on the board, till the culture process finishes and the young abalones are removed from the board. The process is 30 d. The method is: take a polyethylene film, wash it thoroughly in 1 L seawater taken from the original pool, be sure all the organisms on the board have been removed. Then preserve the samples in 4 % formaldehyde solution; concentrate to 50 mL after deposition. Get a few samples of living body for identifying the species at the same time.

1.3 Quantitative analysis of samples

Shake up the samples, get 0.1 mL, and count the amount of the ciliates and diatom under the microscope. Then take 1 mL of the sample, count the number of abalones and measure their length and width under the microscope, and take their average value.

1.4 Qualitative analysis of samples

By using the method of live observation and protargol silver staining to identify part of the ciliates, the variety identification and the classification system follow the description and identification key of Kahl, Carey, Yunfen Shen and Weibo Song[5~8].

2 Results

2.1 The abalones growth condition and the process of variation

After being hatched from the zygote, through the swimming stage to creeping larva stage, peristomial shell larva stage, and ending in the swimming life and landing on the polyethylene film, the abalone turns into the life of crawling and lapping the diatom. As Fig. 1 shows, the number of the abalone crawling on the polyethylene film increases gradually, and reaches its maximal on the ninth day, and the density is 0.86 cell • cm^{-2}. Then the density reduces gradually, and at the end of the culture, decreases to 0.02 cell • cm^{-2}, so the survive rate is lower. At this time, the individual of the abalone increases to 1.544 mm in length and 1.208 mm in width.

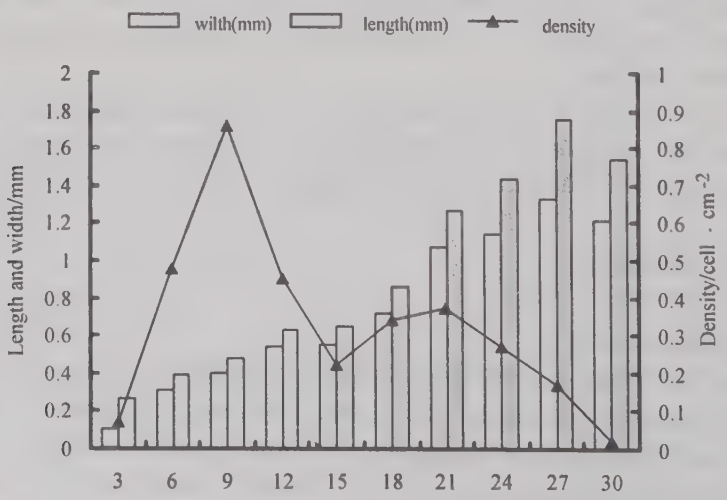

Fig. 1 Growth and density change during young abalone cultivation

2.2 Ciliate composition in the abalone culture pond

Totally 68 species of ciliates, belonging to 3 classes, 16 orders and 46 genus, are found (Table 1). In all order, the species of Hypotrichida is maximal (13); and then Cyrtophorida and Haptorida(10); But the genus of Cyrtophorida Chilodonella is maximal (6). During the study, the genera *Aspidisca* and *Vorticella* appear all the time, *Euplotes* is absent only in one sample, and the other species appear in samples for a short time or discontinuously.

Tab. 1 A list of ciliates in young abalone culture ponds

Ciliophora	Trichostomatida	Peritrichida
Kinetofragminophorea	25 *Plagiopyla marina*	46 *Cothurnia oblonga*
Prostomatida	26 *Sonderia vorax*	47 *Rhabdostyla ringens*
1 *Cyclotrichium Sphacricum*	Colpodida	48 *Vorticell* sp.
2 *Holophyr simplex*	27 *Cyrtolophsis bursaria*	Polymenophorea
3 *Urotricha globosa*	Synhymeniida	Heterotricha
Haptorida	28 *Chilodontopsi* sp.	49 *Chlamydodon triquetrus*
4 *Dileptus anser*	29 *Nassula* sp.	50 *Condylostoma minima*
5 *Dileptus bincleatus*	Cyrtophorida	51 *Caenomorpha levanderei*
6 *Enchelydium labeo*	30 *Chilodonella bavariensis*	52 *Peritromus ovalis*
7 *Enchelys simplex*	31 *Chilodonella caudata*	Oligotrichida
8 *Lacrymaria pupula*	32 *Chilodonella heligolandica*	53 *Sirombidium* sp.
9 *Lacrymaria sapropelica*	33 *Chilodonella psammophila*	54 *Tintinnopsis tuboiduloses*
10 *Trachelophyllum chlense*	34 *Chilodonella subtias*	55 *Tintinnopsis mayor*
11 *Trachelius ovum*	35 *Chilodonella uncinata*	Hypotrichida
12 *Mesodinium acarus*	36 *Trochilia* sp.	56 *Holosticha alviolata*
13 *Mesodinium rubrum*	37 *Dysteria calkinsi*	57 *Opisthotricha Parallelis*
Pleurostomatida	38 *Dysteria marina*	58 *Oxytricha bifaria*
14 *Litonotus camella*	39 *Atapochilodon arenifer*	59 *Oxytricha marina*
15 *Litonotus fasciola*	Suctorida	60 *Keronopsis* sp.
16 *Loxophyllum rostratum*	40 *Acineta foetida*	61 *Steinia* sp.
17 *Loxophyllum hecus*	41 *Podophrya fixa*	62 *Diophrys appendiculata*
18 *Loxophyllum uninuoleatum*	Oligohymenophorea	63 *Diophrys scutum*
19 *Amphileptus litonotiformis*	Hymenostomatia	64 *Euplotes moebiusi*
20 *Amphileptus marina*	42 *Colpidium* sp.	65 *Euplotes rariseta*
21 *Amphileptus rotunda*	43 *Frontonia acuminata*	66 *Aspidisca leptaspis*
22 *Amphileptus* sp1.	44 *Frontonia depressa*	67 *Aspidisca steini*
23 *Amphileptus* sp2.	Scuticociliatida	68 *Aspidisca turrita*
Karyorelictida	45 *Cyclidium oblongum*	
24 *Remanella obtusa*		

2.3 The density change of the dominant genus

During the study, the genera *Aspidisa*, *Vorticella* and *Euplotes* occupy the maximum proportion,

and *Aspidisa*, *Vorticella* exist throughout the culture stage. The maximal density of *Aspidisca*is 5.5 cell • cm^{-2}, and it is the first dominant genus in most time. *Vorticella* reaches its maximum density of 1.52 cell • cm^{-2}, and becomes the first dominant in the later stage. *Euplotes* exists in most time, and its maximal density is 1.01 cell • cm^{-2} (Fig. 2). The dominant species are *Aspidisca leptaspis*, *Vorticella* sp. and *Euplotes rariseta*.

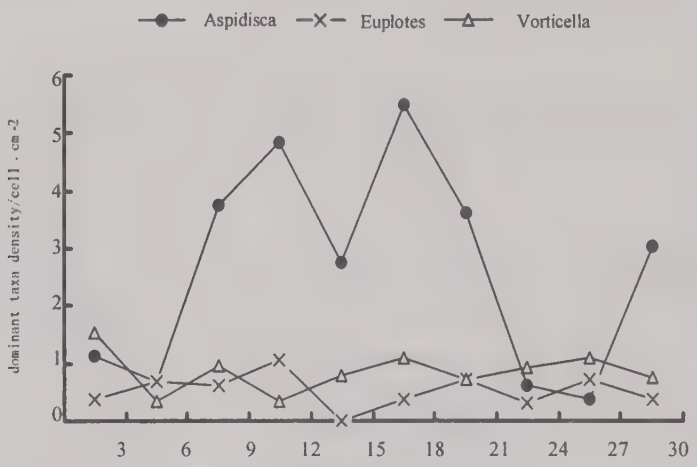

Fig. 2 Dynamic processes of dominant species of ciliates during young abalone cultivation

2.4 The density change of the diatom and ciliates in the abalone culture pond

Figure 3 shows the density change of the diatom and ciliates in the abalone culture pond. The

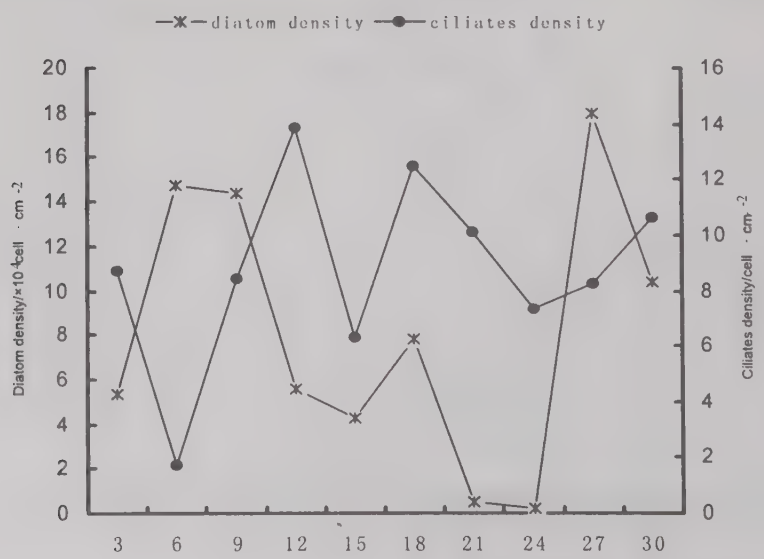

Fig. 3 Change of total density of diatom and harmful ciliates during young abalone cultivation

density of diatoms reaches its maximum on the sixth day: 14.76 cell • cm^{-2}, and slightly reduces on the ninth day: 14.39 cell • cm^{-2}. Then it fluctuates somewhat and on the 21st day and the 24th day, the density is minimum. But on the 27th day the density reaches its second maximum: 17.96 cell • cm^{-2}. The ciliate density reaches its maximum on the 12th day, then fluctuates, and reaches its second maximum on the 27th day too.

2.5 The density and species change of ciliates during culture

Figure 4 shows the density and species change of ciliates during culturing; the number of species is 9 at the most, and 4 at the least.

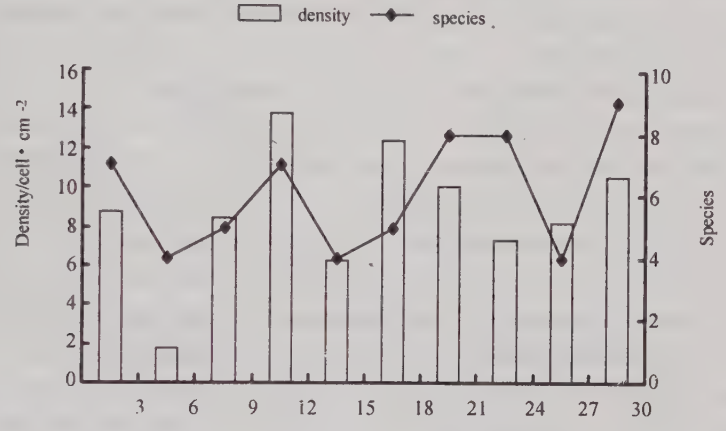

Fig. 4 Change of species and total density of harmful ciliates during young abalone cultivation

3 Discussion

Because different ciliates have different life styles and food habits, the composition and dominant species under different circumstances are different. In the prawn culture seawater environment, the main ciliate species are planktontic, and the dominant order is Oligotrichida[4]. In the abalone larva foodstuff culture pond, because the samples are collected from the polyethylene film, the ciliates are primarily the sessile type, and the dominant species are Hypotrichida species, *Aspedisca stein* and *Aspidisca turrita* [3]. In this study, the sample is also from the polyethylene film. The dominant genera are Hypotrichida *Aspidisca* and *Euplotes*, and the dominant ciliates are *Aspidisca leptaspis*, *Vorticella* sp. and *Euplotes rariseta*. These show Oligotrichida order ciliates are adapted for living on the polyethylene film in seawater culture environment for their flat body, poor freeswimming ability, can crawl on the board with its ventral cirr, and their main food is germ and diatom, which makes them the dominate genus.

There are some commensal ciliates in culture water, such as Peritrichida and Suctorida order ciliates, whose damage to the culture is known very well[3]. In this study, totally 5 species are found, and they are Peritrichida *Cothurnia oblonga*, *Rhabdostyla ringens* and *Vorticella* sp.; Suctorida*Acineta foetida* and*Podophrya fixa*, of which *Vorticella* sp. is the dominant species, and appeared during the study and its quantity is quite large. Before the young abalone larva land on the polyethylene film, the

diatom should be inoculated and cultured on the board, the time of the polyethylene film in the water is longer. So the species and density of Peritrichida and Suctorida on the board are more than those in the diatom stage (*Epistylis* sp. and *Vorticella* sp.)[3].

With the abalone larva upgrowth, its density on the polyethylene film increases gradually at first, and reaches its maximum: 0.86 cell • cm^{-2}. At the same time, the diatom absorbs the nourishment and multiplies. The abalone larva is smaller, and its ability of consuming the diatom is lower than the speed of the diatoms multiplication, so the density of the diatom on the board increase still. But with the extension of culture time, some abalone larva are eliminated out for aplasia; the edible diatom decreases, the other harmful organisms living on the board contend with the abalone larva for food; The water quality becomes worse; Some Peritrichida and Suctorida even directly live on the abalone larva surface *etc.*. All these factors may affect the normal growth of the abalone larva, and cause its survival rate to drop significantly.

The abalone larvae lap the diatom and crawl on the polyethylene film. This affects the ciliate's density, species composition and the quantity of each species. In the diatom culture pond, the dominant species are *Aspedisca stein* and *Aspidesca turrita*; the size is 25 μ m or so, and the maximal density is 21.55 cell • cm^{-2} [3]. But in the abalone larva culture pond, the dominant species are replaced: The dominant species *Aspidisca leptaspis*is 60 μ m or so, the size of *Euplotes rariseta* is 40 μ m or so; the sessile species *Vorticella* sp. also becomes the dominant species; the density of ciliates reaches 13.87 cell • cm^{-2} . Therefore, compared with the relatively stable conditions in the diatom culture pond, as abalone larvae exist on the polyethylene film, although the dominant species *Aspidisca stein* and *Aspi disca sanchi* appear in the abalone larva culture pond, they are not dominant species any more, and are replaced by the bigger species: *Aspidisca leptaspis* and *Euplotes rariseta*, and the density drops.

In mariculture, the fresh-water-bath and low-salinity water treatment are used to control the ectoparasitical ciliates (such as *Trichodina* spp.) on the *chlamys farrer* and *Haliotis discus*, but the host gill epithelia are sensitively, to the freshwater and low-salinity water, as a result of which, lots of the host die[9]. During the abalone cultivation, to raise the abalone survival rate, some medicines (such as potassium permanganate, dipterex, formaldehyde *etc.*) are used to kill the harmful organisms, but those medicines must be less poisonous to abalone larva and diatom; and the poisoning time must be strictly controlled. From the results of this study, it can be seen that the density of the ciliates rises and falls with the density of the diatom, showing that the medicine in moderate concentration may kill some harmful micrometazoa such as Copepods[10], but is inefficient to the ciliates. Because the abalone larva culture pond is half open, there are a lot of ciliates on the polyethylene film during the diatom culture; The water has been filtrated, but the small ciliates and its cyst can't be eliminated efficiently; the ciliates can also spread with the aid of the tools and even the air. Therefore, it is meaningful to employ an ideal method, control the ciliates quantity in the abalone cultivation environment, reduce its harmfulness, and increase the survival rate of abalone larvae.

References

[1] Li Hui, Hu Jianxing, Xu Chunmei. The Species and Dynamics of Harmful Organisms in Culture Ponds for Larvae and Juveniles of Chlamys nobille. Jin Quzeng. The Biology and Mariculture of Scallop Chlamys Nobilis. Beijing: Science Press, 1996, 48-52.

[2] Song Weibo. The Harmful Ciliate in Mariculture Water. Marine Sciences, 1993, 4: 41-46.

[3] Xu Runlin, Miao suying, Yu Mianyu, Sun yi-xiang. Harmful Ciliates and Dominant Population in Cultured Ponds of Algae. *Tropic Oceanology*, 2000, 19(3), 20-26.

[4] Lu Jinrang, Zhang Hongyan, Li Deshang, Lei Yanli, Xu Kuidong. Population Growth and Production Estimation of Planktonic Ciliates in A Experimental Ecosystem of A Shrimp Pond. Journal of Fishery Sciences of China, 1997, 4(5): 50-54.

[5] Kahl A. Urtiere Oder Protozoa. In: Dahled. Die Tierwelt Deuschlands. 1935, 1-886.

[6] Carey P G. Marine Interstitial Ciliates. London: Chapman & Hall, 1992, 1-358.

[7] ShenYunfen. Protozoology. Beijing: Science Press, 1999, 431-509.

[8] Song Weibo. Progress in Protozoology. Qingdao: Qingdao Ocean University Press, 1999, 65-76.

[9] Xu Kuidong Song Weibo. A Primary Study on the Trichodinosis of Marine Mollusca and Its Control Approach. Journal of Ocean University of Qingdao, 1996, 26(2): 172-178

[10] Chen Chui, Yan Lixin Yan Haibo. Culture of Abalone. Guangzhou: Guangdong Science & Technology Press, 1998, 121.

The Relation of Standard Metabolic Rate to Water Temperature and Body Weight of Schlegels Black Rockfish (*Sebastodes Fuscescens*)

Ma Zhimin (马志敏)[1,2], Sun Yao (孙 耀)[2], Zhang Bo (张 波)[2], Tang Qisheng (唐启升)[2]
1 Ocean University of China, Qingdao 266003, *Shandong, China*
2 Yellow Sea Fisheries Research Institute, Chinese Fisheries Science Acadmy, Qingdao 266071, *Shandong, China*

Abstract Standard metabolic rates of Schlegels black rockfish with different body weights are determined in laboratory by using the flow-through respirometer at 11.2 ℃, 14.7 ℃, 18.0 ℃ and 23.6 ℃. The results indicate that the standard metabolic rates increase with the increase of body weight at different temperatures. Relationship between them could be described as $Rs = a \ln W^{b}$. The mean of standard metabolic rate is significantly different among groups, but the b values are not. The standard metabolic rates of amended standard body weights decrease with the increase of temperature, and the mean of standard metabolic rate is also significantly different among groups when the standard body weights are 48.6 g, 147.9 g, and 243.1 g. Relationship between them could be described as $Rsw = m e^{-bT}$. The relations of standard metabolic rate (*Rs*) or relative metabolic rate (*Rs*) to body weight and temperature yield the following equations: $Rs = 1.160\ W^{0.752}\ e^{-9.494/T}$ and $Rs' = 1.160\ W^{0.254}\ e^{-9.494/T}$.

Keywords Standard metabolic rates, Body weight, Temperature, Schlegels black rockfish

Introduction

Standard metabolism of fish is defined as the minimum metabolic rate in the starveling and static state[1]. The widely adopted method is to determine indirectly the standard metabolic rate (SMR) of fish through respiratory experiment[2, 3]. As it is very difficult to keep fish in standard state when practically determined, most SMR of fish are usually obtained under an approximate standard state. Obviously, the diverse level of controlling the above-mentioned standard state may result in experimental errors. Concerning the determination of fish standard metabolism, there has not been a unified standard method to follow until now. So far, the SMR of many fish species has been quantitatively determined, and the quantitative mathematical models have been established to describe the relationship of SMR to the influence factors, such as temperature, body weight, ration level, and so on[4~11]. However, those studies have been still limited to some fresh water or euryhalinous fish species. Experimental studies and published reports on marine fish have seldom been seen. So whether some regular patterns found from this study are suitable for marine fish species still needs further verification.

Schlegels black rockfish (*Sebastodes fuscescens*) is an economically important species in inshore of the Bohai Sea and Yellow Sea. As a bottom-dwelling carnivorous fish, it has no significant behavioral trait of gregarousness and overwintering migration. This fish possesses broad representativeness in the Bohai Sea and Yellow Sea. By using the self-designed flow-through respirometer, this study determines SMR of Schlegels black rockfish and the effects of temperature and body weight, and establishes the interaction mathematical model of SMR with body weight and temperature. This study will assuredly

Received on January 18, 2004

help to disclose the metabolic energy characteristic of this fish species.

1 Materials and Methods

The experiment was carried out at the Maidao Experimental Station for Fishery Sciences, Yellow Sea Fisheries Research Institute, in 1997—1998.

1.1 Source of materials and acclimation

The test fish were caught in the coastal area of Qingdao, P.R China. After being treated with 2~4 mg/L chloramphenicol solutions, the fish was put into the glass fiber reinforced plastic tanks (1 000 L) for acclimation for about 15 days. When feeding and growth went to normal, the test fish was transferred to the trial tanks (100 L) for further acclimation for about 7 days. Acclimation was conducted on flow-through conditions. During acclimation, the fish was fed with piece of fresh Sand launce (*Ammodyte personatus*), the size of which was taken to being swallowed by test fish.

1.2 Experimental Apparatus

The experiment adopted a self-made flow-through respirometer to determine the standard metabolic rate of Schlegels black rockfish (for its structure, see Figure 1).

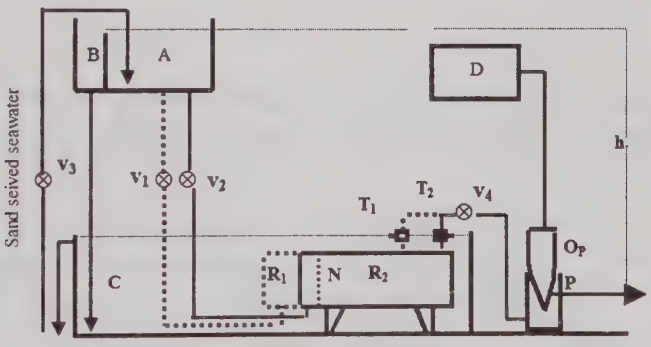

Fig. 1 Schematic diagram of the flow-through respirometer for fish

After passing precipitation and high pressure sand filtration, the natural sea water ($S = 29$) entered superior water reservoir (A), and then came into the respiratory chambers R_1 and R_2 through spherical valves V_1 and V_2. Through adjusting spherical valves V_1 to keep excessive water overflowing from the chamber A, stable water level difference, viz. stable amount of water flowing through the respiratory chamber, could be maintained during the experiment. The water overflowing from the chamber A came into the constant temperature test chamber through the lateral water chamber B, making the water in the reservoir C at the flowing state, and thereby keeping the seawater temperature relatively stable. Water from the respiratory chamber entered the dissolved oxygen measurement chamber P by connection T_1 or T_2 and spherical regulation valve (V_4), the rate of flow being 180 ~ 220 mL/min. D is the instrument for measuring DO and temperature (YSI-model, ±0.03 mg/L, Made in USA). O_P is DO measurement probe. During the experiment, the respiratory chamber of 6 cm·30 cm or of 10cm·40cm is selected and the position of moving restricted net is adjusted according to the body size of fish so as to reduce spontaneous activity of test fish as far as possible.

1.3 Methods

Based on the natural fall of seawater temperature and the relative stability in the process of temperature change from Aug. to Nov. along the coast of Qingdao, acclimation was conducted at four natural seawater temperatures, namely, (11.2 ± 1.98) ℃, (14.7 ± 0.57) ℃, (19.4 ± 1.12) ℃ and (23.6 ± 0.46) ℃. As the metabolism determination time was rather short, the scope of temperature variation was relatively small. The body weight of test fish was from 29.6 to 358.1g. 84 Schlegels black rockfish were measured. Generally two fish of similar body weight were merged into one group in the determination for small fish. Before the determination, the experimental fish fasted for 2～4 d, the fasting time being fixed in accordance with the temperature. The respiratory chamber R_1 was set as the control in each determination. After fasting, the experimental fish were transferred into the respiratory chamber R_2, and the three-junction was adjusted to connect T_1 with DO mobile measurement chamber P and T_2 was emptied. After keeping steady for 0.5 h, determine the DO value of water flowing from the control respiratory chamber R_1 firstly. Then empty T_1, connect T_2 with P, and determine DO value of water from the test fish respiratory chamber R_2. The oxygen consumption of Schlegels black rockfish is the products of the dispersion of two measured DO values and water velocity flowing through the respiratory chamber. At the end of the experiment, the body weight of the experimental fish was determined immediately.

2 Results

2.1 Relationship between SMR and body weight of Schlegels black rockfish

Figure 2 shows the relationship of SMR (*Rs*) and relative SMR (*Rs*) to body weight in the

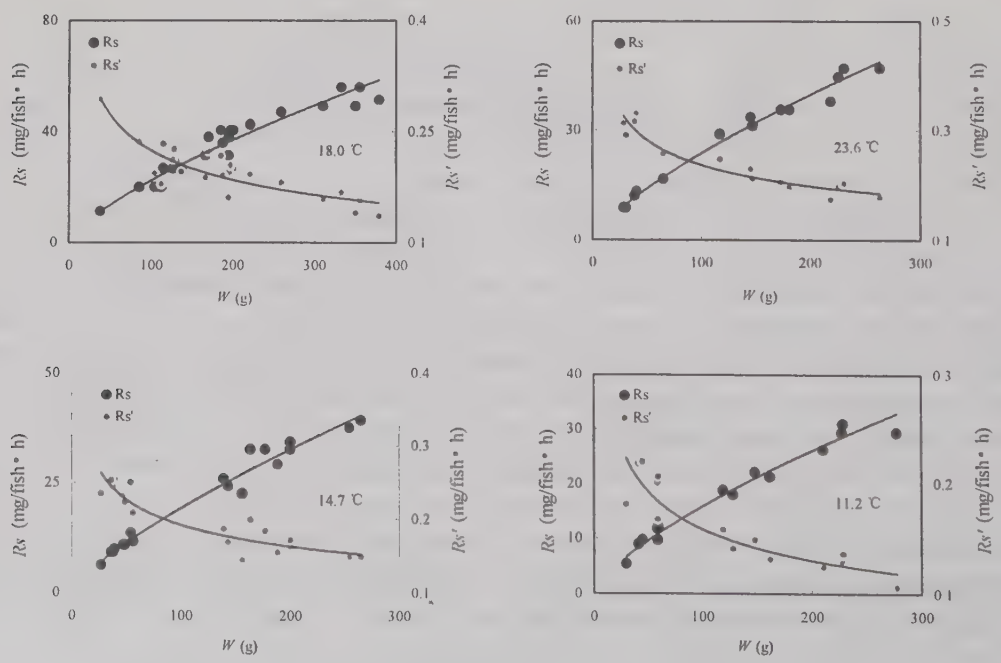

Fig. 2 The relationship between *Rs* or *Rs'* and body weight at differert temperatures

experimental temperature range.

Apparently, *Rs* increases with the increase of body weight without exception, but *Rs'* appears to the contrary. By regression analysis, it could be found that the results have accorded with the general relationship of standard metabolism to body weight of fish, viz., $Rs = a\ W^{b}$. However, all the body weight exponent of *Rs'* is positive, while all the body weight exponent of R_s is negative; and the relevant relationship of the entire fitted curve shows a high level of significance.

Table 1 shows the parameters of fitted equation at different temperatures and the relevant test results. By transforming the above-mentioned power function into linear form, and using analysis of covariance, it could be seen that (1) the average SMR of Schlegels black rockfish at different temperatures has significant difference among groups ($F_{(3,65)} = 7.64$, $P < 0.01$); (2) the body weight exponent b values of regression equation at different temperatures have no significant difference ($F_{(3,64)} = 1.01$, $P > 0.05$); (3) the intercept ln (a) differs significantly ($F_{(3,64)} = 62.16$, $P < 0.01$).

Tab. 1 The parameters of fitted equation and statistics test on the relationship between Rs and body weight

Temp.(C)	Number of fish	*Rs*				*Rs'*			
		a	*b*	r^2		*a*	*b*	r^2	
11.2	14	0.586	0.716	0.968		0.586	−0.284	0.828	
14.7	18	0.578	0.761	0.982	P < 0.01	0.578	−0.239	0.845	P < 0.01
18.0	22	0.818	0.719	0.944		0.818	−0.281	0.722	
23.6	15	0.763	0.746	0.990		0.763	−0.254	0.911	

2.2 Relationship between SMR of Schlegels black rockfish and temperature

Sixty-nine experimental fish are divided into 3 groups according to their body weight, and the mean body weight of each group is adopted as the relatively standard body weight (*Ws*). Then SMR of each group under standard body weight could be calculated with the following formula:

$$Rsw = (Ws / W)^{b} \times Rs$$

Where, *Rsw* is the SMR under the standard body weight, *Ws* is the standard body weight of the fish, *W* is the measured body weight of the fish, *Rs* is the SMR and *b* is the body weight exponent at different temperatures.

Rsw value of different standard body weight tends to retardatively increase with the increase of temperature (see Fig.3). Within the experimental temperature range, their relationship could be quantitatively described with the same curve form, viz.:

(48.6 ± 14.2) g: $Rsw = 18.76e^{-7.56/T}$, $R^2 = 0.996\ 8$

(147.9 ± 20.7) g: $Rsw = 49.73e^{-9.64/T}$, $R^2 = 0.996\ 8$

(243.3 ± 35.8) g: $Rsw = 71.35e^{-9.57/T}$, $R^2 = 0.959\ 9$

Statistical analysis proves that the above-mentioned relationship has significant correlation.

Analysis of covariance on the linear relationship of ln*Rsw* to 1/*T* indicates that: (1) the mean standard metabolism of Schlegels black rockfish has significant difference among different body weight groups ($F_{(2,62)} = 266.33$, $P<0.01$); (2) the body weight exponent *b* of regression equation at different temperatures doesn't have significant difference ($F_{(2,61)} = 0.45$, $P > 0.05$), but the difference among intercept ln(a) is significant ($F_{(2,61)} = 924.81$, $P < 0.01$).

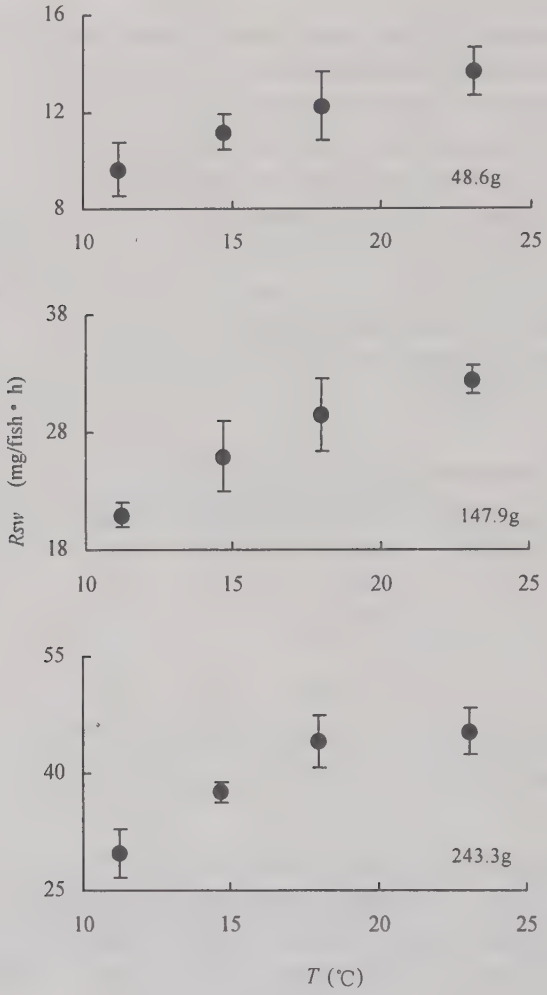

Fig. 3 Changes of Rsw with temperature at different body weights

2.3 The model for interaction of SMR, temperature and body weight

Based on the result of the present study, the model for interaction of SMR, temperature and body weight presented by Cui Yibo (1989) is revised as follows:

$$\ln Rs \text{ or } \ln Rs' = A\ln W + B / T + \ln C$$

By multiple regression operation on the measured results using the above equation, it could be obtained that

$$\ln Rs = 0.752 \ln W - 9.494 / T + \ln 1.160 \quad \text{or}$$

$$\ln Rs' = -0.254 \ln W - 9.494 / T + \ln 1.160$$

($N = 69$, $R^2 = 0.9796$ or 0.8663, $|t\ (\ln W)| = 52.11$ or 17.52, $|t\ (1/T)| = 13.92$ or 13.34). Both the negative coefficient and the partial coefficient shows a high significance level ($P < 0.01$). The above equations may also be transformed into the following forms:

$$Rs = 1.160\ W^{0.752} e^{-9.494/T} \quad \text{or} \quad Rs' = 1.160\ W^{-0.254} e^{-9.494/T}$$

3 Discussion and Conclusions

Compared with many other marine carnivorous fish species, feeding and swimming activity of Schlegels black rockfish are relatively weak, so the proportion of metabolic energy to the general energy output is lower. Even then, the relative metabolic rates in this study are dispersed in the scope of 124 ~ 329 mg/kg • h, with the general average value being 198 mg/kg • h, which is remarkably higher than 89 mg/kg • h, a statistical average value for 34 fish species (Brett &Groves, 1979)[1]. As most of the 34 fish species selected by Brett & Groves are of fresh water, so further studies are needed on whether there is a system diversity of metabolic level between marine and freshwater fish species.

The standard metabolism of fish increases along with the increase of body weight. The relationship could generally be described by the power function $Rs = aW^b$, where b is body weight exponent. With regard to body weight exponent b, two points need to be elucidated.

Firstly, it is uncertain whether there is diversity of b value among species. Winberg (1956) suggested firstly that the body weight exponent of fish was about 0.8[12]. Later, Elliott (1979) proposed that the extreme scope of b value was 0.5 ~ 1.0, most values being between 0.7 ~ 0.9[13]; but Brett & Groves (1979) and Cui &Liu (1990) claimed that there were no significant differences of b value among most fresh water fish species, the average being about 0.86. The present study indicates that the b value for Schlegels black rockfish is 0.73 6 ± 0.022, which is in the scope of b value presented by Elliott, but far from those suggested by Brett and Cui.

Secondly, it is related to whether temperature could affect b value. Fry (1979) thought that b value was independent of temperature[14]. The present study and the studies on Atlantic herring (*Brevoortia tyrannus*)(Hettler, 1976)[15] demonstrated this viewpoint. But there are also some different study results. For example, the b value for African crucian carp(*Orechromismossambicus* and *Orechromisniloticus*) increases along with the rise of temperature[13, 16] , while the b value for south catfish (*Silurus meridionabis*) and European eel (*Anguilla anguilla*) decreases with the increase of temperature[5, 11].

Generally, the SMR of fish increases with temperature, but the mathematical models used to describe the relationship vary greatly. The SMR of brown trout (*Salmo trutta* L.) and European minnow (*Phoxinus phoxinus* L.) increases post with the increase of temperature. The relationship between them is described by an exponent function curve[7, 17], but it turns to be a power function curve for southern catfish (*Silurusasotus* L.)[11].

In this study, SMR of Schlegels black rockfish increases at a decreasing speed with the increase of temperature distinctly. It's difficult to describe the relation by a curve often adopted in the previous studies. Though the function $Rsw = m\, e^{n \cdot T}$ adopted in this study is not very reasonable for the speculated result of SMR when the temperature extends down, the statistical test indicates that this function is best suitable within the scope of this study.

As the variance features of SMR of Schlegels black rockfish with temperature and body weight differ greatly from those indicated by the published reports[4, 10, 18~23], it is not feasible to describe the interaction of Schlegels black rockfishs SMR with temperature and body weight by using the known empirical formula. By comparison, this study has chosen the empirical formula[2] which has close variance features, revised it according to the results of this study, and then presented the mathematical model applied to the interaction of Schlegels black rockfishs SMR with temperature and body weight. Nevertheless, as few studies have related to marine fish so far, further studies are needed to testify whether the above-mentioned model is fit for other marine fish.

Acknowledgements

We thank Professor Chen Minshan for constructive criticism of our earlier draft and his help on the translation.

This paper is financially supported by the Major Program of National Natural Science Foundation (No. 497901001), Key Basic Research and Development Program (No. G1999043710) of China

References

[1] Brett J R, Groves T D D. Physiological energetics. In: Fish physiology (W. S. Hoars eds). New York: Academic Press, 1979, 8: 279-352.

[2] Cui Y. Bioenergetics of fishes: theory and methods. Acta Hydrobiol. Sin., 1989, 13(4): 369-383.

[3] J P Herrmann & E.C. Enders. Effect of body size on the standard metabolism of horse mackerel. J. Fish Biol., 2000, 57: 746-760.

[4] Cui Y & Wootton R J. The metabolic rate of the minnow, *Phoxnus phoinus L.*, in relation to ration, body size and temperature. Funct. Ecol., 1988, 2: 157-162.

[5] Dengi G & Gallagher M K. The influence of body size and temperature on oxygen consumption of the European eel, *Anguilla anguilla.* J. Fish. Biol., 1989, 34: 19-24.

[6] D W Sims. The effect of body size on the standard metabolic rate of the lesser spotted dogfish J. Fish Biol., 1996, 542-544.

[7] Elliott J M. Energy losses in the waste products of brown trout (*Salmo trutta L.*). J. Anim. Ecol., 1976, 45: 561 -580.

[8] G Claireaux & J P Lagardere. Influence of temperature, oxygen and salinity on the metabolism of the European sea bass. J. Sea Res., 1999, 42, 157-168.

[9] H Schurmann & J F Steffensen. Effects of temperature, hypoxia and activity on the metabolism of juvenile Atlantic cod. J. Fish Biol., 1997, 50: 1 166-1 180.

[10] Jiashou Liu, Yibo Cui & Jiankang Liu. Resting metabolism and heat increment of feeding in mandarin fish (*Siniperca chuatsi*) and Chinese snakehead (*Channa argus*). Comp. Bio. Physio (Part A), 2000, 127: 131-138.

[11] Yang Z, Xie X & Sun R. The resting metabolic rate of the common catfish (*Silurus Asotus*) as a function of body weight,temperature and sex. Acta Hydrobiol. Sin., 1995, 19(4): 368-372.

[12] Wingerg G G. Rates of metabolism and food requirements of fishes. Fish. Res. Bd Can. Transl. Series, 1956, 194.

[13] Elliott J M. Energetics of fresh teleosts. In: Fish Phenology: Anabolic Adaptiveness in Teleosts. Symp. Zool. Soc. Lond. 44 (P.J. Miller eds). London: Academic Press, 1979, 29-61.

[14] Fry F E J. The effect of environmental factor on the physiology of fish. In: Fish physiology (W. S. Hoars eds), New York: Academic Press, 6: 1-98.

[15] Hettler E F. Influence of temperature and salinity on routine metabolic rate and growth of young Atlantic menhaden. J. Fish. Biol., 1976, 8: 55-65.

[16] Cui Y & Liu J. Comparison of energy budget among six teleosts, II Metabolic rates. Comp. Biochem. Physiol., 1990, 97: 169-174.

[17] Cui Y & Wootton R. J. Components of the energy budget in the European Minnow, Phoxinus phoxinus (L.) in relation to ration,body weight and temperature. Acta Hydrobiol. Sin., 1990, 14(3): 193-204.

[18] Beamish F W H. Respiration of fishes with special emphasis on standard oxygen consumption. II. Influence

of weight and temperature on respiration of several species. Can. J. Zool., 1964, 42: 177-188.

[19] Beamish F W H & Mookherjii P S. Respiration of fishes with special emphasis on standard oxygen consumption. Ⅰ. Influence of weight and temperature on respiration of goldfish,*Carassius auratus* L. Can. J. Zool., 1964, 42: 161-175.

[20] Dengi G & Gallagher M L. The relationship between growth, food conversion and oxygen consumption in developed and undeveloped American eels, *Anguilla rostrata* Leseueur. J. Fish Biol., 1985, 27: 635-641.

[21] Eccles D H. The effect of temperature and mass on routine oxygen consumption in the South African cyprinid fish *Barbus aeneus Burchell.* J. Fish Biol., 1985, 27: 155-165.

[22] Ross B, Ross L G. The oxygen requirements o*toreochomis niloticus* under adverse conditions. In: Fishelson. C.M. (Eds.), Proceedings of the International Symposium on Tilapia Aquaculture. Tel Aviv., 1983, 134-143

[23] Xie X & Sun Y. The bioenergetics of the southern catfish (Silurus meridionalis Chen). Ⅰ. Resting metabolic rate as a function of body weight and temperature. Physiol. Zool. 1990, 63: 1 181-1 195.

Bottom Sediment Transport in the Flood and Ebb Channels of the Changjiang Estuary

Liu Gaofeng (刘高峰)[1,2], Shen Huanting (沈焕庭)[1], Wang Yonghong (王永红)[1],
Wu Jiaxue (吴加学)[2]

1 *State Key Laboratory of Estuarine and Coastal Research, East China Normal University, Shanghai* 200062, *China*;

2 *Estuary and Coast Science Research Center, Ministry of Communications, Shanghai* 201201, *China*;

3 *School of Ocean and Earth Scienece, Tongji University, Shanghai*, 200092, *China*

Abstract Nanxiaohong and Nangang main south channel are chosen as the typical flood and ebb channels. Hydrodynamics analysis based on field hydrological and sediment data is conducted with Gao-Collins model to analyse sediment transport trends. Also, the grain size distribution analysis of the bottom sediment sampled in Sep. 2001 is used as the base of the analysis. The result shows that the sediment in Nanxiaohong is from the rive mouth area. The sediment transports upwards with the flood flow which is stronger than the ebb flow, *i.e.*, in the direction of SE-WN. The sediment in main south channel comes from upward. They transport downwards with the ebb flow, which is stronger than the flood flow, *i.e.*, in the direction of WN-SE. The directions, sources and mechanism of sediment transport are identified according to comprehensive analyses of the observed data on hydrodynamics and sediment.

Keywords Flood channel, Ebb channel, Changjiang Estuary ,Sediment transport

Introduction

The phenomenon of the route divergence of the flood and ebb current is obvious in the Changjiang estuary. The direction of the ebb current deflects south by south, and the flood current deflects north by north. This is caused by many factors. The Coriolis force is the important one of those that shouldnt be neglected [1]. The route divergence of the current results in the difference of river channel property. Two kinds of different channel appear in the Changjiang estuary: one is the ebb channel, such as the main channel of south branch, south channel and north channel, whose main dynamics is the ebb current because of the great deal of runoff, the other is the flood channel, such as north branch, Xinqiao channel in south branch and Nanxiaohong and Beixiaohong near Changxing Island, whose main dynamics is the flood current as a result of energy aggregation of the landform[2]. The two kinds of channel may change into each other under some special conditions. For example, the main path of the runoff was north branch 150 years ago, so the north branch was an ebb channel at that time. Afterward the main path of runoff shifted to the south branch, the north branch changed into a flood-dominant channel since the flood became comparatively stronger. Generally ebb channel is the main channel while the flood channel is the ancillary one[3]. The flood channel differs from the ebb channel not only in the hydrological sedimentary character, also in the transport direction of bed sediment. The former has been studied deeply by Shen[2, 3], while the later has been studied rarely.

Received on October 20, 2003

The determination of bed sediment transport pathway is essential if predictions of the response of estuarine geomorphology to both natural events and human activities are to be made[4]. A number of sediment properties, including radionuclide concentrations, mineral magnetic parameters and sediment chemistry have been adopted over the past decade as sediment tracers to identity the sources of sediment [5]. For example, Yinqiang has identified the sediment transport pathway in the Huangmaohai sea area according to the analysis of neutron activation in tracer sand[6]. In addition, sediment transport pathways can be deduced from grain size distribution. During sediment movement, the effects of dynamic process, sedimentation, selective transport and abrasion of particles cause grain size spatial variation [4]. Observation shows that the different distribution of grain size is related to the sediment transport pathway[7]. The study on spatial distribution of grain size will benefit cognition of various processes of sediment transport. Based on this, McLaren developed a model which could predict the sediment net transport trend according to the trend in the mean, sorting and skewness of particle size[8, 9]. This model has been widely used to identify estuarine and coastal sediment transport[10~12]. This model chooses a possible sediment transport pathway to estimate sediment transport probability, so it is a one-dimensional model. Based on this model, S. Gao developed a two-dimensional sediment grain size trend analytic model[13, 14]. This model could be used to study sediment transport direction in the open estuarine and coastal area. In this paper, the typical flood and ebb channels: Nanxiaohong and main channel of Nangang are chosen as research objects and based on the grain size data of 20 sediment samples and comprehensive analyses of hydrodynamics and sediment observed data, Gao-Collins model is used to study the bed sediment transport trends in this area. The result would provide basis for studying evolution and exploitation of flood and ebb channels.

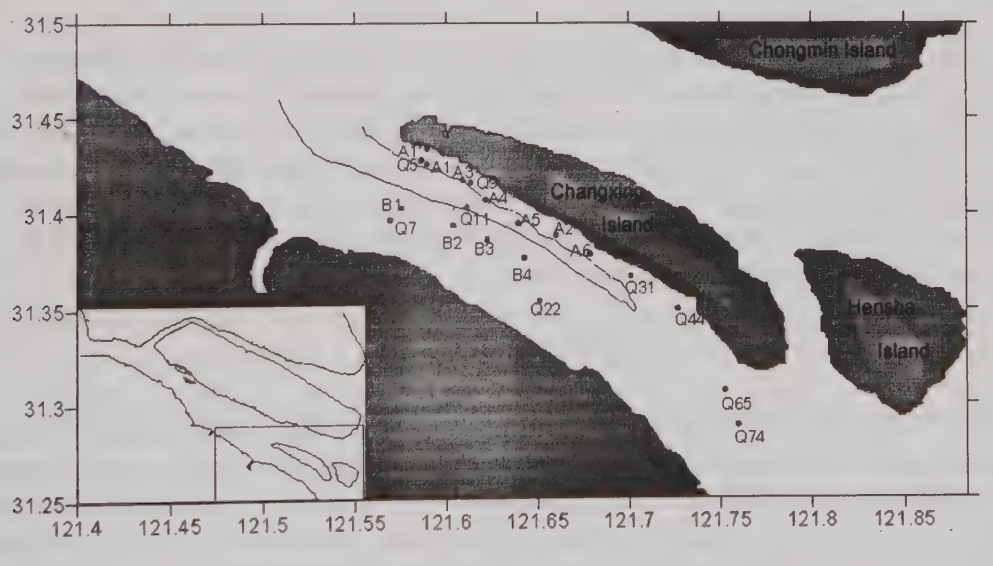

Fig. 1 Research area and position of sampling points

1 Introduction to the Gao-Collins model

In the Gao-Collins model, grain-size distribution of sediment in transport process can be related to the source with the energy transition function. This function has defined the relative probability of

particle erosion and transport in some interval[10]. Eight possible trends may occur during analyzing the trend in mean (μ), sorting (σ) and skewness (S_k) of particle size distributions when Sample A is compared with Sample B[8] (Table 1).

Tab. 1 Possible case using three grain size parameters

Type	Parameter		
1	$\sigma_A > \sigma_B$	$\mu_A < \mu_B$	$Sk_A < Sk_B$
2	$\sigma_A < \sigma_B$	$\mu_A < \mu_B$	$Sk_A > Sk_B$
3	$\sigma_A < \sigma_B$	$\mu_A > \mu_B$	$Sk_A > Sk_B$
4	$\sigma_A > \sigma_B$	$\mu_A > \mu_B$	$Sk_A < Sk_B$
5	$\sigma_A > \sigma_B$	$\mu_A < \mu_B$	$Sk_A > Sk_B$
6	$\sigma_A < \sigma_B$	$\mu_A < \mu_B$	$Sk_A < Sk_B$
7	$\sigma_A < \sigma_B$	$\mu_A > \mu_B$	$Sk_A < Sk_B$
8	$\sigma_A > \sigma_B$	$\mu_A > \mu_B$	$Sk_A > Sk_B$

Of these trends, only those which satisfy the following condition are indicative of the bedload sediment transport: (1) The significance probability of some movement direction is higher than that of the inverse direction in some trends; (2) The trend will not appear if there are no reciprocal interchange between sediment samples. Only case 1 and case 2 which accord with the above conditions could indicate the sediment transport trend[9].

This is the one dimensional McLaren model. Based on the model, Gao-Collins developed a two dimensional data processing method[13]. (1) After collecting bed sediment samples in horizontal grid in study area. The mean sorting and skewness are obtained through grain size analysis. (2) The maximal separation distance could be used as characteristic length D_{cr} to ascertain adjacent points. Those samples should be compared with each other and then distribution trend of grain size will be obtained. Trend vector (unit length) can be drawn from high sorting points to low sorting points. All vectors of each point compose the overall sediment transport trend vector.

$$\vec{R}(x,y) = \sum_{1}^{n} \vec{r}(x,y)_i \tag{1}$$

Where, n is the number of trend vectors, while $\vec{r}(x,y)_i$ is the ith vector, and $\vec{R}(x,y)$ is the overall vector. (3) The distribution trend of grain size between every two points may accord or discord with the sediment transport trend, while the probability of the two trends according with each other is higher than that of the two trends discording with each other. Those trends discording with sediment transport are chaos, which could be filtered through semi-quantitative analysis.

$$\vec{R}_{av}(x,y) = \frac{1}{k+1}\left[\vec{R}(x,y) + \sum_{1}^{k} \vec{R}_j\right] \tag{2}$$

Where, $\vec{R}_j$ is the composed vector of adjacent points, $\vec{R}_{av}(x,y)$ is averaged trend vector after filtration, and k is the number of adjacent points. The residual patterns composed from the averaged

trend vector can represent sediment transport patterns[7]. It should be noted that the trend arrowhead denotes the possible direction of sediment transport and the vector length denotes the significance of grain size distribution trend, but they dont denote sediment transport strength..

2 Sampling and analysis

Twenty sediment samples were obtained from the observing sites in South Harbour of Changjiang Estuary (Figure 1) on September 17, 2001. The samples were analyzed with the Coulter grain-size analysis instrument and the result was reported by Coulter LS Control Program. The whole distribution of grain size, mean, sorting and skewness of samples were obtained. The LS Control Program calculates the three parameters using the following formulas.

$$\mu = \sum_{1}^{n} P_i d_i \tag{3}$$

$$\sigma = \sqrt{\sum_{1}^{n} P_i (d_i - \mu)^2} \tag{4}$$

$$S_k = \sqrt[3]{\sum_{1}^{n} P_i (d_i - \mu)^3} \tag{5}$$

Where, P_i is the percent of the ith group grain size d_i, n is the overall number of grain groups. Gao-Collins model has some requirements for the sampling deployment[11,8]. (1) The sampling grid points should be in the same sedimentary environment. (2) The sampling depth should be limited in the sediment transport thickness. (3) The space between sampling points should not be too large or too small. The samples are got from the same sedimentary environment and the sampling depth is about 10 cm, which is less than the sediment transport thickness. The space between sampling points is about 322 ~ 4 835 m, which approximately accords with those requirements.

3 Results and discussion

3.1 Grain size of bed sediment in south channel and transport trend

Distribution of sediment grain size in Nanxiaohong and main channel of Nangang (Fig. 2) shows that the variation of sediment mean diameter is similar to that of sorting. But the variation of sediment skewness is contrary to those of mean diameter and sorting. The skewness is small (large) if the mean and sorting is large (small). The three parameters vary obviously from upstream to downstream. The three parameters increase in Nanxiaohong and they change in upstream more greatly than in downstream.

From upstream to downstream, the mean and sorting in the main channel of Nangang become smaller and then become larger gradually. The skewness has the similar change trend, but upstream change is larger than downstream change. The distribution of the three particle parameters in the whole Nangang area (Fig. 3 (A ~ C)) shows that the mean and sorting of sediment on shoal between flood channel and ebb channel are very large. So the two parameters have peak regions on the shoal. The peak region of mean diameter appears on the upstream shoal and the peak region of sorting appears in the middle reaches of the shoal, while the peak region of skewness appears in the downstream Nangang.

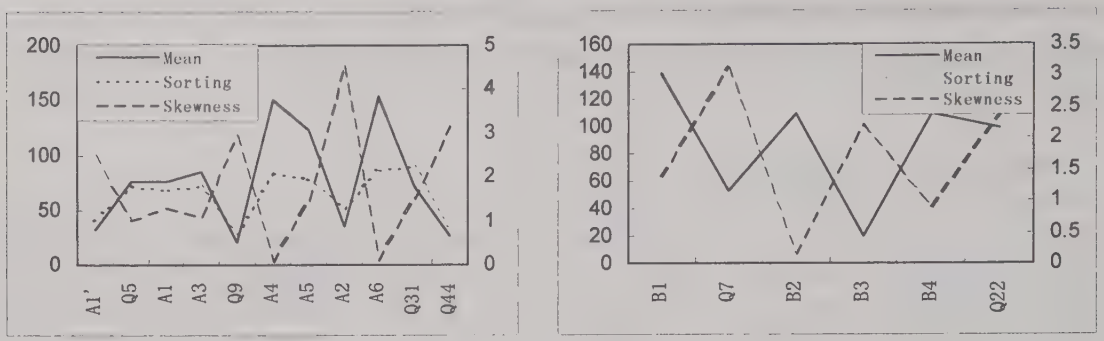

Fig. 2 Distribution of particle parameters in Nanxiohong (Left) and the main channel of Nangang (Right)

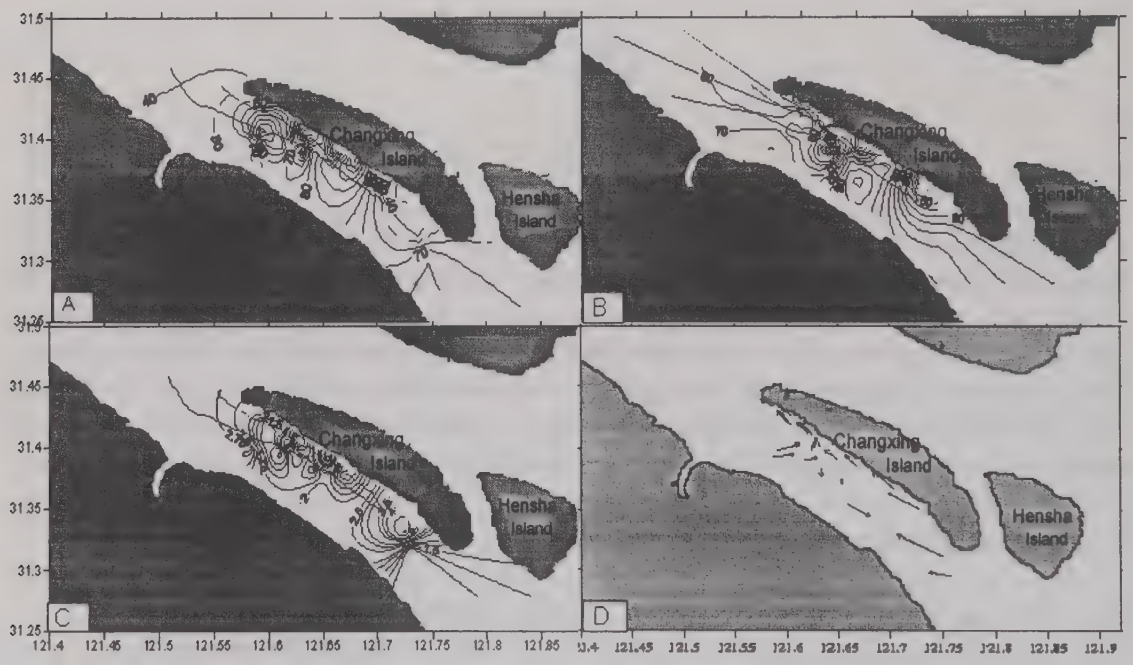

Fig. 3 Distribution pattern of particle parameter and residual patterns in bed sediment transport
(A mean grain size; B sorting coefficient; C skewness; D residual patterns)

Residual patterns of bed sediment transport in Nangang (Fig 3D) show that: (1) The sediment in Nanxiaohong transports from the outside mouth to the inside mouth, The direction is SE-WN. A great number of samples have the similar direction. Only A6 points to Changxing Island but the vector is small. (2) The sediment in the main channel of Nangang transports from inside the mouth to the outside mouth, and the direction is WN-SE. That B1 and Q7 point to Nanxiaohong shows some sediment transport to Nanxiaohong. (3) Sediment on shoal between flood channel and ebb channel mainly transports downstream, but some transport to Nanxiaohong. For example, Q11 points to Nanxiaohong directly, but the trend is small.

3.2 Analysis of cause about the bed sediment transport trend

Nanxiaohong and the main channel of Nangang are typical flood channel and ebb channel respectively and there are lots of differences in hydrology and sediment characteristics between them. Hydrological measurement was carried out at the site A1 and the site B1 in Sep., 2001. A1 and B1 locate in Nanxiaohong and the main channel of Nangang respectively and are basically on the same section. The six-layer method is adopted, which means that the samples at the surface, 0.2H, 0.4H, 0.6H, 0.8H and the bottom are taken. Current velocity, direction and suspended sediment concentration are measured simultaneously. Average current velocity and tide period are calculated at different layers. Results are listed in Table 2.

Tab. 2 Tidal data of the sites A1 and B1

Site	Layers	Surface		0.2 H		0.4 H		0.6 H		0.8 H		Bottom	
		Flood	Ebb	Flood	Ebb	Flood	Ebb	Flood	Ebb	Flood	Ebb	Flood	Ebb
A1	Time (h)	5.43	7.35	5.37	7.37	5.25	7.53	5.11	7.66	5.03	7.66	4.89	7.82
	Velocity (m/s)	1.55	1.44	1.48	1.41	1.38	1.36	1.24	1.30	1.08	1.20	0.89	1.00
B1	Time (h)	4.82	8.18	4.67	8.33	4.75	8.25	4.54	8.46	4.53	8.47	4.33	8.66
	Velocity (m/s)	1.22	1.25	1.16	1.21	1.02	1.17	0.92	1.08	0.83	1.01	0.69	0.85

From Table 2, some conclusions can be drawn: (1) Average current velocity during flood is larger than that during ebb at every layer of A1 station. It is contrary to B1 station, in which average current velocity during flood is smaller than that during ebb. (2) The flooding period and flooding current velocity at every layer at A1 are larger than those at B1, and the ebb period at B1 is longer than that at A1.

Tab. 3 The data of sediment at the sites A1 and B1

Sites	Maximal SSC (kg/m^3)		Average SSC (kg/m^3)		Sediment transport rate (10^3 kg/m)	
	Flood	Ebb	Flood	Ebb	Flood	Ebb
A1	1.56	1.43	1.25	1.058	263.38	258.71
B1	0.90	0.95	0.78	0.81	136.37	240.01

From Table 3, some conclusions can be drawn: (1) The maximal SSC, average SSC and sediment transport rate during flood are bigger than those during ebb at A1. However, the results at B1 are exactly opposite. (2) The maximal SSC, average SSC and sediment transport rate of B1 are smaller than those of A1.

Based on the above analysis, some understanding is obtained: Nanxiaohong is a typical flood channel. Flood current is strong in the flood channel, which means that the average current velocity and period during flood are bigger than those of ebb. And the SSC during flood tide is bigger than that during ebb tide, which leads to the fact that the sediment carried by flood current cannot be taken away by the ebb current. So the net transport is towards upriver. It is clearly demonstrated by the process of bed sediment transport trend at Nanxiaohong (Fig 3 D). The sediment mainly comes from the river mouth area and is carried by flood current. The sediment source includes the sediment from the sea and the sediment from the ebb channel. The sediment mainly deposits in the upper area of Nanxiaohong

during spring tide and deposition occurs at the middle and lower areas.

The main channel of Nangang is a typical ebb channel. The characteristics of hydrology and sediment in the ebb channel are contrary to those of the flood channel. The details are ebb current velocity is bigger than flood current velocity, and the ebb period is longer than flood period, SSC during ebb tide is bigger than that during flood tide and net sediment transport is towards lower river. The sediment mainly comes from upriver and some of the sediment conveyed by ebb tide may transport back to Nanxiaohong by flood tide.

Due to the asymmetrical tidal characteristics between flood channel and ebb channel, the phase difference at the same section in different channels is produced. There is tide level discrepancy at the same time between flood channel and ebb channel. The flood and ebb tides are earlier at the flood channel compared with the ebb channel. Thus a transverse slope will appear and further leads to transverse sediment transport. Sediment transport of the above 4 sites at Figure 3D slightly pointing to Nanxiaohong is an evidence.

4 Conclusions

(1) Nanxiaohong and the main channel of Nangang are typical flood and ebb channel respectively. Their properties differ from each other distinctly. Net sediment transport is determined by different hydrology and sediment characteristics between flood channel and ebb channel. The grain size distribution trends of bed sediment in the two channels give some clues to the net sediment transport direction. The bed sediment in Nanxiaohong transports from upstream to downstream while that in Nangang transports towards downstream. The water body exchanges frequently between the Nanxiaohong and the main channel of Nangang due to the existence of a circulatory flow between the flood channel and the ebb channel, and thus some part of sediment on the shoal is carried towards Nanxiaohong.

(2) The sediment in Nanxiaohong which is taken by the flood current mainly comes from the mouth area. Sediment in the main channel of Nangang which is almost carried by the ebb current mainly comes from upriver.

(3) The grain size analysis of Nangang shows that the Gao-Collins model, a two dimensional sediment grain size trend model, which is based on the McLaren model, can be used to calculate the sediment transport direction, route and source. In order to obtain satisfying results , attention should be paid to analysis combined with hydrodynamics when this model is applied.

Acknowledgements

In translating this paper, Wu Hualing , Liu Yuanfeng and Wang yuanye have given lots of advice and help.

Reference

[1] Chen Jiyu, Yun Caixing, Xu Haigeng and Dong Yongfa. The Development Model of Changjiang Estuary in 2000 Years. Porcesses of Dynamics and Geomorphology of the Changjiang Estuary, Shanghai Scientific & Technical Publisher Press, 1988.

[2] Shen Huanting *et al.*. The Relationship of Channel Evolution with the Characteristics of Residual Currents in the Chhangjiang Estuary. Proceedings of Symposium of Geomorphology. Chinese Geographical Society. China Science Press, 1988, 80-121.

[3] Shen Huanting, Li Jiufa and Jin Yuanhuan. Evolution and Regulation of Flood Channel in Estuaries. Oceanologia et Limnologia Sinica, 1995, 26(1): 83-89.

[4] Russell R D. Effects of Transportation of Sedimentary Particles. In: Trask, P.D. (editor), Recent Marine Sediments. The Society of Economic Paleontologists and Mineralogists, Tulsa (Oklahoma). 1939, 32-47.

[5] Yoshimasa Kurashige, Yuichiro Fusejima Source Identification of Suspended Sediment from Grain-size Distributions: I. Application of Nonparametric Statistical Tests. Catena 31, 1997, 39-52.

[6] Ying Qiang, Cao Mingxiong, and Kong Xiangbai. Determination of Sediment Depositional Range in HuangMao Bay, Advance in Water Science, 1997, 8(1): 48-53.

[7] Gao S and Collins M B. Analysis of Grain Size Trends for Defining Sediment Transport Pathways in Marine Environments. Journal of Coastal Research, 1994, 10: 70-78.

[8] McLaren P. An Interpretation of Trends in Grain Size Measurements. Journal of Sedimentary Petrology. 1981, 51: 611-624.

[9] McLaren P, Bowles D. The Effects of Sediment Transport on Grain-size Distributions. Journal of Sedimentary Petrology, 1985, (55): 457-470.

[10] Gerhard Masselink. Longshore Variation of Grain Size Distribution Along the Coast of the Rhone Delta, Southern France: A Test of the McLaren Model. Journal of Coastal Research, 1992, 2: 286-291.

[11] R W Duck, J S Rowan, P A Jenkins and I Youngs. A Multi-Method Study of Bedload Provenance and Transport Pathways in an Estuarine Channel. Phys. Chem. Earth(B), 26(9): 747-752.

[12] Wu Jiaxue ,and Shen Huanting. Bottom Sediment Transport in Huangmaohai Estuary, South China: the Problems of the Application of McLaren Model in Estuarine Environments. Journal of Sediment Research, 1999, 3: 26-32.

[13] Gao Shu, Collins Michael. An Cretique of the McLaren Method for Defining Sediment Transport Paths. Journal of Sediment Petrology, 1991, 61:143-146.

[14] Gao Shu, Coillins Michael. Net sediment Transport Patterns Inferred from Grain-size Trends, Based upon Definition of Transport Vectors. Sedimentary Geology, 1992, (81): 47-60.

[15] Yang Ou and Liu Cangzhi. Analysis on Sediment Transport Patterns and Sediment Sources of North Branch of Changjiang Estuary. ShuiLI XueBao, 2002, 2: 79-84.

[16] Shen Huanting *et al.*. The Characteristics of Tidal Current and its Effects on the Channel of the Changjiang Estuary Proceedings of Symposium of Geomorphology. Chinese Geographical Society. China Science Press, 1988, 80-90.

[17] Shen Huanting *et al.*. The Characteristics of Tidal Wave and its Effects on the Channel of the Changjiang Estuary Proceedings of Symposium of Geomorphology. Chinese Geographical Society. China Science Press, 1988, 73-80.

[18] Gao Shu, Michael Collins. The Use of Grain Size Trends in Marine Sediment Dynamics: A Review. Chinese Journal of Oceanology and Limnology, 2001, 19(3): 265-271.

Marine Science Bulletin

Marine Science Bulletin publishes papers on marine science and technology including physical oceanography, chemical oceanography, marine biology, marine geology, environmental oceanography, estuarine & coastal sciences, marine technology, digital ocean, coastal zone management, ocean engineering, marine economics, etc., and aims to promote international academic exchange.

Editor-in-Chief: Lin Shaohua（林绍花）
Deputy Editor-in-Chief: Lin Shaohua（林绍花） He Guangshun（何广顺）
Yang Ying （杨 鹰）
Executive Editor: Lin Baofa（林宝法） He Xuewu （何学武） Zhang Deshan（张德山）
Zhang Xiaoxian（张潇娴） Wang Zhankun（王占坤）
Computer typist: Cheng Xiuchun （程秀春）

Marine Science Bulletin **(Vol . 6 No. 1 May 2004)**

Responsible Institution:
State Oceanic Administration of China
Edited and Published Semi-annually by:
National Marine Data and Information Service
Address: 93 Liuwei Road, Hedong District, Tianjin 300171, China
E-mail: msb@mail.nmdis.gov.cn

ISSN1000-9620
CN12-1271/N